GeoScienceWorld
Lithosphere
Volume 2022, Article ID 4584611, 45 pages
https://doi.org/10.2113/2022/4584611

Lithosphere

Research Article

Age and Chemostratigraphy of the Finlayson Lake District, Yukon: Implications for Volcanogenic Massive Sulfide (VMS) Mineralization and Tectonics along the Western Laurentian Continental Margin

Matthew J. Manor[1], **Stephen J. Piercey**[1], **Donald C. Murphy**[2] **and Corey J. Wall**[3,4]

[1]*Department of Earth Sciences, Memorial University of Newfoundland, Room 4063, Alexander Murray Building, 9 Arctic Ave, St. John's, NL, Canada A1B 3X5*
[2]*Yukon Geological Survey, Box 2703 (K14), Whitehorse, Yukon, Canada Y1A 2C6*
[3]*Isotope Geology Laboratory, Department of Geosciences, Boise State University, 1910 University Drive, Boise, ID 83725, USA*
[4]*Pacific Centre for Isotopic and Geochemical Research, Department of Earth, Ocean and Atmospheric Sciences, University of British Columbia, Vancouver, British Columbia V6T 1Z4, Canada*

Correspondence should be addressed to Matthew J. Manor; mjmanor@mun.ca

Received 12 January 2022; Accepted 9 March 2022; Published 20 June 2022

Academic Editor: Jiyuan Yin

The Yukon-Tanana terrane in the Finlayson Lake district, Yukon, represents one of the first arc–back-arc systems that formed adjacent to the Laurentian continental margin in the mid-Paleozoic. Back-arc rocks contain many large and high-grade volcanogenic massive sulfide (VMS) deposits. This study integrates U-Pb zircon geochronology, lithogeochemistry, and Hf-Nd isotopes to establish precise controls on tectonomagmatic activity adjacent to the western Laurentian margin in the Late Devonian to Early Mississippian. High-precision chemical abrasion- (CA-) ID-TIMS U-Pb zircon geochronology defines coeval arc (ca. 363.1 to 348 Ma) and back-arc (ca. 363.3 to 355.0 Ma) magmatism in the Finlayson Lake district that intruded continental crust of Laurentian affinity (e.g., Snowcap assemblage). Mafic and felsic rocks display geochemical and isotopic characteristics that are consistent with being formed from mixtures of depleted asthenosphere and enriched lithospheric mantle sources. These melts variably entrained Laurentian continental crust via high-temperature crustal melting due to basaltic underplating. The high-temperature back-arc felsic magmatism occurs at specific time periods coinciding with VMS deposits and supports previous genetic models for VMS mineralization that suggest elevated heat flow and hydrothermal circulation were due to regional-scale rift-related magmatism rather than from local subvolcanic intrusions. The short timescales and transient nature of tectonomagmatic events in the Finlayson Lake district suggest that rapid and complex subduction initiation of oceanic and continental crust fragments facilitated coeval compression, extension, and magmatism in the arc and back-arc regions. We thus reevaluate the presently accepted tectonostratigraphic framework of the Finlayson Lake district and suggest revised interpretations that shed light on VMS depositional environments and a possible broader association with the ca. 358 Ma Antler Orogeny. Results of this study have implications for incipient tectonics, magmatism, and mineralization along the western Laurentian continental margin and other orogenic belts globally.

1. Introduction

The Yukon-Tanana terrane represents the largest arc–back-arc terrane in the northern Cordillera and is a critical component for deciphering the early tectonomagmatic and metallogenic evolution of the peri-Laurentian realm [1, 2]. Rocks that comprise Yukon-Tanana terrane have geochemical, isotopic, and metallogenic links to the Laurentian continent (e.g., [3–6]) yet display magmatic, metamorphic, structural, and sedimentary characteristics that differentiated it from the neighboring platformal strata, thus defining an allochthon-parautochthon relationship [1, 7]. The Finlayson

Lake district is the most stratigraphically intact segment of Yukon-Tanana terrane rocks in the northern Cordillera and has been the locus of research since the mid-1980s [4, 8]. There was increased interest in the area due to the discovery of numerous volcanogenic massive sulfide (VMS) occurrences in the mid-1990s [9–11], which has resulted in the discovery of >40 Mt of polymetallic ore, including the ~18.1 Mt Kudz Ze Kayah, ~1.5 Mt GP4F, ~10 Mt Kona, and 6.2 Mt Wolverine VMS deposits [12–14]. Coincident mapping, geochemical, tracer isotope, and U-Pb geochronological work defined the chronology and chemostratigraphy of the Finlayson Lake district and illustrated that it formed as an evolving arc–back-arc system between ca. 366 Ma and 345 Ma [15–17].

The geochronological work that underpinned much of the previous work was based on traditional, multigrain zircon fractions and air abrasion methods [18] prior to significant advancement in the field of U-Pb geochronology with the invention of chemical abrasion pretreatment techniques [19]; thus, issues remain with regard to the accuracy and resolution of various plutonic and volcanic events and the timing of VMS mineralization in the Finlayson Lake district (e.g., [20]). Advances in high-precision U-Pb geochronology have revolutionized our understanding of ore systems and have allowed refinement of the timing of volcanic and plutonic activity related to mineralization on relatively short time scales from 10 s to 100 s of thousands of years [21–25]. Refinement of the chemical abrasion pretreatment technique [19] and application of the EARTHTIME standard [26] to U-Pb zircon geochronology have increased precision and relative uncertainties to as low as ~0.1% for single crystals and ~0.02% for weighted means, compared to laser ablation methods that achieve closer to ~1% [27]. In VMS districts, this precision provides the ability to define mineralized horizons on a regional scale and assess the timing of past volcanic eruptions and plutonic activity and their relationships to VMS mineralization [28, 29]. In the Finlayson Lake district, these high-precision geochronology methods have defined the ages of the Kudz Ze Kayah, GP4F, and Wolverine VMS deposits [30]; however, the age relationship to local plutons with respect to the proposed heat sources to the VMS systems remains unclear.

Magmatism is critical in the formation of VMS deposits, with magmatic heat interpreted to be the thermal driver of VMS-related hydrothermal circulation in the upper crust [31–34]. While it remains uncertain if plutons and subvolcanic intrusions spatially associated with VMS camps provide enough heat to form large deposits [35, 36], especially in light of recent models of incremental pluton assembly in arc settings [37–40], it is clear that high-temperature felsic volcanism is commonly associated with VMS mineralization in continental-dominated terranes [17, 41–44]. This high-temperature magmatism is often expressed as high concentrations of high field strength elements (HFSE; e.g., Nb, Th, Y, and Zr) and rare earth elements (REE; [17, 41, 43, 45]) and has been suggested that this is due to basaltic underplating of continental crust that provides higher than normal geothermal gradients, induces greater dissolution of HFSE-REE minerals in the crust during melting, and by association has the potential for the genesis of large VMS deposits [17, 36, 41, 43]. To test this underplating-crustal melting hypothesis, petrological (i.e., MLA-SEM) and radiogenic tracer isotope geochemical data is critical for validating and quantifying the relative abundance of crust versus mantle components involved in VMS-related felsic magma genesis; however, this requires both detailed lithostratigraphic and chronostratigraphic controls and VMS-bearing and VMS-barren stratigraphy with similar continental basement, to properly assess magmatic controls on VMS genesis (e.g., [42, 46]).

In this contribution, we report new high-precision CA-ID-TIMS and LA-ICP-MS U-Pb zircon dates, whole-rock lithogeochemistry, MLA-SEM modal abundances, and Hf-Nd isotopes for the earliest arc–back-arc environments that formed immediately adjacent to the western Laurentian continental margin in the Late Devonian to Early Mississippian. Specifically, we report new results for back-arc rocks in the Big Campbell thrust sheet and arc rocks in the Cleaver Lake thrust sheets in the Finlayson Lake district of the Yukon-Tanana terrane. We present a revised interpretation of Yukon-Tanana terrane evolution that incorporates early and recent interpretations of the ultramafic rocks and their volcanic cover sequences in the district (e.g., [4, 8, 47–50]). In this new context, our results constrain the timing and petrogenesis of upper-crustal plutonism and volcanism in the back-arc rift and provide constraints on the timing, duration, and host rock composition of VMS mineralization at or below the seafloor. In the arc regions, these new data increase temporal resolution for the earliest-known arc magmatism in the district and further constrain the longevity of the arc during a period of active back-arc extension. These data significantly contribute to our understanding of the nature and timescales of magma-rich arc rifting and associated VMS mineralization along an established and attenuated continental margin setting along the ancient Cordilleran margin of Yukon, Alaska, and British Columbia.

2. Previous Interpretation of the Finlayson Lake District

The Finlayson Lake VMS district of southeastern Yukon is a fault-bounded block of the Yukon-Tanana and Slide Mountain terranes that formed off the western continental margin of Laurentia in the mid- to late-Paleozoic (Figure 1; [8, 16, 49]). Rocks that comprise Yukon-Tanana terrane arc and back-arc assemblages are variably deformed and metamorphosed volcanic, plutonic, and sedimentary rocks that locally retain primary geological and geochemical characteristics; these rocks were deposited or intruded above a pre- to Late Devonian basement [1, 5, 7, 16]. The Jules Creek transform fault juxtaposes the Yukon-Tanana terrane adjacent to ophiolitic rocks of the Slide Mountain terrane [16], which were then together thrust above North American platformal strata along the Inconnu thrust in the Late Jurassic to Early Cretaceous [51]. The current geographical configuration of the Yukon-Tanana terrane in central Yukon was attained in the Eocene following ~430 km of displacement along the Tintina strike-slip dextral fault system, which resulted in

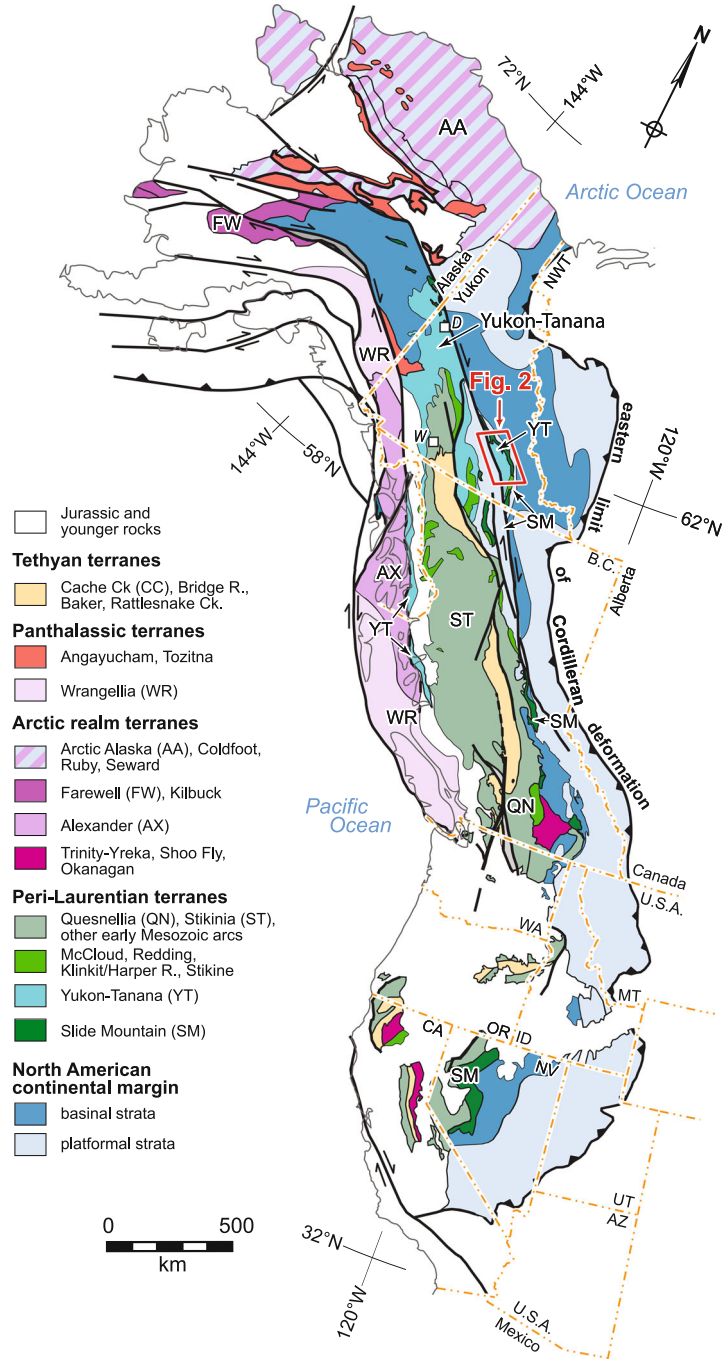

FIGURE 1: Paleozoic to early Mesozoic terranes of the North American Cordillera of Canada and the United States of America (modified after [150]). Note the terranes are superimposed on the present-day geographic configuration of North America. AZ = Arizona; CA = California; B.C. = British Columbia; ID = Idaho; MT = Montana; NV = Nevada; NWT = Northwest Territories; OR = Oregon; UT = Utah; WA = Washington; W = Whitehorse; D = Dawson City.

the offset sliver referred to as the Finlayson Lake district (Figures 1 and 2; [52]).

In the current interpretation of the structural geometry of the Yukon-Tanana terrane [16], Yukon-Tanana terrane rocks within the Finlayson Lake district are hosted in three distinct structural panels (from structurally deepest to shallowest): the Big Campbell, Money Creek, and Cleaver Lake thrust sheets (Figures 2 and 3; [16]). Upper Devonian and older metasedimentary rocks of the North River formation comprise the basement to both the Big Campbell and Money Creek thrust sheets, but the formation is not observed in the Cleaver Lake thrust sheet. The Big Campbell thrust sheet is bounded below by the post-Late Triassic Big Campbell thrust fault and above by the Money Creek thrust fault (Figures 2 and 4). Rocks in the Big Campbell thrust sheet comprise the basal Upper Devonian and older North River formation and the overlying Upper Devonian mafic and felsic metavolcanic and metasedimentary rocks of the Grass

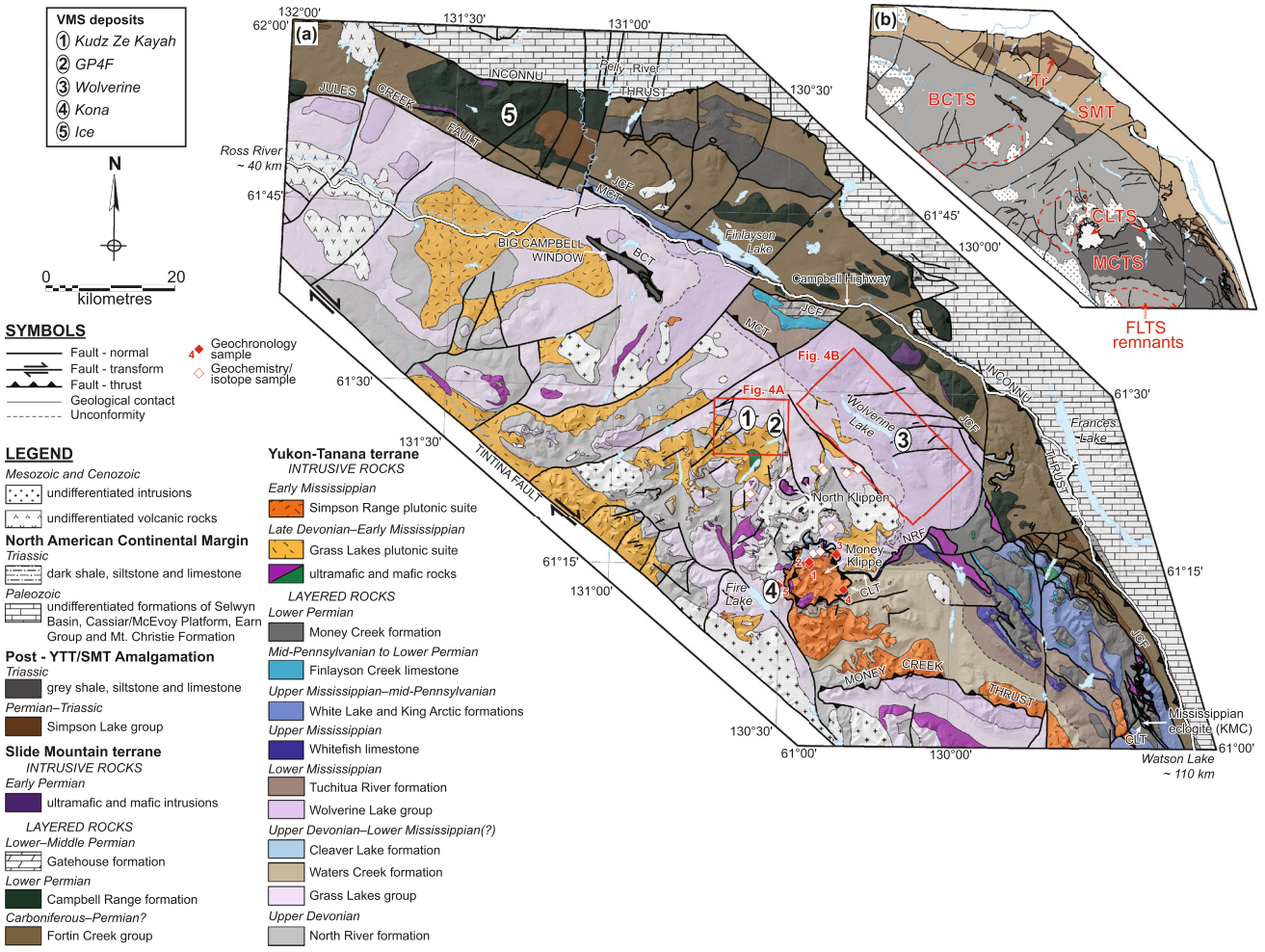

FIGURE 2: Regional geologic setting of the Finlayson Lake district, Yukon-Tanana terrane, showing the spatial relationship to the Slide Mountain terrane and North American continental margin (modified after [6, 54]). (a) Geological map of the district, where numbers indicate locations of prospective VMS deposits in the region. All geological units in legend are described in detail in Murphy et al. [16]. Diamond symbols represent locations of geochronology (red fill) and lithogeochemistry/isotope (white fill) samples outside of detailed maps in Figures 4(a) and 4(b); numbers correspond to sample numbers: 1 = 18MM-107; 2 = 18MM-108; 3 = P99-24; 4 = P99-82; 5 = 17MM-047. (b) Distribution of major thrust sheets in Yukon-Tanana terrane and their location relative to the Slide Mountain terrane (SMT) and Triassic (Tr) overlap assemblages. VMS = volcanogenic massive sulfide; BCT = Big Campbell thrust; MCT = Money Creek thrust; JCF = Jules Creek fault; CLT = Cleaver Lake thrust; NRF = North River fault; KMC = Klatsa Metamorphic Complex; BCTS = Big Campbell thrust sheet; MCTS = Money Creek thrust sheet; CLTS = Cleaver Lake thrust sheet; FLTS = Fire Lake thrust sheet; Tr = Triassic rocks.

Lakes group, which includes the Fire Lake, Kudz Ze Kayah, and Wind Lake formations (Figure 2). Late Devonian gabbroic to dioritic intrusions of the North Lakes intrusion and granitoid intrusions of the Grass Lakes plutonic suite cut the Grass Lakes group and then are all unconformably overlain by Lower Mississippian metaclastic and mafic to felsic metavolcanic rocks of the Wolverine Lake group (Figures 3 and 4). Metasedimentary rocks of the Money Creek formation and metabasalt of the Campbell Range formation, both originally thought to be Lower Permian, are interpreted to unconformably overlie the Wolverine Lake group; we revisit and substantially revise this interpretation below. The Grass Lakes and Wolverine Lake groups contain VMS mineralization felsic volcano-sedimentary stratigraphy that is interpreted to have formed in an evolving continental arc to back-arc basin tectonic setting that represents the earliest stages of mid-Paleozoic rifting on the western peri-Laurentian margin [7, 16, 30, 47, 48, 53].

In the hanging wall of the Money Creek thrust fault, rocks comprising the Money Creek thrust sheet include the Upper Devonian North River formation that is overlain by Upper Devonian to Lower Mississippian felsic to intermediate metavolcanic and metasedimentary rocks (Waters Creek and Tuchitua River formations). These rock units are intruded by granitic rocks of the Early Mississippian Simpson Range plutonic suite, then capped by Mississippian to Lower Permian limestone, mafic metavolcanic, and metaclastic rocks (Figures 2 and 3; [3, 4, 16]). The rocks in the Money Creek thrust sheet are interpreted to have formed in a continental arc (±local back-arc basin) tectonic setting to the southwest of the Big Campbell thrust sheet and are presently not associated with any significant VMS

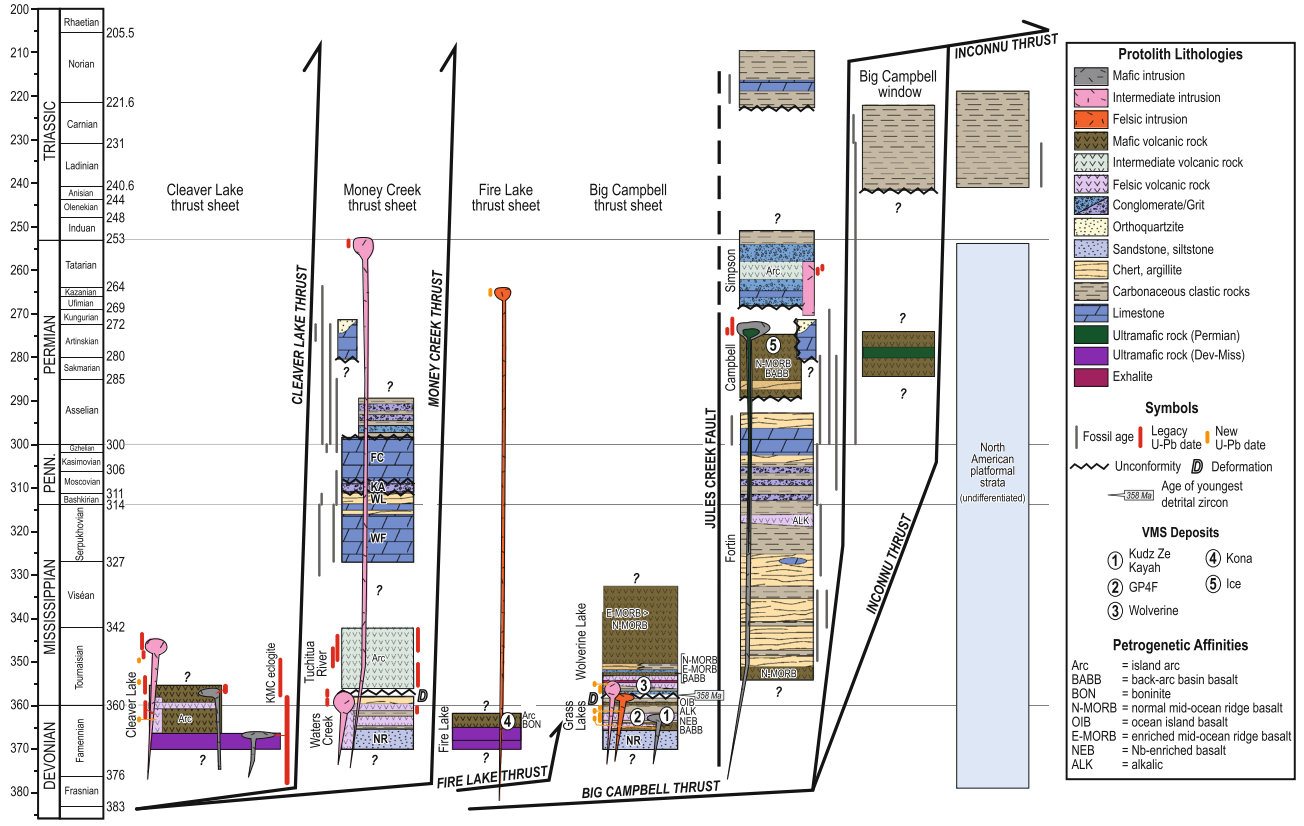

FIGURE 3: Composite chronostratigraphic columns for the Finlayson Lake district with locations of VMS prospects, U-Pb zircon and fossil ages, and petrogenetic affinities (modified after [16]). New U-Pb zircon dates obtained in this study are shown. Late Devonian to Early Mississippian stratigraphy in the Big Campbell thrust sheet has been adjusted to correspond to new age constraints. KMC = Klatsa Metamorphic Complex; NR = North River formation; Penn = Pennsylvanian.

mineralization [3, 7, 16]; however, several mineral occurrences are present [54]. Rocks from the Money Creek thrust sheet were not investigated in this study and will not be further discussed.

The Cleaver Lake thrust sheet structurally overlies the Money Creek thrust sheet and contains relatively undeformed and unmetamorphosed Late Devonian mafic and felsic volcanic rocks (Cleaver Lake formation) that overlie mafic and ultramafic rocks; these rock units are subsequently intruded by Early Mississippian granitoids of the Simpson Range plutonic suite [16, 49, 55]. The Cleaver Lake thrust sheet was thrust above the Money Creek thrust sheet along the Cleaver Lake thrust fault after the Early Permian [16]. Mafic-ultramafic rocks were initially interpreted to have been Permian intrusions that were correlative to the Slide Mountain terrane, thereby constraining the age of thrusting to Permian [16]; however, in this contribution, we revise this interpretation as discussed below. The rocks in the Cleaver Lake thrust sheet are interpreted to have been generated in an intraoceanic arc and subduction complex to the southwest of the Money Creek and Big Campbell thrust sheets and are also not associated with any known VMS mineralization [3, 6, 7, 16, 45].

Slide Mountain terrane rocks are juxtaposed against Yukon-Tanana terrane rocks along the Jules Creek fault (Figure 2; [16]). North and east of the Jules Creek fault, these rocks comprise Early Mississippian to Lower Permian metasedimentary and metavolcanic rocks of the Fortin Creek Group, which are unconformably overlain by Lower Permian mafic metavolcanic rocks and metasedimentary rocks of the Campbell Range Formation and Lower to Middle Permian sedimentary rocks of the Gatehouse formation (Figure 2). The Slide Mountain terrane contains the Lower Permian mafic-type Ice VMS deposit and has been interpreted to form in a back-arc basin to mid-ocean ridge tectonic setting [56–58].

2.1. Previous Geologic Interpretation of the Big Campbell Thrust Sheet

2.1.1. Grass Lakes Group. The Fire Lake formation has traditionally been interpreted to be the stratigraphically lowest volcanic unit overlying the metaclastic rocks of the North River formation [16, 51]. The original definition of the formation comprised mafic volcanic-volcaniclastic rocks with geochemical affinities equivalent to enriched midocean ridge basalt (E-MORB), back-arc basin basalt (BABB), alkalic ocean island basalt (OIB), and low-Ti island arc tholeiite (IAT) to boninite affinities [7, 47, 48]; these mafic volcanic rocks overlie mafic-ultramafic bodies that were originally inferred to be comagmatic intrusions, an interpretation that is revisited herein. Variable Nd isotopes ($\varepsilon Nd_{350\ Ma}$ = –0.3 to +8.5) and trace element signatures suggest they represent

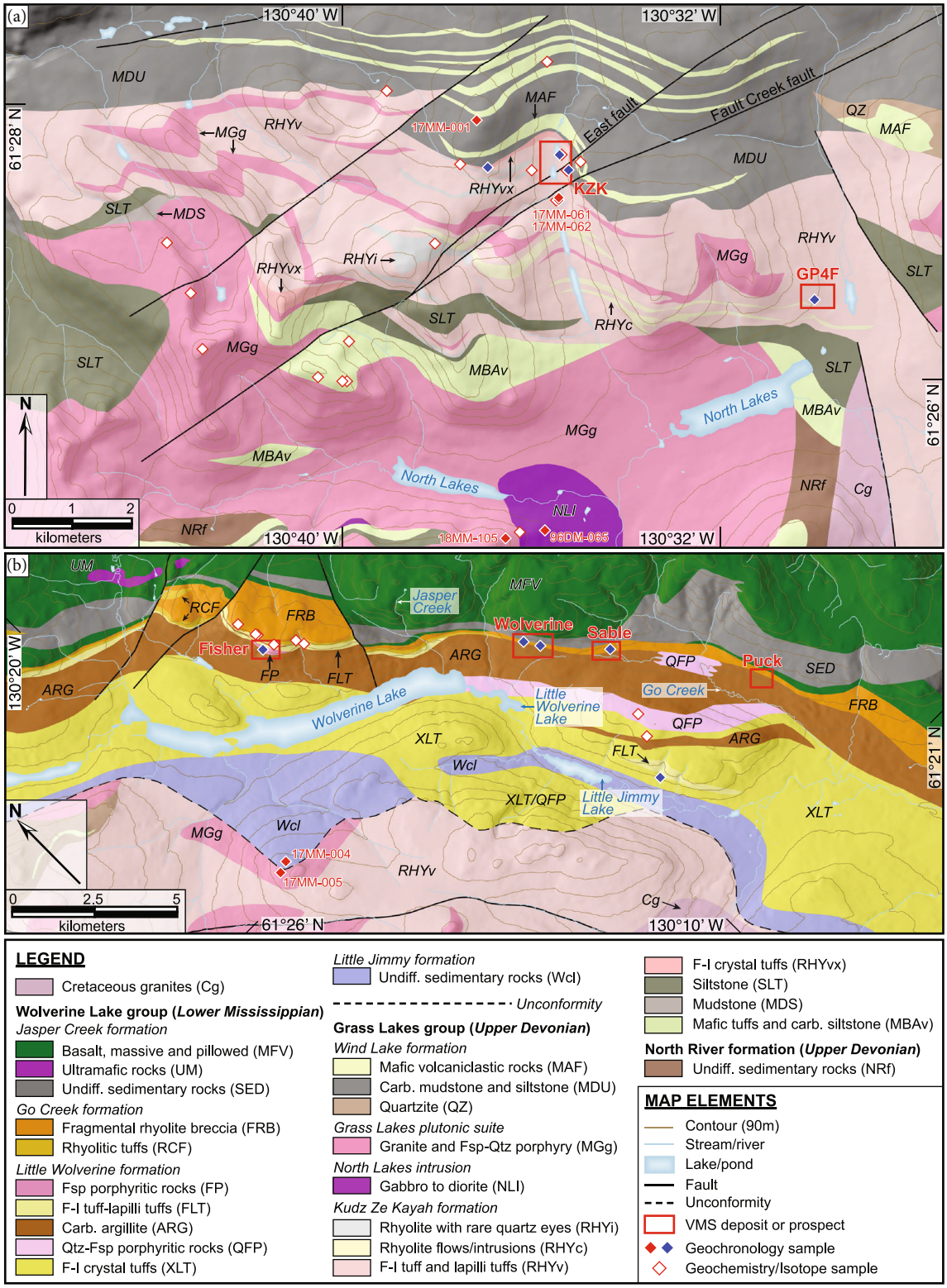

FIGURE 4: Geologic maps of (a) the Grass Lakes group in the vicinity of the Kudz Ze Kayah and GP4F deposits and (b) the Wolverine Lake group, in the south-central Finlayson Lake district, Yukon-Tanana terrane (modified after Baker et al. [60], Manor et al. [30, 63], and [54]). Diamonds represent sample locations for U-Pb (red fill = this study; blue fill = [30]) and lithogeochemistry/isotopes (white fill) as in Figure 2. Fsp = feldspar; F = felsic; I = intermediate; carb = carbonaceous; Qtz = quartz.

varying mixtures of back-arc mantle and arc mantle wedge with or without slab and/or continental crustal contributions that were generated during the onset of back-arc–related rifting along the Laurentian margin [47, 48]. The ~10 Mt Kona Cu-Co-Au VMS deposit is hosted by mafic volcaniclastic rocks (primarily boninitic) and fine-grained turbiditic metasedimentary rocks that are interpreted to have formed in a subaqueous setting [20, 59]. The age of this unit was originally thought to have been pinned by two Late Devonian $^{207}Pb/^{206}Pb$ dates (366.3 ± 10.2 Ma and 365.0 ± 1.3 Ma; [16]) for the North Lakes intrusion, which includes metadiorite-gabbroic rocks originally inferred to be comagmatic with Fire Lake volcanic rocks; we revisit and revise this interpretation below.

The Kudz Ze Kayah formation, originally thought to stratigraphically overlie the Fire Lake formation (see below), contains ~400-1300 m of felsic volcaniclastic rocks and subordinate flows, felsic and mafic subvolcanic intrusive rocks, and mudstones deposited in a rapidly forming, subaqueous back-arc basin [30]. Felsic lithofacies have evolved Nd isotopic signatures ($\varepsilon Nd_{350\ Ma}$ = –8 to –9) but have HFSE and REE enrichment characteristic of A-type, back-arc magmatic rocks; they are interpreted to have formed from melting of Proterozoic to Archean continental crust [6, 45]. The felsic-siliciclastic ~1.5 Mt GP4F and bimodal-felsic ~18.1 Mt Kudz Ze Kayah Zn-Pb-Cu-Ag-Au deposits are hosted in felsic volcaniclastic rocks approximately 4 km laterally and ~500-600 m stratigraphically apart (Figure 4; [13, 30, 60]). The age of felsic volcanism in the Kudz Ze Kayah formation has recently been tightly constrained to ca. 363.3 to 362.4 Ma with four CA-ID-TIMS dates [30]. These new dates define the age of VMS mineralization in the GP4F deposit to 363.254 ± 0.098 Ma, whereas the Kudz Ze Kayah deposit is constrained by two overlapping dates in the Krakatoa and ABM zones (362.847 ± 0.099 Ma and 362.82 ± 0.12 Ma, respectively).

The Wind Lake formation overlies the Kudz Ze Kayah formation and consists of carbonaceous argillite; lesser mafic volcaniclastic, volcanic, and intrusive rocks; and minor felsic volcaniclastic rocks and quartzite. The total thickness of the Wind Lake formation is estimated at ~4500 m; mafic volcanic rocks are only present in the lowest 500 m and are otherwise dominated by carbonaceous argillite (Figure 4; [30, 60]). The mafic rocks have alkalic, OIB-type geochemical signatures with near-chondritic Nd isotope signatures ($\varepsilon Nd_{350\ Ma}$ = –2.8 to +1.1; [61]), suggesting the magmas underwent varying degrees of crustal contamination following extraction from lithospheric or asthenospheric sources. The Wind Lake formation thus represents the cessation of felsic-dominant volcanism in the Grass Lakes group (Figure 4; [61]).

The Grass Lakes plutonic suite comprises a batholith-like intrusive complex composed of variably metamorphosed and deformed, fine to medium-grained peraluminous granodiorite to monzogranite (Figures 2, and 4; [16]). Minor intrusions (dikes and sills) of feldspar ± quartz porphyritic rocks cut the entire Grass Lakes group stratigraphy (Figure 4; [60]). The geochemical characteristics of this rock suite are similar to felsic, A-type, back-arc–related volcanic rocks of the Kudz Ze Kayah formation, with similarly evolved Nd isotope compositions ($\varepsilon Nd_{350\ Ma}$ = –9.5; [6]) and inherited Proterozoic to Archean zircon grains [4, 6, 16, 45]. The granitic rocks of the Grass Lakes plutonic suite range include dates of 362.2 ± 3.3, 359.9 ± 0.9, and 357.3 ± 2.8 Ma [16]. Geochemical and geochronological constraints have led previous workers to suggest a comagmatic relationship between silicic plutonism of the Grass Lakes plutonic suite and the formation of felsic volcanic rocks and associated VMS mineralization in the Kudz Ze Kayah formation [6, 45].

2.1.2. Wolverine Lake Group. Rocks of the Wolverine Lake group unconformably overly the Grass Lakes group following a period of deformation during the Upper Devonian to Lower Mississippian, the kinematic nature of which is poorly known (ca. 357.5 Ma; [16, 62]). Rocks that comprise the Wolverine Lake group include undifferentiated basal, footwall, and hanging wall units [16, 30, 63, 64]. The basal unit, constrained by ca. 357.5 Ma maximum depositional age [16], contains quartzofeldspathic-pebble conglomerate, grit, sandstone, and carbonaceous phyllite. Footwall rocks comprise ~1200-1700 m carbonaceous argillite, felsic volcaniclastic rocks, and high-level quartz-feldspar porphyritic (QFP) and feldspar porphyritic (FP) intrusive rocks (Figure 4). Felsic crystal tuffs in the lower footwall have been previously dated at 356.371 ± 0.091 Ma [30] and 356.2 ± 0.9 Ma [4, 16], and two periods of magmatism are associated with VMS mineralization at (1) ca. 356.1 Ma: pre-VMS QFP intrusions (Sable zone) and (2) ca. 355.2 to 355.0 Ma: syn- to post-VMS FP intrusions and crystal tuffs (Wolverine/Lynx and Fisher zones; [30]). An additional QFP from the Puck zone gave an older date of 356.9 ± 0.5 Ma [17]. Geochemical and isotopic characteristics of the footwall felsic rocks ($\varepsilon Nd_{350\ Ma}$ = –8.2 to –7.8; [6]) are similar to A-type, back-arc affinities of the Kudz Ze Kayah formation and Grass Lakes plutonic suite, with the exception of the porphyritic intrusive rocks where FP rocks are HFSE-REE-rich compared to QFP and volcaniclastic rocks [17, 45]. Hanging wall rocks primarily contain carbonate and silica-pyrite exhalite, iron formation, and carbonaceous argillites that are overlain by fine-grained resedimented rhyolitic tuff/siltstone and rhyolitic breccia and massive basalt flows and minor mafic volcaniclastic rocks with juvenile ($\varepsilon Nd_{350\ Ma}$ = +6.9) N-MORB, enriched- (E-) MORB, and BABB geochemical affinities [6, 16, 30, 53, 64, 65]. The basalts in the Wolverine Lake group hanging wall were initially mapped as being part of the Campbell Range formation of the Slide Mountain terrane, an interpretation which is reconsidered in a subsequent section.

2.2. Previous Geologic Interpretation of the Cleaver Lake Thrust Sheet. In the core region of the Finlayson Lake district, the Cleaver Lake thrust sheet is a klippe that contains two primary, relatively undeformed geological units: (1) the Upper Devonian Cleaver Lake formation and (2) Early Mississippian Simpson Range plutonic suite [16, 55]. The Cleaver Lake formation consists of both calc-alkaline and island arc tholeiitic basalt and rhyolite that are intruded by quartz-rich porphyritic rocks; the latter intrusions show local evidence for magma mingling with basaltic dikes and are interpreted to be the volcanic feeders to the extrusive

rocks [55]. Geochemically, these rocks have arc-like signatures, and Nd isotopic signatures ($\varepsilon Nd_{350\,Ma} = -4.8$ to $+0.1$; [6]) indicate this arc was built above a basement composed of both oceanic and continental rocks [3, 6, 45, 48]. Rocks in the Cleaver Lake formation have crystallization ages of 360.5 ± 1.9 Ma and 356.1 ± 0.9 Ma for felsic and mafic intrusive rocks, respectively, and indicate that the primary volcanic succession is likely coeval in age to the Grass Lakes group [4, 7, 16]. The Simpson Range plutonic suite contains hornblende- and biotite-bearing monzodiorite, granodiorite, and quartz diorite, all with evolved geochemical signatures of arc affinity ($\varepsilon Nd_{350\,Ma} = -12.9$ to -7.4; [3, 6]); these granitoids exhibit cross-cutting relationships with rocks of the Cleaver Lake formation [3, 55]. U-Pb zircon dates for three granitoids in the Simpson Range plutonic suite include 354.9 ± 1.8, 348.4 ± 0.8, and 345.9 ± 1.2 Ma [3, 4, 16] and define a clearly younger age than the Cleaver Lake formation.

In the southeastern Finlayson Lake district, the Cleaver Lake thrust sheet also includes the Klatsa metamorphic complex. The Klatsa metamorphic complex comprises bodies of serpentinized mafic-ultramafic rocks structurally imbricated with eclogite-facies sedimentary rocks and basalt and represents an Early Mississippian subduction complex [15, 66].

3. New Stratigraphic and Structural Interpretations

In this study, we revise the stratigraphic and structural framework of the Finlayson Lake district presented above in light of our new results and the adoption of the reinterpretation of mafic and ultramafic bodies in the region presented by van Staal et al. [50], which follows early work by Tempelman-Kluit [49], Mortensen and Jilson [8], and Mortensen [4]. Geological observations are presented here as a basis for reporting geochronological, geochemical, and isotopic data below and described further in the discussion.

3.1. Fire Lake and Kudz Ze Kayah Formations. Traditionally, the Fire Lake formation has been considered to be in stratigraphic succession between the North River and Kudz Ze Kayah formations, which contained mafic-ultramafic bodies that were interpreted as coeval intrusions. However, we have adopted the reinterpretation by van Staal et al. [50] that follows others [4, 8, 49], where the ultramafic-mafic slabs represent allochthonous slices of mantle and lower crust as opposed to intrusions [11, 16]. This reinterpretation requires that the base of the mafic-ultramafic bodies be a thrust fault, and the relationship of the Fire Lake formation to the North River and Kudz Ze Kayah formations therefore requires reevaluation. The Fire Lake formation and underlying ultramafic-mafic rocks define a new thrust sheet that overlies the North River formation and also possibly the Kudz Ze Kayah formation if the North Klippen is correlated with the Fire Lake thrust sheet (Figure 2). This reinterpretation indicates that (1) the Fire Lake formation no longer stratigraphically overlies the North River formation but instead is structurally juxtaposed against it (Figure 5), and (2) the mafic rocks of non-arc affinity (BABB, E-MORB, and OIB) between the Kudz Ze Kayah and North River formations, initially correlated with the Fire Lake formation [48, 67–69], are no longer in the same thrust sheet and thus not directly correlatable to the Fire Lake formation. The reassignment of these rocks to the Kudz Ze Kayah formation makes the formation a bimodal volcanic succession that directly overlies the North River formation, which includes BABB and E-MORB-affinity mafic rocks with juvenile isotopic signatures ($\varepsilon Nd_{350\,Ma} > +8$; [48]). The placement of these mafic units into the Kudz Ze Kayah formation requires that only those volcanic and volcaniclastic rocks that overlie the occurrences of mantle ultramafic rocks or are demonstrably part of the Fire Lake thrust sheet are included in the Fire Lake formation (e.g., boninite and IAT affinity; Figure 2).

3.2. Wolverine Lake Group. Rocks in the Lower Mississippian Wolverine Lake group have previously not been differentiated into formations but described as basal, footwall, and hanging wall assemblages with respect to VMS mineralization [16, 30, 63, 64, 70]. We herein propose definitions for four informal "formations," named after lakes and creeks present within the Wolverine Lake group based on lithological, geochemical, and geochronological characteristics presented in this paper and in previous work (e.g., [16, 17, 45]): (1) Little Jimmy formation, (2) Little Wolverine formation, (3) Go Creek formation, and (4) Jasper Creek formation (Figure 4(b)).

The Little Jimmy formation is the basal unit of the Wolverine Lake group and consists of mixed quartzofeldspathic-pebble conglomerate, grit, sandstone, and carbonaceous phyllite (Figure 4(b); [16]); previously, the rocks of this unit have been mapped as unit "U-5l" [62]. The Little Jimmy formation (ca. 357.6 to 356.4 Ma) is named after the Little Jimmy Lake, approximately 3.5 km directly south of the Wolverine mine site, and the type locality is immediately east of the regional unconformity between the Grass Lakes and Wolverine Lake groups (NAD83 9U 429446 mE, 6812106 mN; Figure 4(b)).

The Little Wolverine formation (ca. 356.4 to 355.0 Ma) stratigraphically overlies (and is locally intercalated with) the Little Jimmy formation and consists of felsic volcanic rocks, intercalated argillite, and high-level porphyritic intrusive rocks that host the ~6.2 Mt Wolverine Zn-Pb-Cu-Ag-Au deposit and other regional VMS prospects [16, 17, 71]. The Little Wolverine formation is named after Little Wolverine Lake that is immediately southeast of Wolverine Lake (Figure 4(b)). The rocks in this unit comprise what has previously been termed "footwall" or "U-5f/qfp," "U-5cp," and "U-6FW" [45, 62] and "Unit 1" within the Wolverine/Lynx zones [71].

The Go Creek formation stratigraphically overlies the Little Wolverine formation and is composed of rocks in the immediate hanging wall of the VMS deposits, including exhalites, iron formations, resedimented volcanic rocks, and carbonaceous argillite (Figure 4(b)). This unit is named after Go Creek, a watercourse that flows downhill through the Go Creek formation from the topographic highs in the Campbell Range basalts, joining with the Money Creek to the southeast (Figure 4(b)). Rocks of this unit have previously been classified as the "hanging wall" or "U-6HW" [45, 62] and include both "Unit 2" and "Unit 3" within the Wolverine/Lynx zones [71].

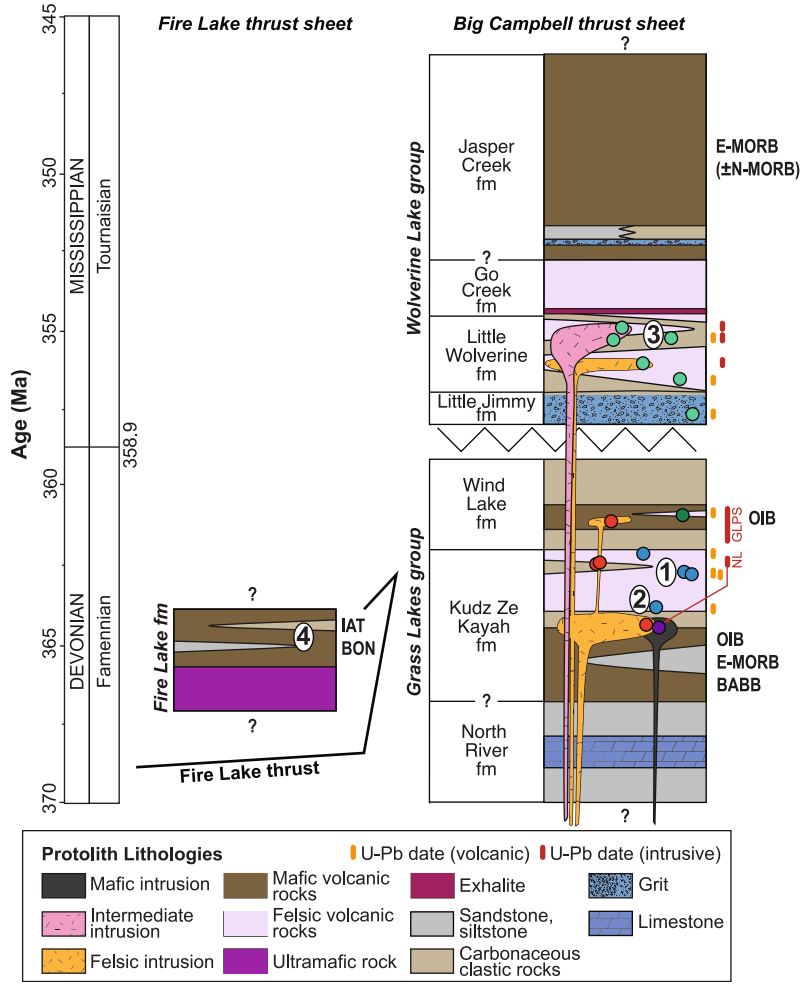

FIGURE 5: Composite chronostratigraphic column for the Big Campbell and Fire Lake thrust sheets, zoomed in to the Late Devonian to Early Mississippian section (modified after [30, 64]). Colored units indicate protolith rock types. Numbers correspond to VMS deposits in the district as in Figure 2. Vertical orange and red lines to the right of the figure indicate new U-Pb geochronology constraints from this study and Manor et al. [30]. The zig-zag line represents an angular unconformity between the Grass Lakes and Wolverine Lake groups [51]. GLPS = Grass Lakes plutonic suite; KZK = Kudz Ze Kayah; fm = formation; NL = North Lakes intrusion; BABB = back-arc basin basalt; BON = boninite; E-MORB = enriched midocean ridge basalt; N-MORB = normal midocean ridge basalt; IAT = island arc tholeiite; OIB = ocean island basalt.

The formation includes a diverse group of rocks that are distinct in lithology and geochemistry from the underlying Little Wolverine formation (e.g., [45]).

Lastly, the Jasper Creek formation lies stratigraphically above the Go Creek formation and caps the Wolverine Lake group (Figure 4; [16]). The Jasper Creek formation contains massive to pillowed basalts and minor greywacke and carbonaceous argillite. This formation is named after Jasper Creek, which originates at high levels in topography north-northeast of the southern end of Wolverine Lake (Figure 4(b)). Previous work has placed this unit into "U-6HW" [62] or "Unit 4" [71] and correlated it with the Lower Permian Campbell Range formation of Slide Mountain terrane. Although the age of the Jasper Creek formation has not been directly determined isotopically or paleontologically, recent mapping leads us to interpret that the Jasper Creek formation is in depositional continuity with the underlying Go Creek formation and does not correlate with the Campbell Range Formation north of the Jules Creek fault [16]; therefore, unconformities no longer exist between lithologic contacts (Figures 3, 4(b), and 5).

3.3. Significance of Mafic-Ultramafic Rocks and Age of Thrust Faults. Several bodies of mafic-ultramafic rocks have been mapped near rocks in the upper part of the Money Creek thrust sheet. These occurrences were originally interpreted as intrusions related to the Lower Permian Campbell Range Formation (i.e., Slide Mountain terrane) that subsequently pinned the timing of major thrust faults in the Finlayson Lake district [16]. Devine et al. [66], however, reinterpreted several of these mafic-ultramafic bodies as being klippen of the Cleaver Lake thrust sheet. We have adopted this interpretation and have reclassified mafic rocks originally mapped as intrusions of Early Permian Slide Mountain terrane to now being related to Late Devonian to Mississippian Yukon-Tanana terrane stratigraphy (see above regarding Jasper Creek formation; Figure 2). These discrete mafic-ultramafic bodies are interpreted to represent klippen

of Devonian to Mississippian rocks that occur along an east-southeasterly trend between the Money Klippe and Klatsa metamorphic complex. As these rocks are no longer interpreted as intrusions, they provide no age constraints for the thrust faults that bound the Big Campbell, Money Creek, and Cleaver Lake thrust sheets; thrusting must have occurred post-deposition of the Money Creek formation but prior to intrusion of Early Cretaceous granitoids. Therefore, we propose that all three major thrust faults in the Finlayson Lake district can be reasonably interpreted as synthetic faults to the Jura-Cretaceous Inconnu thrust fault system that obducted Yukon-Tanana and Slide Mountain terranes onto the Laurentian continent (Figure 3).

4. Analytical Methods

Analytical procedures are outlined below and presented in detail in Supplementary Materials along with standard data and results from reproducibility monitoring (Tables S1, S4, and S5 and Figure S7). Sample preparation, mineral separation and extraction, annealing, and imaging for U-Pb zircon geochronology samples were carried out at Memorial University of Newfoundland (MUN; Figures S3–S5). Laser ablation- (LA-) ICP-MS and chemical abrasion- (CA-) ID-TIMS analyses were performed at the Isotope Geology Laboratory at Boise State University, Idaho (BSU). Laser ablation was performed on each grain using a New Wave Research UP-213 Nd:YAG UV laser (213 nm), where ablated material was analyzed on a ThermoElectron X-Series II quadrupole ICP-MS for U-Th-Pb isotopic ratios and trace element concentrations. Following LA-ICP-MS analysis, individual zircon grains were plucked from the epoxy mount and chemically abraded following the same procedure as in Manor et al. [30]. Isotopic determinations for CA-ID-TIMS analyses follow the methodology of Davydov et al. [72] and Schmitz and Davydov [73]. U-Pb ratios were measured using an IsotopX PhoeniX-62 thermal ionization mass spectrometer at BSU.

Sample preparation and measurement of major and trace element lithogeochemical data were performed at ALS Laboratories in North Vancouver, British Columbia, and Sudbury, Ontario; Geoscience Laboratories (Geo Labs) of the Ontario Geological Survey in Sudbury, Ontario, for transition metals, base metals, and semimetals; and Pacific Centre for Isotopic and Geochemical Research (PCIGR) at the University of British Columbia for trace elements on a subset of samples. At ALS, samples were fused with a lithium metaborate flux, digested in a HNO_3-HCl mixture, and analyzed by ICP-AES for major elements and ICP-MS for trace elements. At Geo Labs, samples were digested on hot plates using a four-acid mixture and analyzed on a Perkin-Elmer Elan 9000 ICP-MS following the methodology of Burnham [74]. At PCIGR, samples prefaced by 98DM-, P98-, P99-, and P00- [6, 17, 45, 61] were processed using high-pressure dissolution techniques [75] and analyzed on a Thermo Finnigan Element2 HR-ICP-MS.

Whole-rock Hf and Nd isotope ratios were measured at PCIGR using separate aliquots of sample powders used for trace element analyses. The Nd and Hf isotope ratios were measured by MC-ICP-MS following Weis et al. [76, 77] and normalized to the JNDi and JMC 475 standards for Nd and Hf isotopes, respectively. Analyses were normalized to JNDi with a $^{143}Nd/^{144}Nd = 0.512116$ [78] and JMC 475 with a $^{176}Hf/^{177}Hf = 0.282160$ [79]. All reference data presented as comparison fields have been renormalized to the accepted values of JNDi and JMC 475 as above. The present-day CHUR values used include $^{143}Nd/^{144}Nd = 0.512638$ [80] and $^{176}Hf/^{177}Hf = 0.282785$ [81], and parent-daughter ratios are $^{147}Sm/^{144}Nd = 0.1967$ [82] and $^{176}Lu/^{176}Hf = 0.0336$ [81]. Depleted mantle model ages (T_{DM}) for Hf were calculated on using $^{176}Hf/^{177}Hf = 0.283238$ and $^{176}Lu/^{177}Hf = 0.03976$ [83]; for Nd, the T_{DM} ages were calculated using $^{143}Nd/^{144}Nd = 0.513113$ and $^{147}Sm/^{144}Nd = 0.2114$ [84].

Mineral liberation analysis (MLA) of polished thin sections of U-Pb TIMS samples was performed using a FEI Quanta 650 scanning electron microscope (SEM; CREAIT facility, MUN) equipped with MLA software. Each thin section was mapped to establish the modal abundances and varieties of minerals present in each rock. Quantitative modal abundances and false color thin section maps can be found in Table S6 and Figure S2, respectively.

5. Chemical Abrasion ID-TIMS and LA-ICP-MS U-Pb Zircon Geochronology

The CA-ID-TIMS U-Th-Pb data for zircon in the Finlayson Lake district provide significantly greater resolution than U-Pb dates obtained by LA-ICP-MS methods (Tables 1 and 2). Results are presented as $^{206}Pb/^{238}U$ isotopic ratios for all the CA-ID-TIMS and LA-ICP-MS samples < 1 Ga; those grains with dates > 1 Ga are reported as $^{207}Pb/^{206}Pb$ dates. Presentation of the U-Pb dates follow the nomenclature of Schoene et al. [85] whereby the weighted mean U-Pb dates include uncertainties as $\pm X/Y/Z$ ($\pm 2\sigma$), where X is the internal error without all systematic errors, Y includes tracer calibration error, and Z includes uncertainty related to both tracer calibration and decay constant error. Unless otherwise noted, uncertainties below are reported as $\pm X$ as the dates originate from the same laboratory. High-precision CA-ID-TIMS dates are used in the text below to aid interpretations related to the primary magmatic crystallization history and tectonic evolution of the district; the LA-ICP-MS results for CA-ID-TIMS samples are provided in Supplementary Materials. Detailed U-Th-Pb CA-ID-TIMS and LA-ICP-MS geochronology results are reported in Table 1 and Table S2, respectively, and a summary table compares the results of each method in Table 2. The CA-ID-TIMS and LA-ICP-MS U-Pb results are displayed as Wetherill concordia diagrams in Figures 8 and 9 and Figures S7 and S8. The CA-ID-TIMS data for the Kudz Ze Kayah formation and Wolverine Lake group (except sample 17MM-004) were previously reported in Manor et al. [30].

5.1. Fire Lake Thrust Sheet

5.2. Fire Lake Formation. Zircon was separated from a felsic intrusion (17MM-047) that cuts mafic tuffs and lapilli tuffs

Table 1: Chemical abrasion-ID-TIMS U-Pb zircon isotopic data for rocks in the Finlayson Lake district.

Sample[†]	Compositional parameters[§]					Radiogenic isotope ratios[#]									Isotopic ages[††]					
	Th/U	$^{206}Pb^*$ ($\times10^{-13}$ mol)	mol%/$^{206}Pb^*$	Pb^*/Pb_c	Pb_c (pg)	$^{206}Pb/^{204}Pb$	$^{208}Pb/^{206}Pb$	$^{207}Pb/^{206}Pb$	% error	$^{207}Pb/^{235}U$	% error	$^{206}Pb/^{238}U$	% error	R	$^{207}Pb/^{206}Pb$	±	$^{207}Pb/^{235}U$	±	$^{206}Pb/^{238}U$	±
Wolverine Lake group																				
17MM-004—quartzofeldspathic grit (429446 E, 6812106 N)																				
z1	0.268	1.2845	99.79%	132	0.23	8429	0.084	0.05365	0.077	0.422204	0.138	0.057071	0.067	0.957	356.58	1.7	357.63	0.42	357.79	0.23
z2	0.267	1.6415	99.89%	250	0.15	15949	0.084	0.05368	0.070	0.422285	0.131	0.057050	0.065	0.964	357.84	1.6	357.68	0.39	357.66	0.23
z3	0.364	0.8741	99.74%	109	0.19	6817	0.115	0.05367	0.098	0.422019	0.152	0.057029	0.067	0.882	357.24	2.2	357.49	0.46	357.53	0.23
z4	0.220	1.8221	99.87%	221	0.19	14308	0.069	0.05368	0.083	0.422223	0.138	0.057045	0.067	0.904	357.71	1.9	357.64	0.42	357.63	0.23
z5	0.321	2.5956	99.89%	256	0.24	16139	0.101	0.05366	0.068	0.422037	0.129	0.057047	0.065	0.968	356.63	1.5	357.51	0.39	357.64	0.23
z6	0.179	0.1864	97.98%	13	0.32	892	0.056	0.05364	0.455	0.422028	0.507	0.057058	0.077	0.712	356.13	10.3	357.50	1.53	357.71	0.27
z7	0.404	1.8530	99.86%	217	0.21	13349	0.127	0.05385	0.073	0.429771	0.132	0.057886	0.065	0.951	364.67	1.6	363.01	0.40	362.75	0.23
z8	0.377	1.3381	99.81%	152	0.21	9460	0.119	0.05386	0.073	0.429931	0.134	0.057897	0.065	0.971	365.07	1.6	363.13	0.41	362.82	0.23
Grass Lake plutonic suite (GLPS)																				
17MM-005—granodiorite (429291 E, 6812095 N)																				
z1	0.481	1.2892	99.74%	113	0.28	6817	0.152	0.05376	0.092	0.426718	0.148	0.057563	0.069	0.887	361.20	2.1	360.84	0.45	360.79	0.24
z2	0.463	0.5234	99.03%	30	0.43	1854	0.146	0.05380	0.291	0.427331	0.335	0.057610	0.073	0.678	362.59	6.6	361.28	1.02	361.08	0.26
z3	0.344	0.6912	99.49%	56	0.29	3546	0.109	0.05379	0.125	0.427110	0.176	0.057590	0.067	0.837	362.21	2.8	361.12	0.53	360.95	0.24
z4	0.430	0.4570	99.26%	40	0.28	2441	0.136	0.05378	0.183	0.426861	0.229	0.057565	0.074	0.724	361.87	4.1	360.95	0.69	360.80	0.26
z5	0.377	0.7619	99.60%	72	0.26	4456	0.119	0.05375	0.112	0.426700	0.165	0.057579	0.069	0.854	360.50	2.5	360.83	0.50	360.88	0.24
z6	0.434	0.2852	99.18%	36	0.19	2213	0.137	0.05376	0.221	0.427137	0.266	0.057620	0.072	0.707	361.18	5.0	361.14	0.81	361.14	0.25
18MM-105—granodiorite (414536 E, 6809068 N)																				
z1	0.283	1.4458	99.40%	47	0.73	3003	0.089	0.05376	0.152	0.427794	0.204	0.057716	0.074	0.787	360.91	3.4	361.61	0.62	361.72	0.26
z2	1.527	0.3644	98.90%	34	0.34	1646	0.481	0.05377	0.267	0.427763	0.315	0.057697	0.075	0.708	361.48	6.0	361.59	0.96	361.60	0.26
z3	2.246	2.3804	99.85%	286	0.30	11781	0.708	0.05372	0.082	0.427600	0.139	0.057732	0.068	0.917	359.26	1.8	361.47	0.42	361.82	0.24
z4	1.108	2.2739	99.24%	46	1.44	2379	0.349	0.05370	0.189	0.427600	0.233	0.057750	0.073	0.705	358.53	4.3	361.47	0.71	361.93	0.26
z5	0.672	1.2546	99.59%	76	0.43	4384	0.212	0.05381	0.126	0.428351	0.185	0.057738	0.070	0.898	362.96	2.8	362.00	0.56	361.85	0.25
z6	1.267	0.8044	99.35%	55	0.44	2773	0.399	0.05372	0.201	0.427697	0.245	0.057747	0.072	0.703	359.18	4.5	361.54	0.75	361.91	0.25
z7	1.330	0.5038	99.03%	37	0.41	1860	0.419	0.05373	0.279	0.427561	0.333	0.057714	0.100	0.648	359.74	6.3	361.44	1.01	361.71	0.35
17MM-061—high-level quartz-feldspar porphyry in KZK fm. (415122 E, 6814798 N)																				
z1	1.057	1.1764	99.70%	114	0.30	5969	0.333	0.05378	0.092	0.428062	0.154	0.057723	0.073	0.925	362.04	2.1	361.80	0.47	361.76	0.26
z2	0.910	0.4278	98.73%	26	0.46	1417	0.287	0.05373	0.383	0.412206	0.429	0.055637	0.093	0.581	359.94	8.6	350.46	1.27	349.03	0.32
z3	0.766	0.4034	99.28%	45	0.24	2514	0.241	0.05382	0.247	0.430834	0.296	0.058060	0.095	0.638	363.47	5.6	363.77	0.91	363.82	0.34
z4	1.296	0.2683	98.72%	28	0.29	1409	0.408	0.05378	0.447	0.427828	0.496	0.057697	0.112	0.528	361.81	10.1	361.63	1.51	361.61	0.39
z5	0.450	0.9936	99.50%	60	0.41	3642	0.142	0.05374	0.205	0.427747	0.243	0.057733	0.080	0.607	359.97	4.6	361.58	0.74	361.83	0.28
z6	0.577	2.6771	99.87%	245	0.28	14412	0.182	0.05375	0.077	0.427480	0.137	0.057685	0.071	0.920	360.44	1.7	361.39	0.42	361.53	0.25
z7	1.202	0.2108	98.80%	29	0.21	1501	0.379	0.05380	0.482	0.428263	0.533	0.057738	0.106	0.562	362.53	10.9	361.94	1.62	361.85	0.37

Table 1: Continued.

Sample†	Th/U	Compositional parameters§ $^{206}Pb^*$ ($\times10^{-13}$ mol)	mol%/$^{206}Pb^*$	Pb^*/Pb_c	Pb_c (pg)	Radiogenic isotope ratios# $^{206}Pb/^{204}Pb$	$^{208}Pb/^{206}Pb$	$^{207}Pb/^{206}Pb$	% error	$^{207}Pb/^{235}U$	% error	$^{206}Pb/^{238}U$	% error	R	Isotopic ages†† $^{207}Pb/^{206}Pb$	±	$^{207}Pb/^{235}U$	±	$^{206}Pb/^{238}U$	±
17MM-062—high-level quartz-feldspar porphyry in KZK fm. (415122 E, 6814798 N)																				
z1	0.753	0.2895	99.16%	38	0.20	2154	0.237	0.05376	0.216	0.427997	0.261	0.057746	0.073	0.703	360.81	4.9	361.75	0.80	361.90	0.26
z2	0.774	0.6856	99.60%	79	0.23	4460	0.244	0.05369	0.117	0.427454	0.168	0.057739	0.070	0.836	358.21	2.6	361.37	0.51	361.86	0.25
z3	0.548	2.8649	99.86%	218	0.33	12939	0.173	0.05373	0.074	0.427577	0.133	0.057711	0.067	0.944	359.94	1.7	361.45	0.40	361.69	0.23
z4	0.623	0.4074	99.48%	59	0.18	3468	0.196	0.05373	0.144	0.427868	0.195	0.057759	0.068	0.823	359.62	3.2	361.66	0.59	361.98	0.24
z5	0.650	0.9676	99.70%	105	0.24	6084	0.205	0.05371	0.105	0.427623	0.157	0.057747	0.069	0.856	358.78	2.4	361.49	0.48	361.91	0.24
z6	0.761	0.8291	99.62%	84	0.26	4753	0.240	0.05376	0.115	0.428148	0.167	0.057758	0.069	0.839	361.13	2.6	361.86	0.51	361.97	0.24
z7	0.698	1.4842	99.79%	149	0.26	8522	0.220	0.05379	0.080	0.428309	0.138	0.057750	0.067	0.934	362.28	1.8	361.98	0.42	361.93	0.23
z8	0.712	0.6455	99.33%	47	0.36	2677	0.224	0.05380	0.148	0.428413	0.198	0.057757	0.068	0.813	362.54	3.3	362.05	0.60	361.97	0.24
Wind Lake formation																				
17MM-001—felsic crystal tuff (413749 E, 6815933 N)																				
z1	0.491	0.1938	98.06%	15	0.32	932	0.155	0.05375	0.503	0.426705	0.554	0.057574	0.102	0.566	360.71	11.4	360.83	1.68	360.85	0.36
z2	0.410	0.3715	98.64%	21	0.43	1325	0.129	0.05375	0.285	0.426823	0.332	0.057593	0.080	0.660	360.60	6.4	360.92	1.01	360.97	0.28
z3	0.564	0.3819	99.17%	36	0.27	2166	0.178	0.05374	0.293	0.426684	0.337	0.057587	0.082	0.620	360.07	6.6	360.82	1.02	360.94	0.29
z4	0.533	0.2019	98.23%	17	0.30	1018	0.168	0.05374	0.402	0.426561	0.450	0.057573	0.087	0.620	359.99	9.1	360.73	1.37	360.85	0.31
z5	0.560	0.4001	99.29%	43	0.24	2556	0.177	0.05373	0.182	0.427656	0.236	0.057724	0.075	0.801	359.84	4.1	361.51	0.72	361.77	0.26
z6	0.465	0.2344	98.41%	18	0.31	1133	0.147	0.05372	0.379	0.426328	0.429	0.057555	0.076	0.715	359.47	8.5	360.57	1.30	360.74	0.27
z7	0.537	0.5612	99.55%	68	0.21	4031	0.169	0.05373	0.160	0.426661	0.207	0.057595	0.077	0.727	359.64	3.6	360.80	0.63	360.98	0.27
North Lake metadiorite																				
96DM-065*—hornblende-biotite diorite (415117 E, 6809165 N)																				
z1	2.037	0.6811	98.94%	39.3	0.61	1703	0.642	0.053787	0.110	0.428938	0.125	0.057865	0.037	0.528	361.12	2.48	362.42	0.38	362.63	0.13
z2	0.899	1.3280	99.90%	317.2	0.12	17228	0.283	0.053810	0.062	0.429052	0.083	0.057855	0.047	0.674	362.08	1.40	362.50	0.25	362.57	0.17
z3	0.445	0.4776	99.71%	103.4	0.11	6304	0.140	0.053893	0.142	0.429853	0.159	0.057874	0.034	0.575	365.55	3.20	363.07	0.48	362.68	0.12
z4	2.315	0.9713	99.80%	226.9	0.16	9230	0.730	0.053828	0.057	0.429323	0.075	0.057872	0.034	0.677	362.86	1.29	362.70	0.23	362.67	0.12
z5	1.536	0.9947	99.86%	264.6	0.12	12486	0.484	0.053878	0.087	0.429517	0.100	0.057845	0.034	0.511	364.94	1.97	362.83	0.30	362.50	0.12
z6	1.743	2.0186	99.89%	375.5	0.18	16987	0.549	0.053826	0.040	0.429352	0.059	0.057878	0.033	0.776	362.78	0.90	362.72	0.18	362.71	0.12
Simpson Range plutonic suite (SRPS)																				
P99-24—hornblende granodiorite (428393 E, 6794091 N)																				
z2	0.560	1.8866	99.87%	234	0.21	13797	0.176	0.05354	0.074	0.414489	0.134	0.056153	0.068	0.940	351.54	1.7	352.10	0.40	352.19	0.23
z3	0.550	0.8517	99.50%	60	0.36	3576	0.173	0.05354	0.126	0.414393	0.178	0.056139	0.066	0.863	351.60	2.8	352.03	0.53	352.10	0.23
z4	0.500	2.1258	99.87%	225	0.24	13491	0.158	0.05356	0.072	0.414647	0.132	0.056151	0.065	0.952	352.50	1.6	352.22	0.39	352.17	0.22
z5	0.508	2.7143	99.85%	206	0.33	12361	0.160	0.05353	0.074	0.414298	0.133	0.056128	0.067	0.942	351.51	1.7	351.97	0.40	352.03	0.23
z6	0.485	4.4886	99.92%	372	0.30	22377	0.153	0.05355	0.067	0.414522	0.127	0.056145	0.064	0.968	352.05	1.5	352.13	0.38	352.14	0.22

Table 1: Continued.

Sample[†]	Compositional parameters[§]					Radiogenic isotope ratios[#]									Isotopic ages[††]					
	Th/U	$^{206}Pb^*$ ($\times10^{-13}$ mol)	mol%/$^{206}Pb^*$	Pb^*/Pb_c	Pb_c (pg)	$^{206}Pb/^{204}Pb$	$^{208}Pb/^{206}Pb$	$^{207}Pb/^{206}Pb$	% error	$^{207}Pb/^{235}U$	% error	$^{206}Pb/^{238}U$	% error	R	$^{207}Pb/^{206}Pb$	±	$^{207}Pb/^{235}U$	±	$^{206}Pb/^{238}U$	±
18MM-107*—monzogranite (424291 E, 6792248 N)																				
z1	0.469	1.0561	99.49%	59	0.45	3553	0.148	0.05348	0.164	0.410559	0.181	0.055673	0.045	0.478	349.42	3.7	349.28	0.53	349.26	0.15
z2	0.500	1.2521	99.77%	129	0.24	7724	0.158	0.05348	0.113	0.410389	0.130	0.055653	0.041	0.563	349.31	2.5	349.16	0.39	349.13	0.14
z3	0.465	4.0297	99.90%	299	0.33	18080	0.147	0.05352	0.026	0.410842	0.056	0.055670	0.035	0.937	351.10	0.6	349.48	0.16	349.24	0.12
z4	0.438	1.1246	99.60%	73	0.38	4471	0.138	0.05353	0.071	0.410813	0.100	0.055661	0.036	0.852	351.28	1.6	349.46	0.29	349.19	0.12
z5	0.468	1.2365	99.68%	92	0.33	5602	0.148	0.05354	0.085	0.410839	0.101	0.055658	0.038	0.592	351.58	1.9	349.48	0.30	349.16	0.13
z6	0.489	1.5236	99.84%	186	0.20	11172	0.154	0.05352	0.068	0.410710	0.084	0.055660	0.037	0.623	350.76	1.5	349.39	0.25	349.18	0.13
z7	0.504	2.0426	99.84%	188	0.27	11302	0.159	0.05354	0.051	0.411048	0.071	0.055680	0.038	0.726	351.82	1.2	349.63	0.21	349.30	0.13
Cleaver Lake formation																				
18MM-108*—high-level quartz porphyry (424207 E, 6792698 N)																				
z1	0.470	0.2484	97.53%	12	0.52	730	0.148	0.05381	0.553	0.429973	0.594	0.057951	0.058	0.724	363.20	12.5	363.16	1.81	363.15	0.21
z2	0.628	0.6346	99.34%	47	0.35	2742	0.198	0.05380	0.195	0.429848	0.214	0.057943	0.048	0.500	362.86	4.4	363.07	0.65	363.10	0.17
z3	0.501	0.2763	98.76%	24	0.29	1459	0.158	0.05390	0.396	0.430715	0.429	0.057957	0.046	0.739	366.86	8.9	363.68	1.31	363.19	0.16
z4	0.508	1.1728	99.56%	69	0.43	4137	0.160	0.05386	0.132	0.430510	0.154	0.057969	0.045	0.606	365.30	3.0	363.54	0.47	363.26	0.16
z5	0.435	1.7533	99.74%	115	0.38	7007	0.137	0.05381	0.085	0.430075	0.104	0.057971	0.038	0.629	362.95	1.9	363.23	0.32	363.27	0.14
z6	0.378	0.7804	99.53%	62	0.31	3827	0.119	0.05388	0.189	0.430455	0.205	0.057942	0.048	0.442	366.06	4.3	363.50	0.63	363.10	0.17
z7	0.357	0.2328	98.35%	17	0.33	1090	0.113	0.05387	0.412	0.430450	0.442	0.057949	0.058	0.552	365.78	9.3	363.50	1.35	363.14	0.21
z8	0.497	2.2648	99.55%	67	0.84	4049	0.157	0.05386	0.127	0.430414	0.145	0.057956	0.043	0.541	365.30	2.9	363.47	0.44	363.18	0.15

[†]Sample numbers denoted with an asterisk (∗) indicate the use of the ET2535 tracer solution, whereas the ET535 tracer was used for all other samples; UTM coordinates in NAD83 Zone 9N; z1, z2, etc., are labels for single zircon grains or fragments annealed; only grain labels in bold font are included in weighted mean date calculations. [§]Model Th/U ratio iteratively calculated from the radiogenic $^{208}Pb/^{206}Pb$ ratio and $^{206}Pb/^{238}U$ age; Pb^* and Pb_c represent radiogenic and common Pb, respectively; mol% $^{206}Pb^*$ with respect to radiogenic, blank, and initial common Pb; measured ratio corrected for spike and fractionation only. Fractionation estimated at 0.17 ± 0.03%/a.m.u. for Daly analyses, based on analysis of NBS-981 and NBS-982. [#]Corrected for fractionation, spike, and common Pb; all common Pb was assumed to be procedural blank: $^{206}Pb/^{204}Pb = 18.042 \pm 0.61\%$; $^{207}Pb/^{204}Pb = 15.537 \pm 0.52\%$; $^{208}Pb/^{204}Pb = 37.686 \pm 0.63\%$ (all uncertainties 1-sigma); errors are 2-sigma, propagated using the algorithms of Schmitz and Schoene (2007). [††]Calculations are based on the decay constants of Jaffey et al. (1971). $^{206}Pb/^{238}U$ and $^{207}Pb/^{206}Pb$ ages corrected for initial disequilibrium in $^{230}Th/^{238}U$ using Th/U [magma] = 3.

Table 2: Summary of U-Pb geochronology results.

Sample*	Lithology	Th/U (LA-ICP-MS)†	Th/U (CA-ID-TIMS)†	Weighted mean $^{206}Pb/^{238}U$ LA-ICP-MS date (Ma)§	Weighted mean $^{206}Pb/^{238}U$ CA-ID-TIMS date (Ma)§
Fire Lake thrust sheet					
Permian dike cutting Fire Lake formation					
17MM-047	Felsic dike	0.34–0.81 (0.53)	NA	263.9 ± 3.8	NA
Big Campbell thrust sheet					
Wolverine Lake group					
18MM-102*	High-level feldspar porphyry	0.24–3.21 (1.52)	1.03–1.40 (1.23)	355.5 ± 1.8	354.982 ± 0.068
P00-WV-1C*	High-level feldspar porphyry	0.14–3.67 (1.51)	0.90–1.10 (1.02)	352.8 ± 2.2	355.262 ± 0.066
P99-WV-4K*	Felsic crystal tuff	0.23–5.37 (1.84)	0.92–1.03 (0.99)	353.3 ± 1.7	355.236 ± 0.058
P00-WV-12*	High-level quartz-feldspar porphyry	0.15–2.19 (0.90)	0.46–0.70 (0.59)	354.6 ± 2.1	356.094 ± 0.059
18MM-114*	Felsic crystal tuff	0.16–2.20 (0.81)	0.26–0.80 (0.37)	359.5 ± 2.0	356.371 ± 0.091
17MM-004	Quartzofeldspathic grit	0.11–1.09 (0.56)	0.18–0.36 (0.27)	356.6 ± 2.9	357.658 ± 0.096
Grass Lakes plutonic suite					
17MM-005	Granodiorite	0.15–1.64 (0.71)	0.34–0.48 (0.42)	363.3 ± 2.6	360.94 ± 0.10
18MM-105	Granodiorite	0.16–5.13 (1.87)	0.28–2.25 (1.21)	359.3 ± 2.3	361.801 ± 0.099
17MM-061	High-level alkali feldspar porphyry	0.07–3.04 (1.10)	0.45–1.30 (0.92)	360.7 ± 2.4	361.71 ± 0.13
17MM-062	High-level plagioclase porphyry	0.24–1.90 (1.01)	0.55–0.77 (0.69)	361.5 ± 3.4	361.901 ± 0.086
Wind Lake formation					
17MM-001	Felsic crystal tuff	0.40–0.62 (0.53)	0.41–0.56 (0.51)	359.8 ± 2.8	360.89 ± 0.12
North Lake intrusion					
96DM-065	Hornblende diorite	0.075–6.08 (2.08)	0.45–2.32 (1.50)	355.4 ± 2.9	362.63 ± 0.05
Kudz Ze Kayah formation					
17MM-002*	Felsic lapilli tuff	0.13–2.21 (0.54)	0.16–0.54 (0.39)	365.1 ± 2.7	362.404 ± 0.098
17MM-031*	Felsic tuff to lapilli tuff	0.15–1.76 (0.98)	0.67–1.15 (1.01)	361.2 ± 2.4	362.82 ± 0.12
18MM-133*	Felsic tuff	0.42–3.80 (1.56)	0.20–1.26 (0.99)	360.0 ± 1.6	362.847 ± 0.099
17MM-074*	Felsic crystal tuff	0.13–4.27 (1.21)	0.27–1.20 (0.62)	363.1 ± 2.3	363.254 ± 0.098
Cleaver Lake thrust sheet					
Simpson Range plutonic suite					
P99-24	Hornblende granodiorite	0.38–0.85 (0.54)	0.49–0.56 (0.52)	354.4 ± 2.0	352.12 ± 0.10
P99-82	Hornblende quartz diorite	0.39–0.67 (0.49)	NA	354.1 ± 2.2	NA
18MM-107	Monzogranite	0.48–1.17 (0.70)	0.44–0.50 (0.48)	348.2 ± 1.8	349.207 ± 0.049
Cleaver Lake formation					
18MM-108	High-level quartz porphyry	0.36–1.24 (0.64)	0.36–0.63 (0.47)	363.2 ± 1.7	363.185 ± 0.058

*CA-ID-TIMS dates for samples denoted with asterisk (∗) are reported from Manor et al. (in press). †Th/U ratios only for grains that are included in the weighted mean for each sample. Values in parentheses are mean values for the population. §Refer to Table 1 and Table S2 for complete U-Th-Pb results and Figures 8 and 9 and Figure S8 for CA-ID-TIMS and LA-ICP-MS concordia diagrams, respectively.

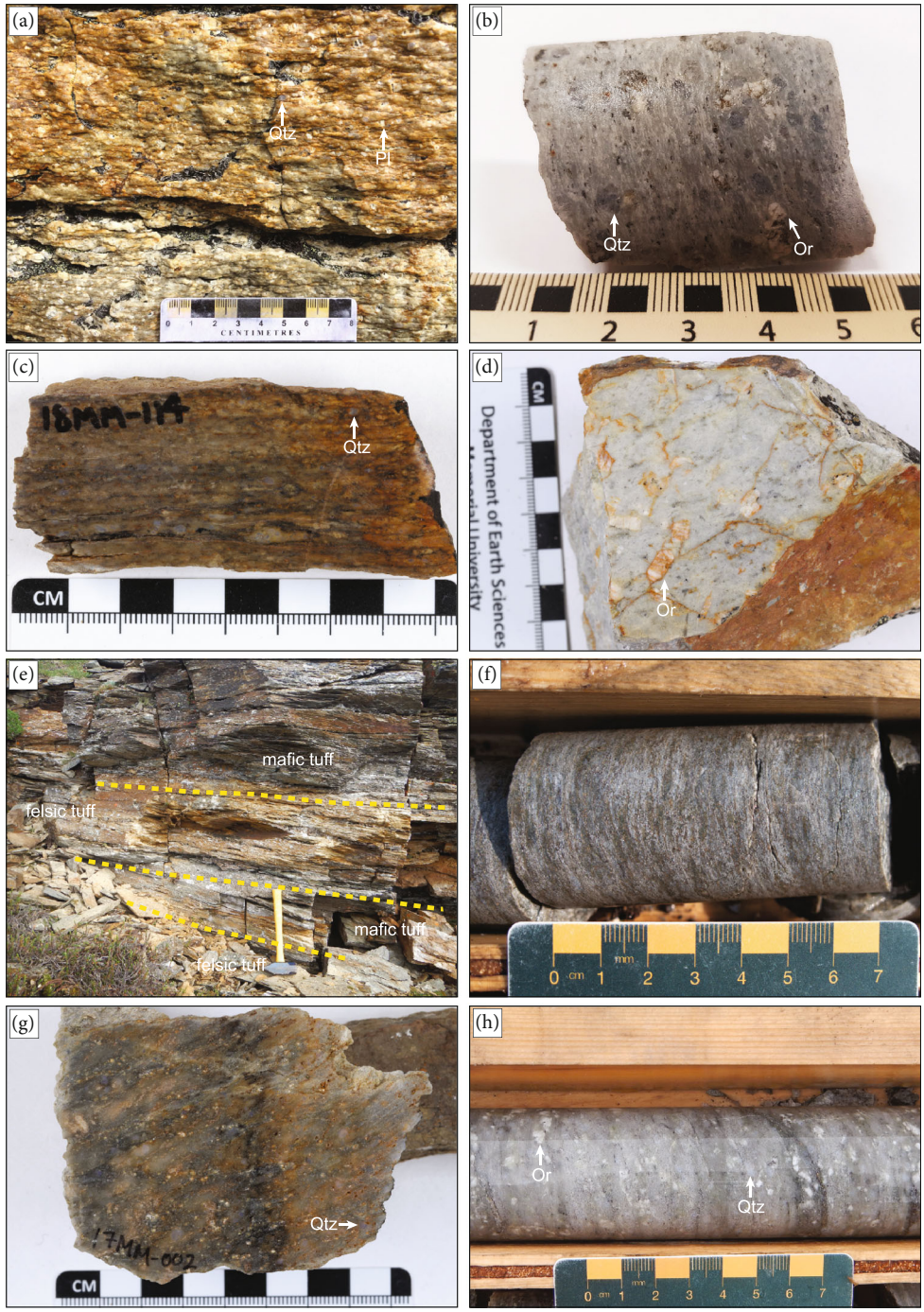

FIGURE 6: Photographs of representative felsic volcanic and high-level intrusive rocks in the Big Campbell thrust sheet, Finlayson Lake district: (a) 17MM-004: Little Jimmy formation, massive and foliated quartzofeldspathic grit; (b) P00-WV-12: Little Wolverine formation (Sable zone), high-level quartz-orthoclase feldspar porphyritic intrusive rock; (c) 18MM-114: Little Wolverine formation (lower), felsic crystal tuff; (d) 18MM-102: Little Wolverine formation (Fisher zone), high-level orthoclase feldspar-porphyritic intrusive rock; (e) 17MM-001: Wind Lake formation, felsic tuff interbedded with mafic tuff ~300 m above contact with Kudz Ze Kayah formation; (f) 18MM-133: Kudz Ze Kayah formation (Krakatoa zone), felsic tuff; (g) 17MM-002: Kudz Ze Kayah formation, felsic crystal-lapilli tuff with blue quartz eyes intercalated with felsic tuff, ~5 m below the Wind Lake formation contact; (h) 17MM-074: Kudz Ze Kayah formation (GP4F), felsic crystal tuff with blue quartz eyes and orthoclase feldspar. Hammer (35 cm) for scale in (e). Qtz = quartz; Or = orthoclase.

in the hanging wall of the massive sulfide mineralization in the Kona VMS deposit (Figure S1; FL97-109; 204 m depth). Ten concordant zircon grains gave a LA-ICP-MS weighted mean $^{206}Pb/^{238}U$ date of 263.9 ± 3.8 Ma (2σ; MSWD = 3.1; Figure S7; Table S2), which is interpreted to be the crystallization age of this rock.

FIGURE 7: Photographs of representative felsic and mafic volcanic, high-level intrusive, and plutonic rocks in the Big Campbell (a–f) and Cleaver Lake (g, h) thrust sheets, Finlayson Lake district. (a) 17MM-005: Grass Lakes plutonic suite: foliated and deformed, massive plagioclase feldspar-quartz granodiorite; (b) 18MM-105: massive, equigranular, moderately foliated granodiorite; (c) 17MM-061: Grass Lakes plutonic suite, high-level quartz-orthoclase feldspar porphyritic rock with rare blue quartz eyes that cuts Kudz Ze Kayah deposit footwall; (d) 18MC015/96DM-065: North Lakes intrusion, fine to medium-grained gabbro to diorite intruded by Grass Lakes plutonic suite granitic dikes; (e) 18MM-132: Kudz Ze Kayah formation (Krakatoa zone), high-level chlorite-altered mafic dike in the Krakatoa deposit footwall; (f) 17MM-054: Wind Lake formation, deformed and altered pillow basalts with possible outer selvage; (g) P99-24: Simpson Range plutonic suite, equigranular hornblende granodiorite; (h) 18MM-108: Cleaver Lake formation, high-level quartz-porphyritic intrusive rock. Hammer (35 cm) for scale in (d) and pen (10 cm) for scale in (f). Qtz = quartz; Or = orthoclase; Pl = plagioclase; Hbl = hornblende.

5.3. Big Campbell Thrust Sheet

5.3.1. Wolverine Lake Group. A basal grit (17MM-004) from the Little Jimmy formation was sampled from the same sample locality as the detrital sample of Murphy et al. [16], immediately northeast of the angular unconformity that separates the Grass Lakes and Wolverine Lake groups (Figures 4 and 6(a)). The CA-ID-TIMS results gave six concordant zircon fractions with a consistently low Th/U (0.2–0.4) and a weighted mean $^{206}Pb/^{238}U$ date of 357.658 ± 0.096 Ma (2σ; MSWD = 0.53; Figure 8(a); Table 1), which is inferred to represent the maximum depositional age of this rock.

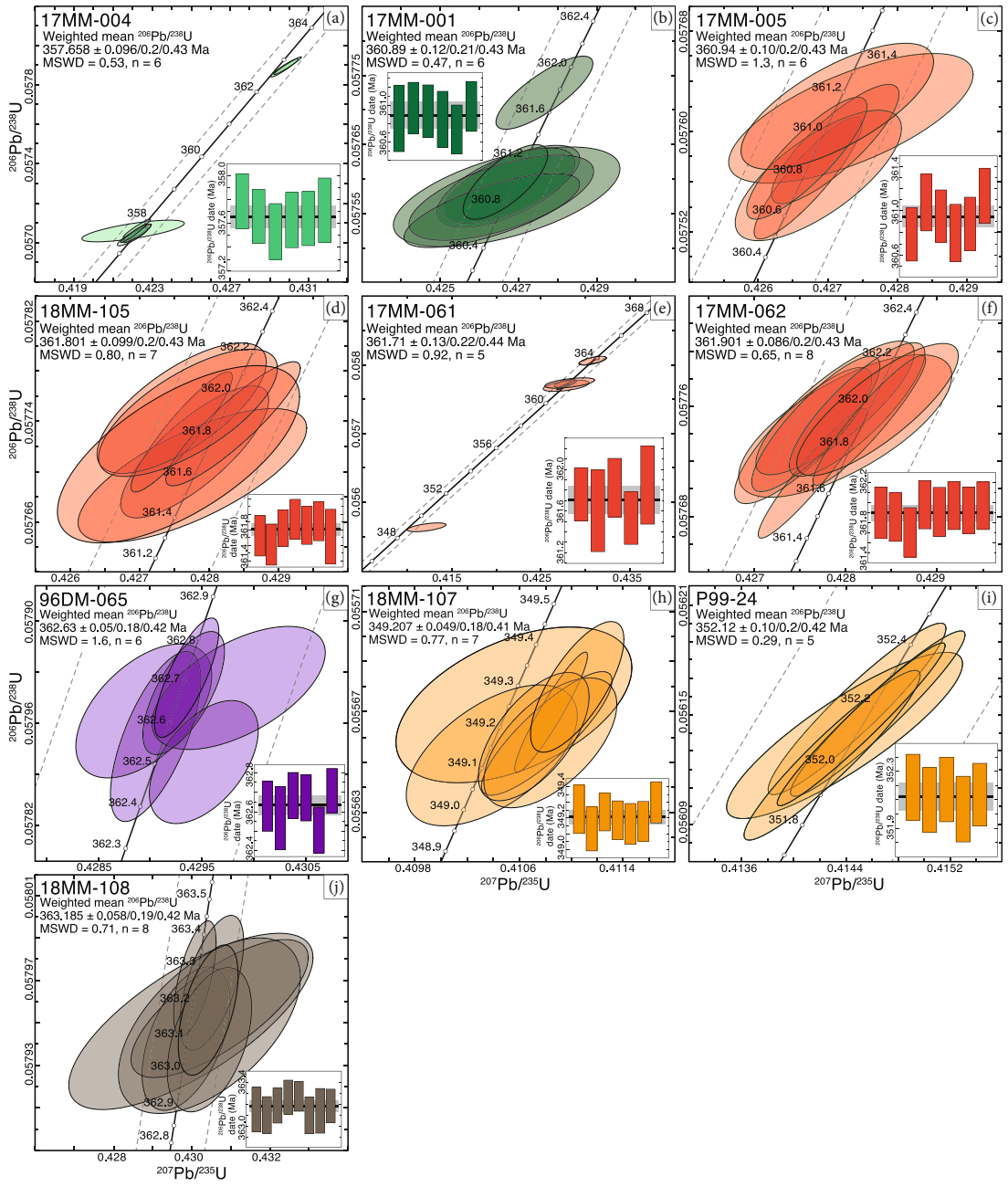

FIGURE 8: Concordia diagrams displaying CA-ID-TIMS U-Pb geochronology results for zircon in the Big Campbell and Cleaver Lake thrust sheets, Finlayson Lake district: (a) quartzofeldspathic grit from the Little Jimmy formation, immediately above the basal WLG unconformity (17MM-004); (b) GLPS granodiorite, immediately below the basal WLG unconformity (17MM-005); (c) GLPS granodiorite (18MM-105); (d) high-level alkali feldspar porphyritic intrusive rock, GLPS (17MM-061); (e) high-level plagioclase porphyritic intrusive rock (17MM-062); (f) felsic crystal tuff interbedded with mafic tuffs in the Wind Lake formation (17MM-001); (g) hornblende diorite, North Lakes intrusion (96DM-065); (h) SRPS hornblende granodiorite (P99-24); (i) SRPS monzogranite, locally observed mingling with gabbroic intrusions (18MM-107); (j) high-level quartz porphyritic intrusive rock, Cleaver Lake formation (18MM-108). Each individual ellipse encompasses the 2σ error on a single zircon analytical result. The grey dashed lines represent the range of decay constant uncertainty on the concordia curve. The inset panels show individual grain analyses with their included 2σ error (vertical bars); the solid black line indicates the calculated weighted mean $^{206}Pb/^{238}U$ date, and the larger grey region indicates the error associated with external reproducibility of the analyses. Ellipse and bar colors correspond to the ranked bars in Figure 3. MSWD = mean square of the weighted deviates; HW = hanging wall; FW = footwall.

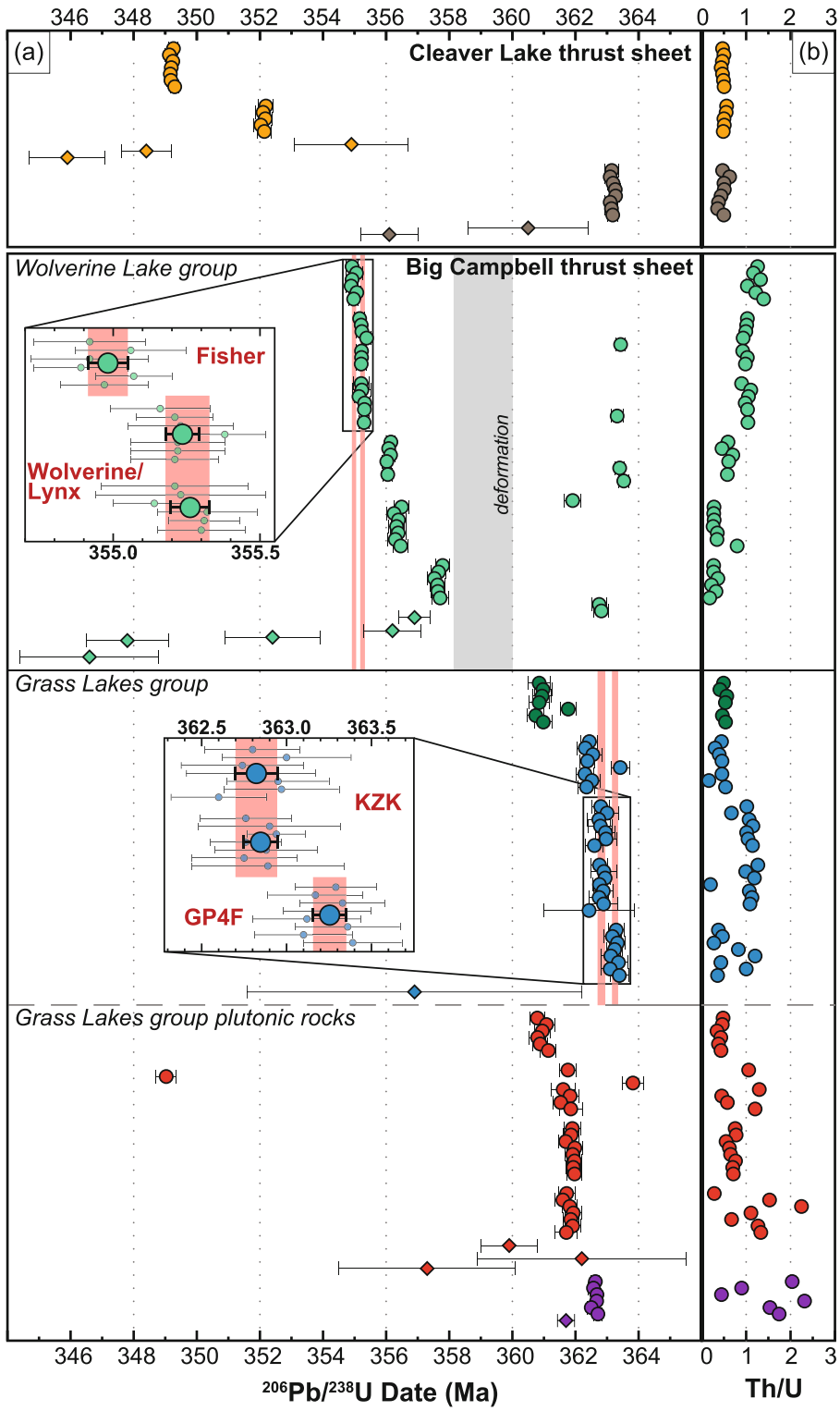

FIGURE 9: Summary of CA-ID-TIMS U-Pb zircon geochronological results for the Finlayson Lake district (a), with associated Th/U (b). Each symbol represents one individual zircon analysis as its $^{206}Pb/^{238}U$ date with associated uncertainty ($\pm 2\sigma$). Th/U for individual zircon grains, which correspond to a specific U-Pb analysis shown in (a). Analyses for the Wolverine Lake group and Kudz Ze Kayah formation are from Manor et al. [30], shown here as a compilation of new U-Pb dates in the district. Insets show individual $^{206}Pb/^{238}U$ dates (small symbols) and their calculated weighted mean date ($\pm 2\sigma$), which define distinct periods of VMS mineralization in the district (vertical red bars). Symbols: circles = this study and from Manor et al. [30]; diamonds = historical U-Pb zircon dates from Mortensen [4], Piercey [151], Murphy et al. [16], and Piercey et al. [17].

5.3.2. Grass Lakes Group

(1) Grass Lakes Plutonic Suite. Rocks dated by U-Pb geochronology from the Grass Lakes plutonic suite include two granitoids (17MM-005 and 18MM-105) and two feldspar porphyritic rocks (17MM-061 and 17MM-062; Figures 7(a)–7(c) and Figure S1). A moderately deformed, medium-grained granodiorite (17MM-005) was collected immediately southwest of the angular unconformity that juxtaposes the Grass Lakes and Wolverine Lake groups (Figure 4). The CA-ID-TIMS data reveal six concordant fractions with Th/U = 0.3 – 0.5 and a weighted mean $^{206}Pb/^{238}U$ date of 360.94 ± 0.10 Ma (2σ; MSWD = 1.3; Figure 8(b); Table 1), interpreted as the crystallization age of the rock. Sample 18MM-105 is a medium to coarse-grained granodiorite located south of the Kudz Ze Kayah formation in the North Lakes area and represents one from the most voluminous part of the Grass Lakes pluton (Figure 4). For CA-ID-TIMS, seven concordant zircon fractions give highly variable Th/U (0.3–2.3), similar to the North Lakes diorite. A weighted mean $^{206}Pb/^{238}U$ date of 361.801 ± 0.099 Ma (2σ; MSWD = 0.80; Figure 8(c); Table 1) is inferred to be the crystallization age of this granitoid.

A quartz-feldspar porphyritic intrusive rock (17MM-061) was sampled from a ~50 m thick intrusion in the upper 130 m of drill hole K16-372, which is interpreted to be near to the same stratigraphic level as the Kudz Ze Kayah VMS deposit. This sample contains medium-grained alkali feldspar phenocrysts and lesser quartz grains in a grey, glassy matrix (Figure 7(c)). Five of seven grains yielded concordant U-Th-Pb results, with Th/U between 0.5 and 1.3 and a weighted mean $^{206}Pb/^{238}U$ date of 361.71 ± 0.13 Ma (2σ; MSWD = 0.92; Figure 8(d); Table 1), interpreted as the crystallization age of this intrusive rock. Of the other two grains, one older grain (z3) gave an older $^{206}Pb/^{238}U$ date of 363.82 ± 0.34 Ma and is interpreted as a xenocryst; the other (z2) is significantly younger with a $^{206}Pb/^{238}U$ date of 349.03 ± 0.32 Ma but is much more discordant (~3%) relative to the other grains (<0.5%). This younger grain is interpreted to have not seen complete mitigation of Pb-loss through the chemical abrasion process. An additional feldspar-rich porphyritic intrusive rock (17MM-062) was sampled at the bottom of hole K16-372 (585 m depth). In contrast to 17MM-061, this rock is dominantly composed of plagioclase and quartz phenocrysts. Eight concordant zircon fractions yield moderate Th/U (0.6–0.8) and a weighted mean $^{206}Pb/^{238}U$ date of 361.901 ± 0.086 Ma (2σ; MSWD = 0.92; Figure 8(e); Table 1), which is interpreted to be the crystallization age of the sample.

(2) Wind Lake Formation. A felsic crystal tuff (17MM-001) was collected at an outcrop locality that displays interbedded felsic and mafic volcaniclastic rocks, ~500 m stratigraphically above the Kudz Ze Kayah–Wind Lake formation contact (Figures 4 and 6(e)). For CA-ID-TIMS, six concordant zircon fractions gave a tight range of Th/U (0.4–0.6) and a weighted mean $^{206}Pb/^{238}U$ date of 360.89 ± 0.12 Ma (2σ; MSWD = 0.47; Figure 8(f); Table 1), inferred as the eruption age for this rock. One zircon fraction yielded a $^{206}Pb/^{238}U$ date of 361.77 ± 0.26 Ma, which is beyond the upper limit of 2σ error of the weighted mean date and inferred to represent an antecryst or xenocryst.

(3) North Lakes Intrusion. Zircon from a diorite in the North Lakes intrusion (96DM-065; [16]) was reanalyzed with modern CA-ID-TIMS techniques for consistency in this study. The CA-ID-TIMS results gave six concordant zircon fractions with high Th/U (0.4–2.3) and a weighted mean $^{206}Pb/^{238}U$ date of 362.63 ± 0.05 Ma (2σ; MSWD = 1.6; Figure 8(g); Table 1). The new results are interpreted to be the crystallization age for this diorite and are outside of uncertainty from previously published results (weighted mean $^{207}Pb/^{206}Pb$ date = 365.0 ± 1.2 Ma; [16]).

5.4. Cleaver Lake Thrust Sheet

5.4.1. Simpson Range Plutonic Suite. Three granitoids from the Simpson Range plutonic suite were dated with LA-ICP-MS (P99-82, P99-24, and 18MM-107) and the latter two samples were dated by CA-ID-TIMS (Table 2, Figures 7(g) and S1). Sample P99-82 is a hornblende quartz diorite from the southeastern margin of the pluton (Figure 4). The LA-ICP-MS U-Th-Pb data reveal 35 concordant zircon fractions with a weighted mean $^{206}Pb/^{238}U$ date of 354.1 ± 2.2 Ma (2σ; MSWD = 1.3; Table S2), which is interpreted as the crystallization age of this granitoid. The hornblende granodiorite (P99-24) is located in the northeastern corner of the pluton (Figure 2). The CA-ID-TIMS results for this sample yielded five concordant fractions with Th/U tightly constrained to 0.5–0.6 and correspond to a weighted mean $^{206}Pb/^{238}U$ date of 352.12 ± 0.10 Ma (2σ; MSWD = 0.29; Figure 8(h); Table 1); this date is interpreted as the crystallization age of this rock. A monzogranite (18MM-107) was sampled near the core of the Simpson Range pluton, about 100 m south of the locality for 18MM-108 (Figure 4). At this location, lobate magma mingling textures are observed between monzogranite and gabbroic rocks. Seven concordant CA-ID-TIMS zircon fractions gave a limited range of Th/U (0.4–0.5) and a weighted mean $^{206}Pb/^{238}U$ date of 349.207 ± 0.049 Ma (2σ; MSWD = 0.77; Figure 8(i); Table 1), interpreted to be the age of crystallization for both this monzogranite and the coeval gabbroic rocks.

5.4.2. Cleaver Lake Formation. A quartz-porphyritic intrusive rock (18MM-108) was sampled from outcrop in the Cleaver Lake formation in the Cleaver Lake thrust sheet (Figure 7(h)), where a sharp contact with the Simpson Range granitoids is observed. The U-Th-Pb results gave eight concordant zircon fractions for CA-ID-TIMS, with moderate Th/U (0.4–0.6) and a weighted mean $^{206}Pb/^{238}U$ date of 363.185 ± 0.058 Ma (2σ; MSWD = 0.71; Figure 8(j); Table 1) that is interpreted to represent the crystallization age of this intrusive rock.

6. Lithogeochemical Results

6.1. Alteration and Element Mobility. The lithogeochemical results from this study show significant element mobility

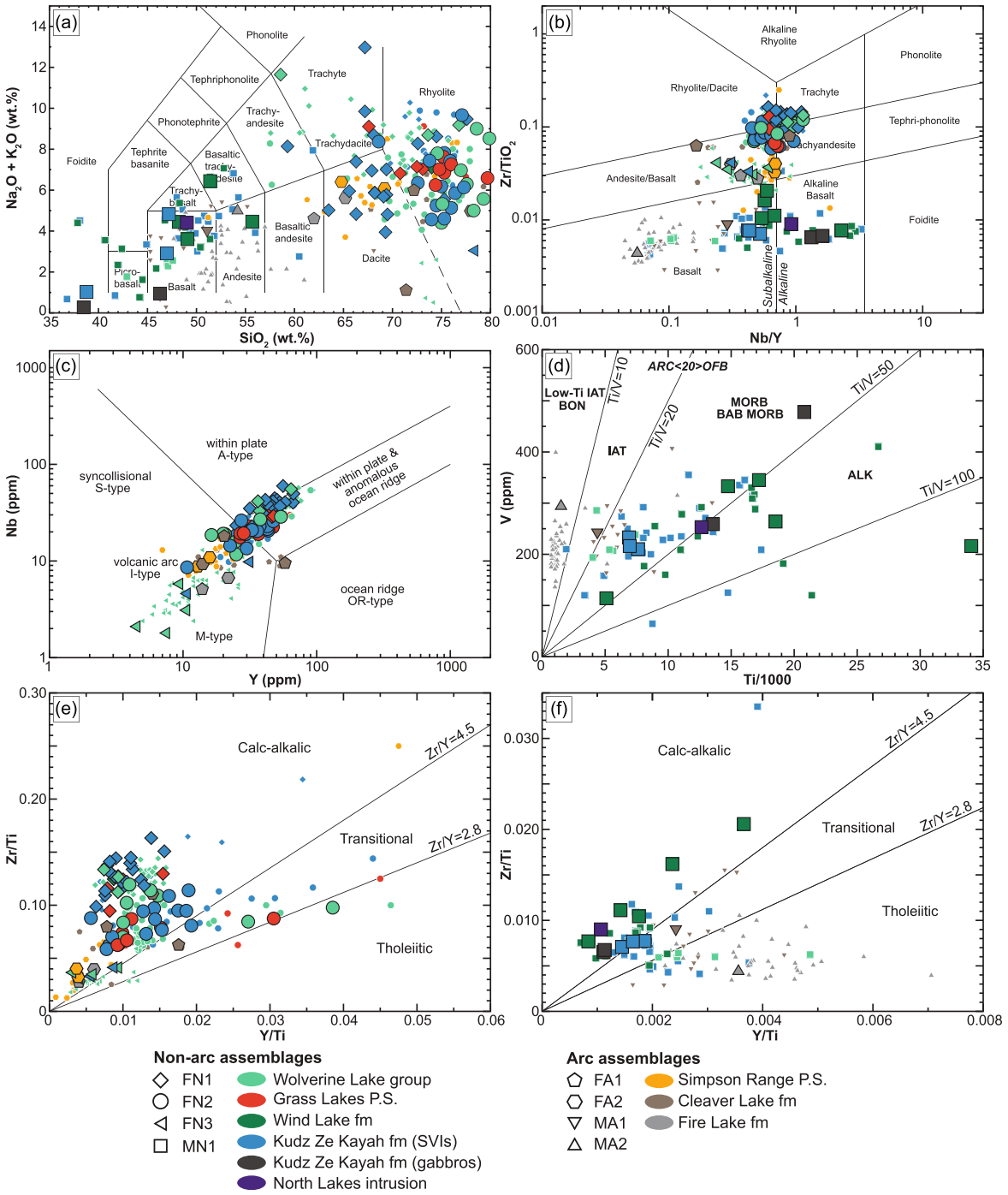

FIGURE 10: Major and trace element discrimination diagrams for felsic and mafic rocks in the Finlayson Lake region. Samples from this study are shown as the largest symbols with black outlines; archival data are smaller symbols with white outlines [6, 7, 17, 45, 47, 48, 53, 61]. (a) SiO_2 vs. Na_2O+K_2O, analyses from the Wolverine deposit hanging wall (i.e., Go Creek formation) have SiO_2 contents above 80 wt.% and are not included; (b) Nb/Y vs. Zr/TiO_2 ([152]; after [153]); (c) Y vs. Nb for felsic rocks [154]; (d) Ti/1000 vs. V for mafic rocks [93]; (e) Y/Ti vs. Zr/Ti for felsic rocks; (f) Y/Ti vs. Zr/Ti for mafic rocks. Panels (e, f) are modified after Lentz [43, 155]; Zr/Y values defining magmatic affinity classes from Ross and Bédard [92]. IAT = island arc tholeiite; BON = boninite; OFB = ocean floor basalt; MORB = midocean ridge basalt; BAB = back-arc basin; ALK = alkaline; SVI = subvolcanic intrusion. Symbol markers represent their assigned geochemical group for non-arc and arc assemblages and are propagated through all subsequent plots. See text for explanation.

due to hydrothermal alteration, notably in alkali (e.g., Na, K, and Ca) and large ion lithophile elements (LILE: Cs, Ba, Rb, K, Sr, and U; e.g., Figure 10(a)). However, several samples have $Al_2O_3/Na_2O < 10$ and Na_2O contents between 2 and 5 wt.%, which are indicative of relatively unaltered rocks (i.e., "least-altered" rocks) as observed in previous studies in the Finlayson Lake district (e.g., [45]). The alteration of least-altered felsic rocks, particularly the extrusive volcanic

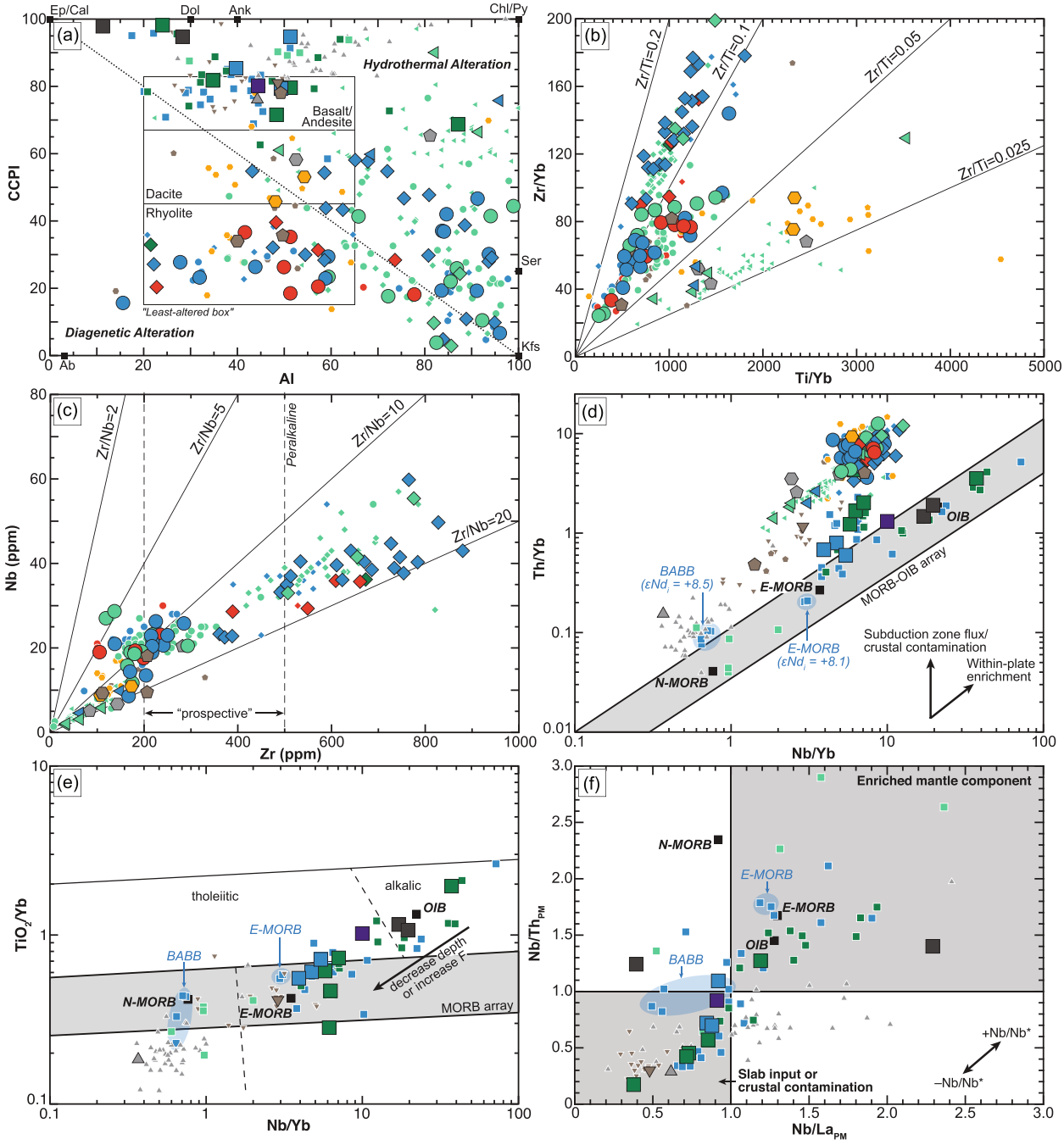

FIGURE 11: Major and trace element diagrams for felsic and mafic rocks in the Finlayson Lake region for alteration assemblages (a), immobile element systematics (b–d), and magmatic differentiation (e, f). (a) CCPI (chlorite-carbonate-pyrite index) vs. AI (Ishikawa alteration index; [86]; from [87]). Ep = epidote; Cal = calcite; Dol = dolomite; Ank = ankerite; Chl = chlorite; Py = pyrite; Ab = albite; Kfs = K-feldspar. (b) Ti/Yb vs. Zr/Yb; (c) Nb vs. Zr; (d) Nb/Yb vs. Th/Yb, after Pearce [94], where vectors indicate trajectories of deviations from the MORB-OIB array with either a subduction zone flux (e.g., as in Fire Lake and Cleaver Lake formations), crustal contamination (e.g., most rocks in the BCTS), or within-plate enrichment (e.g., group FN2 to FN1 felsic rocks). (e) Nb/Yb vs. TiO_2/Yb after Pearce [94]. (f) Nb/Th_{PM} vs. Nb/La_{PM} after Piercey et al. [7]. Reference compositions for N-MORB, E-MORB, and OIB are from Sun and McDonough [91]. Symbols as in Figure 10. F = melt fraction. Blue fields illustrate samples reported in Piercey et al. [48].

or volcaniclastic rocks of the Kudz Ze Kayah formation and Wolverine Lake group, resulted in the dominant sericite and alkali feldspar alteration assemblages with minor chlorite-pyrite overprint; the mafic rocks typically exhibit more abundant carbonate, epidote, and chlorite-pyrite alteration (Figure 11(a); [43, 86, 87]). The methodology outlined by Piercey et al. [45] is utilized here, where HFSE (Zr, Hf, Nb, Ta, and Y), Th, and REE (La to Lu) are assumed to be immobile, and their measured concentrations are indicative of primary petrologic processes rather than secondary alteration

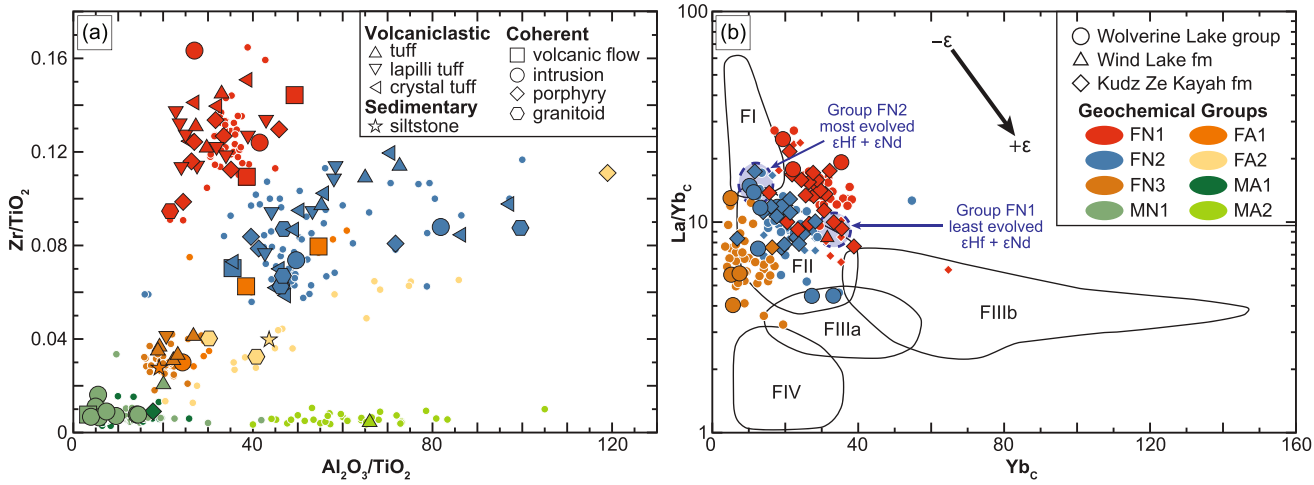

FIGURE 12: Geochemical group discrimination diagrams. (a) Al_2O_3/TiO_2 vs. Zr/TiO_2. Symbols represent lithology, which does not compose any trends with geochemical signature. Colors represent distinct geochemical groups based on distinct Zr/Al_2O_3 ratios. Small circles are data from literature sources as in Figure 10. (b) Yb_C vs. La/Yb_C, for felsic volcanic rocks only; data is normalized to C1 chondrite (C; [91]). Petrochemical discrimination fields (FI to FIV) from Hart et al. [34]. The black arrow shows a general trend of isotopic compositions within each group, and blue shaded regions indicate endmembers.

(e.g., [88]). Moreover, immobile elements and ratios that contain Al_2O_3, TiO_2, HFSE, and REE are used to assess the primary geochemical characteristics of the rocks (Figures 10–14). For additional comparison, felsic rocks have been normalized to upper continental crust (UCC; [89]), mafic rocks to primitive mantle (PM; [90]), and both felsic and mafic rocks to the C1 chondrite for REE (C; [91]). Complete lithogeochemical results are presented in Table S3.

6.2. Fire Lake Formation. Rocks were sampled from the drill core in the Kona VMS deposit including a single mafic tuff, intermediate-felsic clastic sedimentary rocks, and the Permian felsic intrusive rock dated in this study (Figures 2, 3, and S1). The mafic tuff has Nb/Y, Ti/V (<10), and Zr/Y ratios that are indicative of an island-arc tholeiitic to boninitic affinity (Figures 10(b), 10(d), and 10(f); e.g., [47, 48]), with a relatively flat primitive-mantle normalized pattern ($La/Yb_{PM} = 0.4$, $La/Sm_{PM} = 1.2$, and $Gd/Lu_{PM} = 0.4$) that overlaps with the boninite field (Figures 10(d) and 14(c)). Intermediate to felsic rocks consist of clastic sedimentary rocks (siltstones; $SiO_2 = 62–65$ wt.%) and the Permian Si-rich felsic dike ($SiO_2 = 84$ wt.%) that occur proximal to massive sulfide mineralization in the Kona VMS deposit. Trace element ratios (Nb/Y and Zr/Y) indicate that these samples have calc-alkalic arc affinities (Figure 10(e)) and have similar REE abundances ($La/Yb_{UCC} = 0.7–0.9$) and neutral to positive Eu anomalies ($Eu/Eu^*_{UCC} = 1.0–1.3$; Figure 13(d)).

6.3. Grass Lakes Group

6.3.1. Kudz Ze Kayah Formation. Felsic volcaniclastic ($n = 28$) and coherent volcanic and intrusive rocks ($n = 8$) and mafic intrusive rocks ($n = 5$) of the Kudz Ze Kayah formation were sampled (Figures 3–7; Table S3). The rocks show no geochemical preference to lithological variations in the felsic rocks (e.g., volcaniclastic vs. coherent; Figure 12(a)). The felsic rocks display a range of SiO_2 contents (59–78 wt.%) and have variable alkali concentrations due to hydrothermal alteration (Figures 10(a) and 11(a)). These rocks are subalkaline ($Nb/Y = 0.3–0.7$) and calc-alkalic ($Zr/Y > 4.2$; [92]) to alkaline-peralkaline ($Nb/Y = 0.7–1.1$; $Zr > 500$ ppm), both with intraplate A-type affinities (Figure 10). Two distinct groups are defined based on Zr/Al_2O_3, Zr/Ti, and Zr/Nb ratios: (1) group FN1, which includes alkaline and peralkaline dacite, trachyte/trachydacite, and minor rhyolite (e.g., TAS; Figure 10(a)), has within-plate Nb/Y ratios (Figure 10(c)), plots above the FI-FII rhyolite field (i.e., high La/Yb_C vs. Yb_C; Figure 12(b)), and has the highest Nb/Ta values (12–17, mean = 15; Figure 18), and (2) group FN2, which has predominantly subalkaline (to minor alkaline) affinities, falls within the andesite/basalt and trachyandesite fields (Nb/Y plot; Figure 10(b)), straddles the within-plate (A-type)–I-type boundary (Figure 10(c)), dominantly plots in the FII (±FI and FIIIa) rhyolite fields (e.g., [34]), and has lower Nb/Ta than group FN1 (10–14, mean = 12; Figure 18). Upper continental crust-normalized immobile elements yield relatively similar patterns between rocks of groups FN1 and FN2, except for higher absolute trace element abundances in group FN1. The patterns are flat with no significant LREE-enrichment (La/Sm_{UCC}: FN1 = 0.8–1.1; FN2 = 0.8–1.1), relatively higher HREE (Gd/Lu_{UCC}: FN1 = 0.6–1.8, mean = 1.4; FN2 = 0.8–1.9, mean = 1.1), and variably negative Eu (Eu/Eu^*_{UCC}: FN1 = 0.4–0.9, mean = 0.7; FN2 = 0.2–1.3, mean = 0.5) and strong negative Ti (Ti/Ti^*_{UCC}: FN1 = 0.05 – 0.09 ; FN2 = 0.04 – 0.18) anomalies (Figure 13(c)). These results are consistent with A-type volcanic signatures [45], except for samples 18MM-142 (tuff with minor argillite) and 18MM-143 (high-level felsic intrusive rock), which show elevated metal concentrations (Ni, Cu, Zn, Cr, and V; Figure 13(c); Table S3), and 18MM-

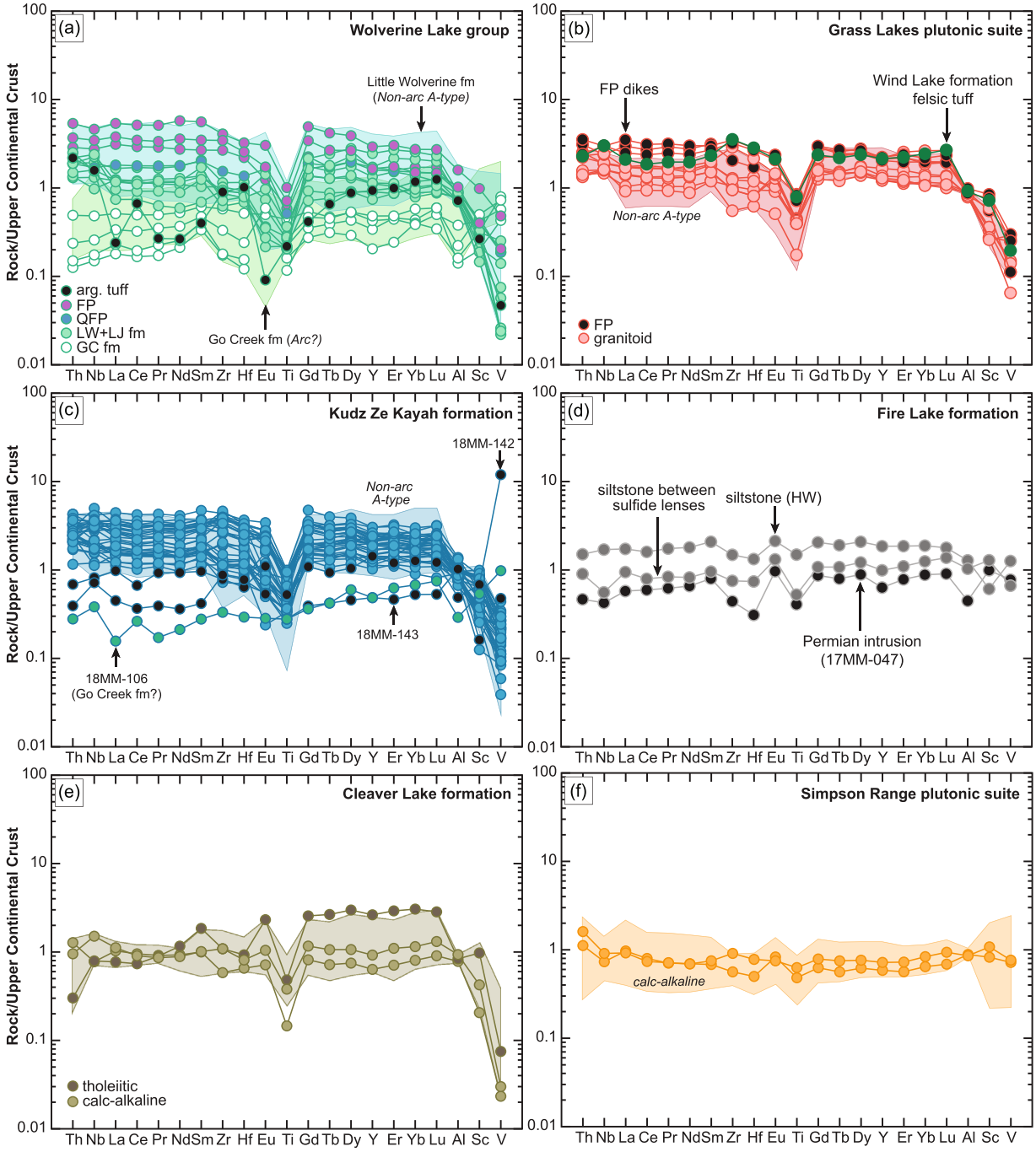

FIGURE 13: Immobile trace element diagrams for felsic rocks in the Finlayson Lake region, normalized to upper continental crust ([89]): (a) Wolverine Lake group; (b) Grass Lakes plutonic suite and Wind Lake formation; (c) Kudz Ze Kayah formation; (d) Fire Lake formation; (e) Cleaver Lake formation; (f) Simpson Range plutonic suite. Shaded fields represent archival data with interpreted magmatic affinities (cf. references in Figure 10). Abbreviations: arg = argillaceous; FP = feldspar porphyritic rhyolite; QFP = quartz-feldspar porphyritic rhyolite; LW fm = Little Wolverine formation; LJ = Little Jimmy formation; GC fm = Go Creek formation; HW = hanging wall.

106 (biotite-rich felsic tuff); all three of these samples have lower La/Yb_{UCC} than typical Kudz Ze Kayah formation rocks (Figure 13(c)).

Mafic rocks sampled from the Kudz Ze Kayah formation comprise (1) fine-grained, subvolcanic intrusive rocks within the area of the Kudz Ze Kayah deposit ($n = 3$) and (2) medium to coarse-grained intrusive rocks (metagabbro) in outcrop stratigraphically below the Kudz Ze Kayah formation ($n = 2$; Figure 4(a)). The subvolcanic intrusive rocks plot within the subalkaline basalt field (Nb/Y = 0.4–0.5) and have MORB/back-arc basin (BABB) affinities (Ti/V = 30–36; Figure 10(d); [93]). The Zr/Y (~4.5) also indicate a transitional to calc-alkalic, E-MORB-like (Th/Nb ~0.1–0.2; Figure 11(d)) affinity. The gabbroic rocks, however,

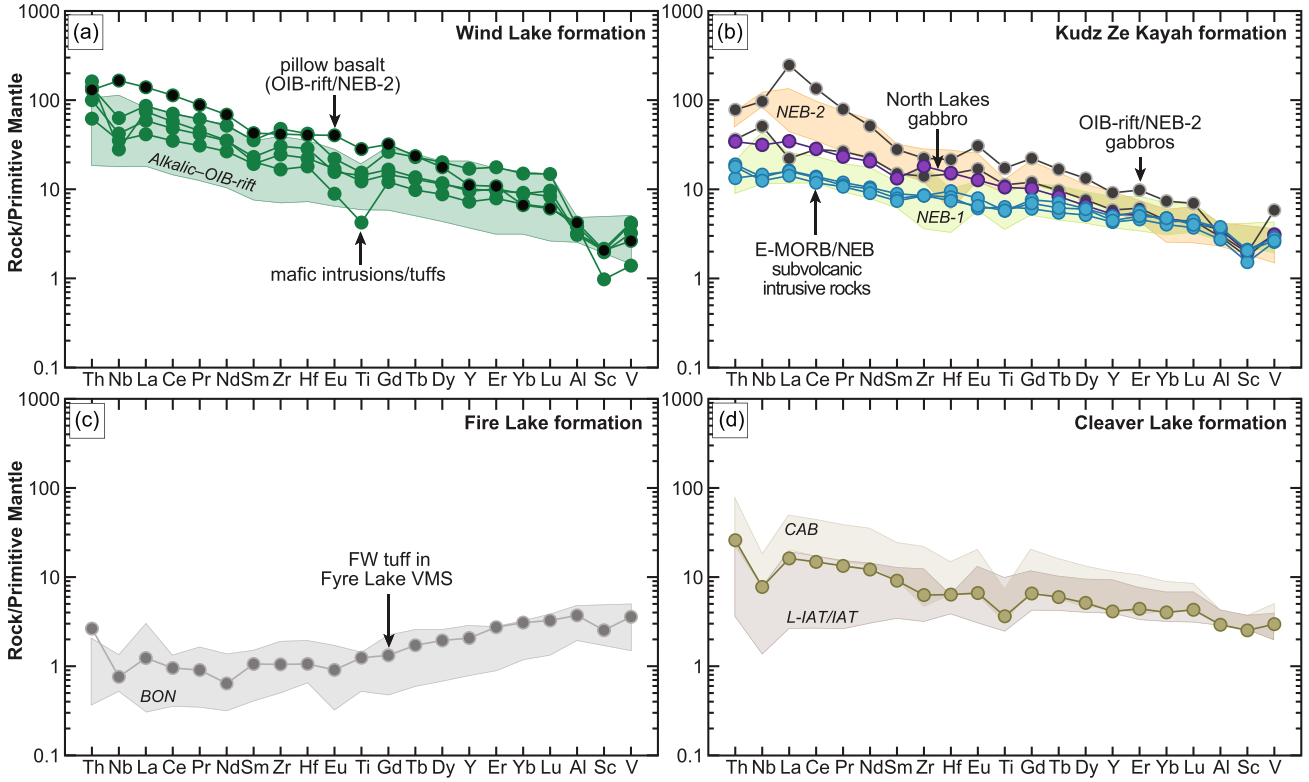

FIGURE 14: Immobile trace element diagrams for mafic rocks in the Finlayson Lake region, normalized to primitive mantle [90]. Shaded fields represent archival data with interpreted magmatic affinities (cf. references in Figure 10): (a) Wind Lake formation; (b) Kudz Ze Kayah formation; (c) Fire Lake formation. NEB = Nb-enriched basalt (after [48]); CAB = calc-alkaline basalt; L-IAT = LREE-enriched island arc tholeiite.

show relatively higher Nb/Y (1.3–1.6) and Ti/V (43–52) ratios indicative of an alkalic affinity (Figures 10(b) and 10(d)); results for these samples plot near the OIB field (Figures 11(d) and 11(e)). The primitive mantle-normalized diagrams for the subvolcanic intrusive rocks show relatively shallow patterns with slightly higher LREE over HREE (La/Yb_{PM} = 3–4), near-neutral Eu and slight negative Nb abundances (Eu/Eu^*_{PM} = 0.88 – 0.96; Nb/Nb^*_{PM} = 0.19 – 0.24). Patterns for gabbroic rocks are steeper (La/Yb_{PM} = 5 – 34) and have higher Nb anomalies (Nb/Nb^*_{PM} = 0.5 – 1.9; Figure 14(b)). Both lithologies show geochemical similarities to other Nb-enriched basalts to E-MORB-type mafic rocks in the district (Figure 14(b); [48, 53, 61]).

6.3.2. Wind Lake Formation. Mafic rocks from the Wind Lake formation have basalt and alkaline basalt to basaltic trachyandesite compositions (Figures 10(a) and 10(b)) and MORB/BABB to alkalic geochemical affinities (Ti/V = 30–160; Figure 10(d)) and straddle the subalkaline to alkaline boundary with Nb/Y = 0.42–2.3 (Figure 10(b)). A pillow basalt sample (17MM-054) gave higher Nb/Y, which falls within the alkaline field, and has elevated Nb/Yb and Th/Yb and plots over the non-arc mantle array; the rest of the mafic rocks are subalkaline and plot above the mantle array (Figure 11(d)). Primitive mantle-normalized diagrams show steep patterns for the mafic intrusions and tuffs with high La/Yb_{PM} (4.5–10) and negative Eu and Nb troughs (Eu/Eu^*_{PM} = 0.6 – 1.0; Nb/Nb^*_{PM} = 0.06 – 0.17); the pillow basalt (17MM-054) has a steeper pattern with a slight positive Eu and more elevated Nb abundance (La/Yb_{PM} = 21; Eu/Eu^*_{PM} = 1.1; Nb/Nb^*_{PM} = 0.3; Figure 14(a)). These are similar to non-arc basalts that have experienced variable crustal contamination (Figure 14(a); [61]). The felsic tuff sample (17MM-001) has higher SiO_2 (74 wt.%) and geochemical characteristics of group FN1 rocks with a trachytic composition (Figure 10(b)) and has an alkalic and peralkaline, within-plate geochemical affinity (Nb/Y = 0.76; Zr/Y = 14.2; Zr/Nb = 125; Figures 10 and 11). The upper continental crust-normalized pattern is relatively flat (La/Yb_{UCC} = 0.86) and overlaps with other within-plate, A-type felsic volcanic rocks in the district (Figure 13(b)).

6.3.3. North Lakes Intrusion. One gabbro (18MC-015) from the North Lakes intrusion has an alkaline basalt composition (Nb/Y = 0.9) and plots on the boundary between MORB/BABB and alkalic fields (Ti/V = 50; Figure 10(d)). The sample yields Th-Nb compositions that fall on the boundary of the non-arc mantle array (Figure 11(d)), between other non-arc mafic rocks in the district. The primitive mantle-normalized signature has a shallow slope with LREE-enrichment relative to HREE (La/Yb_{PM} = 7.4), slightly positive Eu (Eu/Eu^*_{PM} = 1.1), and negative Nb (Nb/Nb^*_{PM} = 0.2) anomalies, indicating these rocks have Nb-enriched basalt affinities (Figure 14(b)).

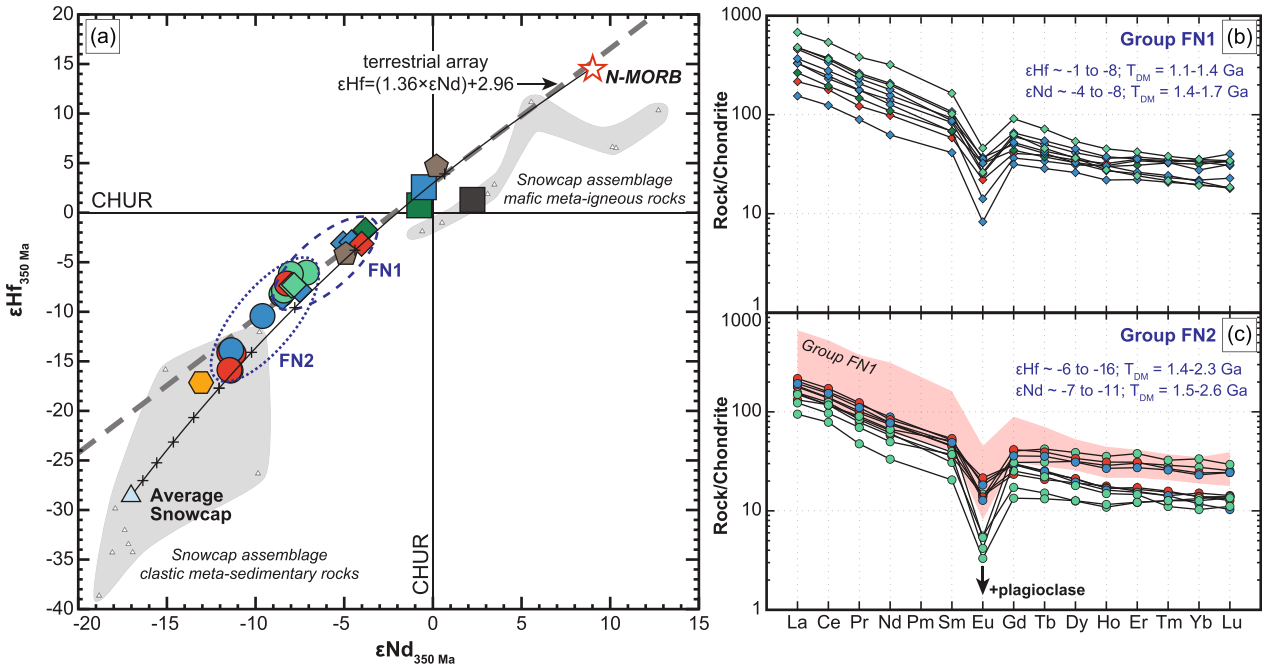

FIGURE 15: (a) εHf vs. εNd (age-corrected to 350 Ma) for mafic and felsic rocks throughout the Finlayson Lake district; (b) chondrite-normalized rare-earth element patterns for group FN1; (c) chondrite-normalized rare-earth element patterns for group FN2. The REE patterns are plotted normalized to Sun and McDonough [91]. Isotope signatures generally plot along the terrestrial array of Vervoort et al. [156] and form a mixing line between a depleted mantle source [83, 84] and metasedimentary rocks of the Snowcap assemblage [5]. A binary mixing curve is shown between N-MORB and average Snowcap assemblage compositions, where graticules are 10% increments. CHUR = chondritic uniform reservoir.

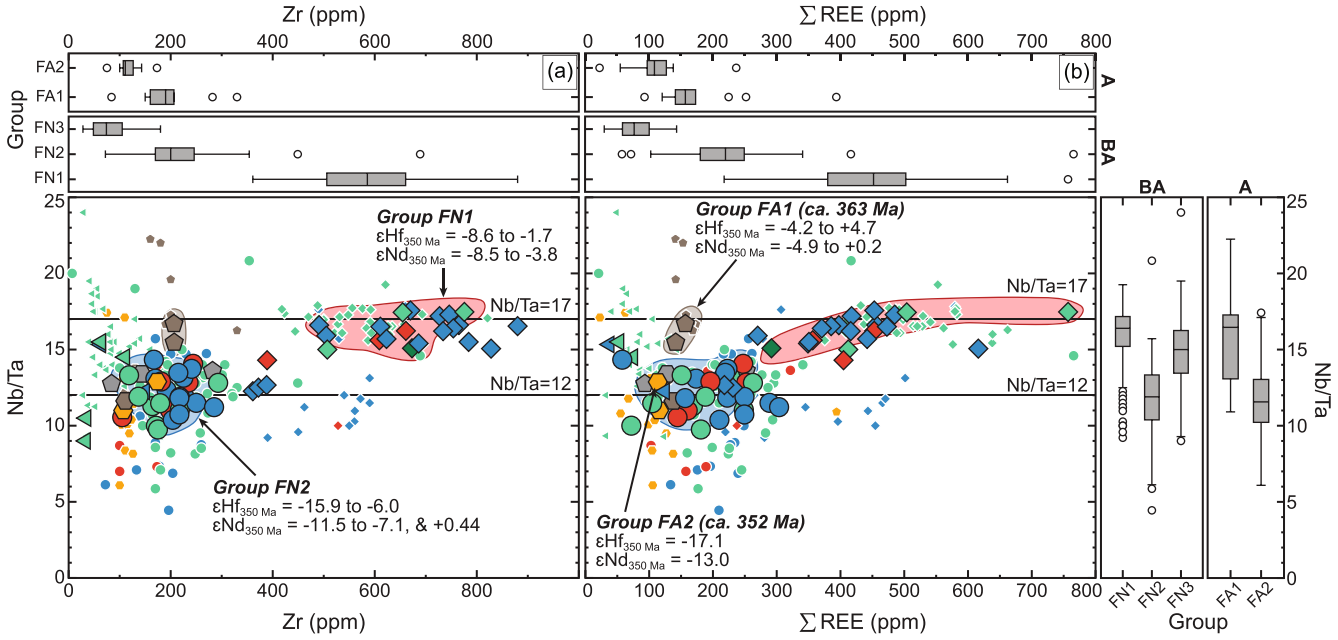

FIGURE 16: Nb/Ta versus (a) Zr and (b) sum of REEs. Reference lines are shown for Nb/Ta where values are ~12 for crust and ~17 for chondrite (i.e., mantle; [89, 98, 99]). Box and whisker plots for each geochemical variable (Nb/Ta, Zr, *ΣREE*) indicate the interquartile range of data in each geochemical group for back-arc (BA) and arc (A) rocks; open circles are outliers in the population. Note the significant increase in trace element concentrations and Nb/Ta ratios for group FN1 relative to group FN2 back-arc rocks. Colored shaded regions represent samples that also have complementary Hf-Nd isotopic compositions, which are also distinct between groups FN1 and FN2. Arc rocks in groups FA1 and FA2 also show a temporal distinction in both trace elements and isotopes, indicative of a transitional environment during the Late Devonian-Early Mississippian.

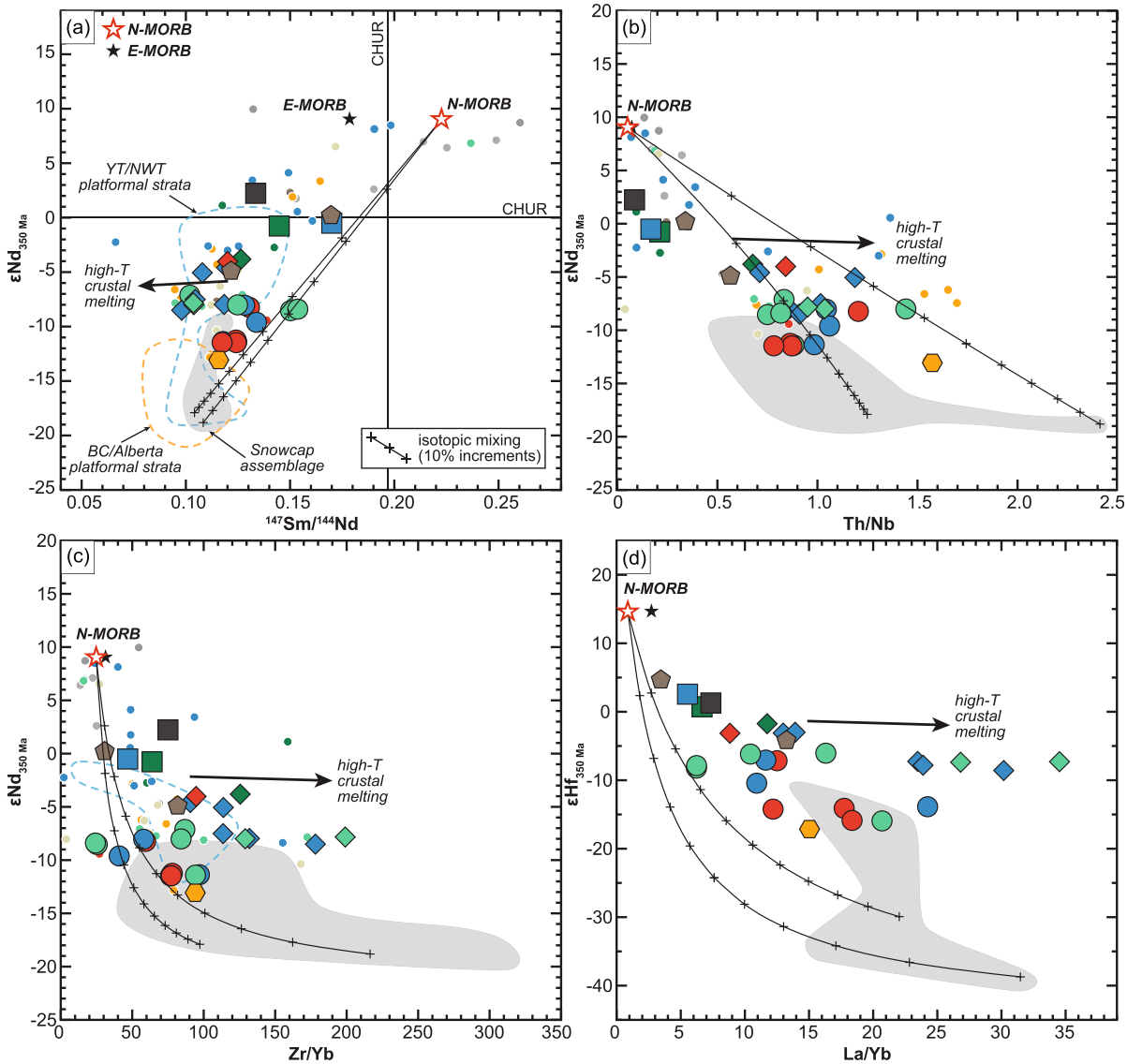

FIGURE 17: Isotope and trace element ratio mixing curves: (a) $\varepsilon Nd_{350\ Ma}$ vs. $^{147}Sm/^{144}Nd$; (b) $\varepsilon Nd_{350\ Ma}$ vs. Th/Nb; (c) $\varepsilon Nd_{350\ Ma}$ vs. Zr/Yb; (d) $\varepsilon Hf_{350\ Ma}$ vs. La/Yb. Endmembers are N-MORB (star), using trace element values from Sun and McDonough [91] and depleted mantle isotopic compositions as in Figure 15, and Snowcap assemblage (grey region; [5, 157, 158]). Dashed lines indicate location of samples from platformal strata of the North American ancenstral margin from Yukon-Northwest Territories (blue; [159]) and BC-Alberta (orange; [160]). Graticules on mixing curves are shown as 10% increments. Symbols and colors as in Figure 10. Data that fall significantly off the mixing curves are interpreted to be results of high-temperature crustal melting (see text for details).

6.3.4. Grass Lakes Plutonic Suite. Samples of the Grass Lakes plutonic suite come from a batholith-sized intrusion and high-level felsic porphyritic intrusive rocks (Figures 2 and 4). Samples from the granitic pluton have high SiO_2 (68–79 wt.%) and HFSE concentrations with within-plate signatures that are transitional to calc-alkaline (Nb/Y = 0.52 – 0.70 ; Zr/Y = 2.9 – 14; Figures 10(b), 10(c), and 10(e)) to slightly alkalic (Nb/Y = 0.70 – 0.80). The suite contains rocks with both FN1 and FN2 group characteristics similar to the Kudz Ze Kayah formation, where FN1 rocks have lower SiO_2 (<73 wt.%) and higher Zr (>390 ppm), Zr/Al_2O_3, Zr/Ti, and Zr/Nb than group FN2 rocks. Upper continental crust-normalized diagrams show distinct trends for the pluton (La/Yb_{UCC} = 0.64 – 0.92) and feldspar porphyritic dikes (La/Yb_{UCC} = 1.1 – 1.8); the dikes have FN1 affinities and contain slightly greater abundances of LREE than group FN2 granitoids. The HFSE and REE abundances for both groups overlap with rocks of the Kudz Ze Kayah formation, Grass Lakes plutonic suite, and Wolverine Lake group footwall (e.g., Eu/Eu^*_{UCC} = 0.4 – 0.9 ; Ti/Ti^*_{UCC} 0.03 – 0.1; Figures 13(b) and 13(c); [6, 45]).

6.4. Wolverine Lake Group

6.4.1. Little Jimmy and Little Wolverine Formations. The Wolverine Lake group samples (n = 12) consist of a lower quartzofeldspathic grit (17MM-004) in the Little Jimmy formation and volcaniclastic rocks (n = 7), a quartz-feldspar

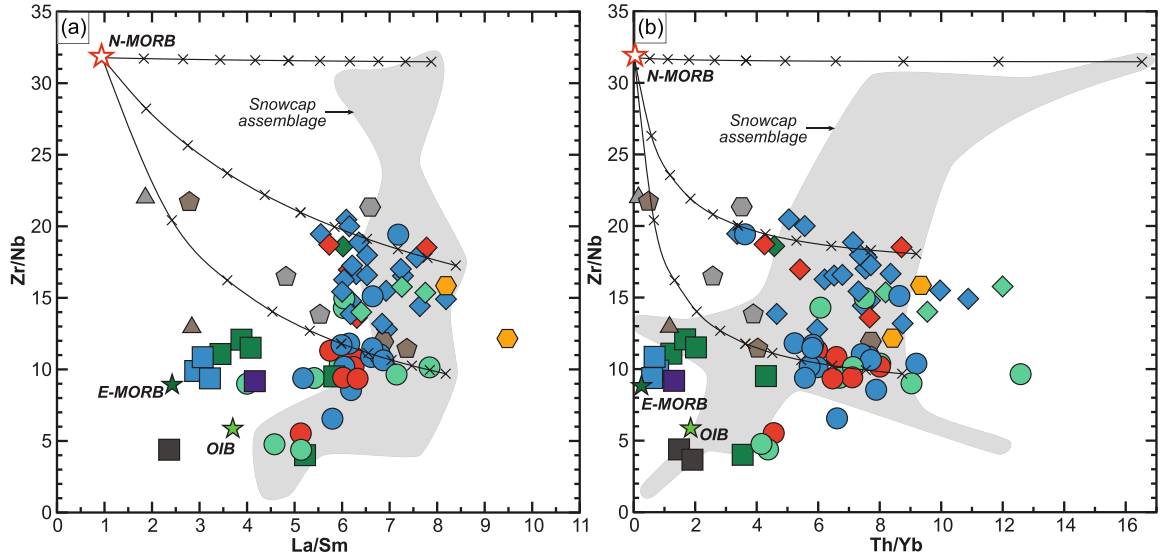

FIGURE 18: Trace element ratio mixing curves: (a) Zr/Nb vs. La/Sm; (b) Zr/Nb vs. Th/Yb. The binary mixing scenario of N-MORB and Snowcap assemblage endmembers (as in Figure 15) is shown as mixing curves with 10% increments. However, this scenario does not necessarily correspond to all rocks in the Finlayson Lake district, and different mixing lines are likely possible where geochemical signatures of mafic melts are mixtures of N-MORB and OIB or E-MORB.

porphyritic intrusive rock (QFP), and feldspar porphyritic intrusive rocks (FP; $n = 3$) from the Little Wolverine formation. Two distinct groupings comprise the geochemical signatures of these rocks, similar to the Kudz Ze Kayah formation: (1) group FN1, which contains only FP intrusive rocks in the upper footwall nearest to VMS mineralization, and (2) group FN2, which contains the basal grit, volcaniclastic, and intrusive rocks throughout the Little Jimmy and Little Wolverine formations. Group FN1 rocks have moderate to high SiO_2 (58–77 wt.%), peralkaline to alkaline trachyte and rhyolite with high Zr/Y (>10), within-plate (Nb/Y = 0.9–1.1), and mostly FI rhyolite affinities (Figure 12(b)) and have high Nb/Ta (15–17.5). Group FN2 rocks have high SiO_2 (75–80 wt.%), fall in the andesite/basalt, trachyandesite, and trachyte fields and contain both within-plate A-type and I-type signatures (Nb/Y = 0.5–1.1; Figure 10(b)), and have tholeiitic to calc-alkaline Zr/Y (2.5–11) and FI, FII, and FIIIa affinities and lower Nb/Ta than rocks in group FN1 (10–13). The upper continental crust-normalized patterns for group FN1 show more abundant REE relative to group FN2 (La/Yb_{UCC}: FN1 = 1.8 – 2.5, mean = 2.1 ; FN2 = 0.5 – 1.5, mean = 1.0), with relatively similar, flat LREE (La/Sm_{UCC} = 1.0 – 1.2 vs. 0.7–1.2, respectively) and steeper HREE slopes (Gd/Lu_{UCC} = 1.3 – 2.3, mean = 1.8) than in group FN2 (Gd/Lu_{UCC} = 0.7 – 1.1, mean = 1.1; Figure 13(a)). Negative Ti and Eu anomalies are similar in group FN1 and FN2 rocks, where Ti/Ti^*_{UCC} = 0.05–0.06 and 0.02–0.07, and Eu/Eu^*_{UCC} = 0.5–0.6 and 0.2–1.0, respectively (Figure 13(a)).

6.4.2. Go Creek Formation. Four samples from the Go Creek formation have distinct geochemical signatures (FN3; e.g., [46] Figures 10–12). The rocks are typically strongly quartz-altered (>83 wt.% SiO_2) that are classified as andesite to basalt (Figure 10(b)), with transitional to calc-alkalic (Zr/Y = 4–12) and volcanic arc, I-type to M-type affinities (Nb/Y < 0.6; Figure 10(b)). They have low Zr/Ti and Zr/Nb (i.e., Zr < 110 ppm) and chondrite-normalized REE (e.g., La/Yb_C vs. Yb_C) signatures that are different than the Little Jimmy and Little Wolverine formations and have arc-like signatures similar to volcanic rocks from the Cleaver Lake thrust sheet (see text below; Figure 13(a)). Upper continental crust-normalized immobile element signatures show flat patterns with slightly positive slopes, but with more depleted abundances compared to the Little Wolverine formation (La/Yb_{UCC} = 0.4 – 1.3). The patterns show neutral to positive Eu anomalies (Eu/Eu^*_{UCC} = 0.9 – 1.3, mean = 1.1) and less negative Ti (Ti/Ti^*_{UCC} = 0.08–0.18, mean = 0.13) that contrast with those lower values from the footwall (Figure 13(a)).

6.5. Cleaver Lake Thrust Sheet

6.5.1. Cleaver Lake Formation. Felsic flows and porphyritic intrusive rocks ($n = 3$) from the Cleaver Lake formation are andesite to rhyolite; two samples (18MM-108 and P99-45) plot as calc-alkalic rhyolites and straddle the subalkaline-alkaline boundary as rhyolite/dacite to trachyandesite (Nb/Y = 0.7 – 0.9), and the third (P99-39) plots as a transitional andesite with a much lower Nb/Y (0.2; Figure 10(b)). The calc-alkalic rhyolites have volcanic arc-like Nb-Y signatures with I-type affinities, whereas the andesite plots in the ocean-ridge (OR-type) field (Figure 10(c)). The upper continental crust-normalized patterns show distinct trends for the andesite, which shows a positive slope with greater HREE relative to LREE (La/Yb_{UCC} = 0.3), compared to the calc-alkalic rhyolites (La/Yb_{UCC} = 1.0 – 1.3), yet HREE show similar, flat patterns (Gd/Lu_{UCC} = ~0.9) where the transitional rocks have more abundant HREE (Figure 13(e)). All three of these rocks have a prominent negative Ti trough (Ti/Ti^*_{UCC} = 0.04 – 0.09),

but the calc-alkalic rocks have negative Eu anomalies compared to a slight positive signature in the transitional rock (Eu/Eu^*_{UCC} = 0.8–1.0 vs. 1.1, respectively). These signatures overlap with those of calc-alkalic to tholeiitic arc rocks from both the Cleaver Lake and Fire Lake formations [45].

One mafic augite porphyritic rock (18MM-109) has a basaltic composition that plots as a transitional island arc tholeiite (IAT; Nb/Y = 0.3 ; Zr/Y = 3.7 ; Ti/V = 18; Figure 10). The rock sample has a Th-Nb composition that plots above the non-arc mantle array, interpreted to indicate contributions from a subducting slab in an arc environment (Figure 11(d)). The primitive mantle-normalized diagrams show elevated LREE over HREE (La/Yb_{PM} = 4.0) and distinct negative Nb and Ti (Nb/Nb^*_{PM} = 0.1 ; Ti/Ti^*_{PM} = 0.1) and slightly negative Eu anomalies (Eu/Eu^*_{PM} = 0.86; Figure 14(d)), characteristic of IAT affinity rocks (e.g., [48]).

6.5.2. Simpson Range Plutonic Suite. A hornblende granodiorite (P99-24) and monzogranite (18MM-107) from the Simpson Range plutonic suite have moderate SiO_2 contents (65–69 wt.%) with subalkaline affinities (Nb/Y = ~ 0.7; Figure 10(b)). The rocks are calc-alkalic (Zr/Y = 8–11), fall within the volcanic arc (I-type) field, and typically have Zr contents < 180 ppm and Nb < 11 ppm that correspond to low Zr/Ti (0.03–0.04) and high Zr/Nb (12–16). The upper continental crust-normalized diagrams have relatively flat patterns (La/Yb_{UCC} = 1.1 – 1.5) with slight negative Nb and Ti (Nb/Nb^*_{UCC} = ~ 0.2; Ti/Ti^*_{UCC} = ~ 0.2) and positive Eu anomalies (Eu/Eu^*_{UCC} = 1.0 – 1.3; Figure 13(f)).

7. Whole-Rock Hf-Nd Isotope Geochemistry

Whole-rock Hf and Nd isotopic compositions (n = 28) were measured for rocks in the Fire Lake, Big Campbell, and Cleaver Lake thrust sheets from the Finlayson Lake district (Tables 3 and 4; Figure 15). The results below are presented by thrust sheet, then in order of stratigraphically lowest to highest. In the Fire Lake thrust sheet, a Permian felsic dike that crosscuts mafic volcaniclastic rocks in the Kona VMS deposit hanging wall gave εHf_i and εNd_i of –4.7 and –7.3, respectively. In the Grass Lakes group, a mafic intrusive rock in the lowest stratigraphic levels of the Kudz Ze Kayah formation (17MM-056; previously mapped as Fire Lake formation) has a juvenile isotopic composition (εHf_i = +1.5 ; εNd_i = +2.4). Felsic rocks from the Kudz Ze Kayah formation (n = 8) gave a range of evolved isotopic compositions of εHf_i = –13.7 to – 2.8 and εNd_i = –11.2 to –4.5. Rocks in the immediate hanging wall and footwall of VMS deposits (e.g., Kudz Ze Kayah and GP4F) have more chondritic isotopic compositions (εHf_i = –7.0 to – 2.9 ; εNd_i = –7.3 to –4.9) relative to those rocks highest in the hanging wall (17MM-002), where εHf_i and εNd_i are –13.7 and –11.2, respectively. A mafic subvolcanic intrusive rock in the footwall of the Kudz Ze Kayah deposit (17MM-060) gave near-chondritic εHf_i = +2.7 and εNd_i = –0.5. Rocks of the Wind Lake formation were sampled either as felsic (17MM-001) or mafic (17MM-003) volcaniclastic rocks. The range of isotope values constrained to near-chondritic relative to the Kudz Ze Kayah formation, yielding εHf_i from –1.6 to +2.7 and εNd_i from –3.7 to –0.5, where the felsic tuff (17MM-001) has the most negative value. Granitoids from the Grass Lakes plutonic suite (n = 5) give the largest range of evolved isotopic compositions across the district (εHf_i = –15.7 to – 3.0 ; εNd_i = –11.4 to –3.9).

In the Wolverine Lake group, the basal quartzofeldspathic grit (17MM-004; Little Jimmy formation) yielded the most evolved isotopic compositions of the unit (εHf_i = –15.8 ; εNd_i = –11.3), which broadly overlap with rocks in the Kudz Ze Kayah formation and Grass Lakes plutonic suite. Four samples from the Little Wolverine formation give restricted, evolved isotope compositions (εHf_i = –8.1 to – 6.0 ; εNd_i = –8.5 to –7.0) that overlap with feldspar porphyritic rhyolites (n = 2) from the Wolverine/Lynx zone (εHf_i = –7.3 ; εNd_i = –7.9) and the Fisher zone (εHf_i = –7.9 ; εNd_i = –7.8).

Three samples from the Cleaver Lake thrust sheet include felsic volcanic rocks of the Cleaver Lake formation (n = 2) and a hornblende granodiorite from the Simpson Range plutonic suite (n = 1). The Hf and Nd isotopic compositions for the Cleaver Lake formation are generally chondritic and correspond to the geochemical affinity of the rocks. Sample P99-39 is of tholeiitic affinity and yields juvenile isotope compositions (εHf_i = +4.8 ; εNd_i = +0.25) relative to P99-45, which is of calc-alkaline affinity and gives evolved values (εHf_i = –4.0 ; εNd_i = –4.8). The Simpson Range plutonic suite granodiorite yields a much more evolved isotopic signature where εHf_i and εNd_i are –17.1 and –13.1, respectively.

8. Regional Geochemical Group Discrimination

Felsic and mafic rocks in the Finlayson Lake district have been subdivided into distinct groups based on their immobile major and trace element concentrations and isotopic compositions (Figure 12). The characteristics of each group are defined by least-altered, precursor rocks with distinct trends in immobile ratio-ratio diagrams (e.g., Figure 12). These groupings are also discussed in terms of stratigraphic packages in the Finlayson Lake district. There are multiple precursor rocks within each rock package, but for the scope of this paper, the details of the causes of these multiple populations are not fully evaluated.

In the Big Campbell thrust sheet, rocks of non-arc affinity (i.e., back-arc) are divided into felsic groups FN1, FN2, and FN3 and mafic group MN1 (Figure 12). Groups FN1 and FN2 comprise rocks of non-arc affinity (i.e., back-arc) and contain most volcanic and plutonic rocks in the Grass Lakes and Wolverine Lake groups (Figure 12). Group FN1 felsic rocks have high HFSE (e.g., Zr > 360 ppm) and REE, low Al_2O_3, similar TiO_2, and less evolved εHf and εNd (>–8) compared to the FN2 group (εHf and εNd < –8). The FN3 group, however, contains Go Creek formation rocks that have arc-related geochemical affinities, despite being located immediately above FN1 and FN2 rocks in non-arc stratigraphy (Figures 4 and 5); these signatures have been attributed to either derivation from extrabasinal arc sources or significant crustal contamination of non-arc magmas [7, 45]. The group FN3 rocks have the lowest Zr (<150 ppm), HFSE, and REE contents of all felsic rocks in the district, Zr/Al_2O_3 like group

Table 3: Whole-rock MC-ICP-MS Lu-Hf isotopic results for rocks in the Finlayson Lake district, Yukon.

Sample	Unit*	Rock type†	UTME§	UTMN§	Age	Group#	Hf ppm**	Lu ppm**	$^{176}Hf/^{177}Hf_m$	2s	εHf_m	$^{176}Lu/^{177}Hf$	$^{176}Hf/^{177}Hf_i$††	εHf_i††	2s	T_{DM}§§	Hf − MORB##	Hf − crust##
17MM-004	LJ	FS	429446	6812106	357.6	FN2	4.50	0.28	0.282171	0.000009	-21.71	0.0087	0.282113	-15.82	0.01	1.81	0.55	0.45
P00-WV-1	LW	FI-HP	439618	6811350	355.2	FN1	18.78	0.87	0.282399	0.000005	-13.66	0.0065	0.282356	-7.27	0.00	1.33	0.74	0.26
P00-WV-11C	LW	FI-HP	434456	6818760	354.9	FN1	14.83	0.47	0.282387	0.000006	-14.06	0.0044	0.282358	-7.20	0.00	1.28	0.74	0.26
98DM-189	LW	FV	435625	6812350	356	FN2	5.36	0.35	0.282453	0.000009	-11.75	0.0090	0.282392	-5.95	0.01	1.35	0.76	0.24
P98-102	LW	FV	439390	6807680	356	FN2	5.04	0.34	0.282451	0.000004	-11.81	0.0093	0.282389	-6.08	0.01	1.37	0.76	0.24
P98-130	LW	FV	434100	6810000	356	FN2	3.99	0.64	0.282479	0.000004	-10.83	0.0224	0.282329	-8.19	0.01	2.29	0.73	0.27
P98-145	LW	FV	434900	6809300	356	FN2	4.59	0.74	0.282492	0.000004	-10.38	0.0227	0.282340	-7.81	0.01	2.30	0.73	0.27
17MM-001	WL	FV	413749	6815933	360.9	FN1	16.50	0.86	0.282563	0.000008	-7.85	0.0073	0.282514	-1.55	0.01	1.10	0.83	0.17
17MM-003	WL	MV	412065	6816318	360.9	MN1	6.30	0.56	0.282667	0.000006	-4.18	0.0124	0.282583	0.89	0.01	1.11	0.86	0.14
17MM-002	KZK	FV	413907	6815182	362.4	FN2	5.20	0.26	0.282218	0.000007	-20.04	0.0070	0.282171	-13.65	0.01	1.64	0.61	0.39
17MM-031	KZK	FV	415049	6815467	362.8	FN1	12.30	0.58	0.282403	0.000005	-13.51	0.0066	0.282358	-7.02	0.01	1.33	0.74	0.26
17MM-033	KZK	FV	415049	6815467	362.8	FN1	18.80	1.02	0.282526	0.000008	-9.14	0.0076	0.282475	-2.89	0.01	1.17	0.81	0.19
17MM-060	KZK	MI-H	415122	6814798	362.8	MN1	2.70	0.30	0.282739	0.000007	-1.62	0.0156	0.282633	2.72	0.01	1.09	0.89	0.11
17MM-074	KZK	FV	419500	6813355	363.3	FN2	7.50	0.62	0.282441	0.000009	-12.17	0.0116	0.282362	-6.87	0.01	1.50	0.75	0.25
P98-19	KZK	FV	427643	6798057	362.8	FN1	12.39	0.80	0.282403	0.000005	-13.51	0.0090	0.282342	-7.60	0.01	1.44	0.73	0.27
P98-24	KZK	FI-H	426400	6806870	362.8	FN2	4.04	0.46	0.282374	0.000008	-14.54	0.0159	0.282266	-10.28	0.01	1.91	0.68	0.32
P98-26	KZK	FV	426100	6807400	362.8	FN1	12.55	0.78	0.282537	0.000007	-8.75	0.0088	0.282478	-2.77	0.01	1.20	0.81	0.19
P98-52	KZK	FI-H	393911	6811945	362.8	FN1	14.62	0.46	0.282351	0.000004	-15.35	0.0044	0.282321	-8.33	0.01	1.33	0.72	0.28
17MM-005	GLPS	FI	429291	6812095	360.9	FN2	5.50	0.36	0.282223	0.000008	-19.89	0.0092	0.282161	-14.05	0.01	1.75	0.60	0.40
17MM-062	GLPS	FI-HP	415122	6814798	361.9	FN2	7.70	0.62	0.282436	0.000008	-12.33	0.0113	0.282360	-6.97	0.01	1.49	0.75	0.25
P98-39	GLPS	FI	430100	6806650	361	FN2	4.70	0.32	0.282228	0.000004	-19.71	0.0094	0.282164	-13.93	0.01	1.76	0.60	0.40
P98-40	GLPS	FI	429750	6811450	361	FN2	4.30	0.33	0.282187	0.000008	-21.16	0.0107	0.282114	-15.70	0.01	1.91	0.55	0.45
P98-42	GLPS	FI	432000	6807050	361	FN1	12.49	0.85	0.282538	0.000007	-8.74	0.0095	0.282474	-2.96	0.01	1.23	0.81	0.19
17MM-047	Dike in FL	FI	419346	6788812	264	FA1	1.80	0.29	0.282651	0.000008	-4.72	0.0226	0.282539	-2.79	0.19	1.80	NA	NA
17MM-056	FL?	MI	411343	6811450	364	MN1	4.20	0.30	0.282667	0.000017	-4.19	0.0100	0.282598	1.51	0.06	1.02	0.87	0.13
P99-24	SRPS	FI	428487	6793907	352.1	FA2	4.52	0.30	0.282141	0.000003	-22.79	0.0092	0.282080	-17.10	0.01	1.89	0.52	0.48
P99-39	CL	FV	426200	6794195	363.2	FA1	5.38	0.91	0.282851	0.000005	2.34	0.0236	0.282690	4.75	0.00	1.27	0.91	0.09
P99-45	CL	FV	424931	6793923	363.2	FA1	4.71	0.42	0.282528	0.000004	-9.10	0.0124	0.282443	-4.01	0.00	1.38	0.79	0.21

*LJ = Little Jimmy formation; LW = Little Wolverine formation; WL = Wind Lake formation; KZK = Kudz Ze Kayah formation; GLPS = Grass Lakes plutonic suite; FL = Fire Lake formation; SRPS = Simpson Range plutonic suite; CL = Cleaver Lake formation. †Rock type: FS = felsic sedimentary rock; FV = felsic volcanic/volcaniclastic rock; FI-HP = felsic high-level porphyritic intrusive rock; FI-H = felsic high-level intrusive rock; FI = felsic intrusion or pluton; MV = mafic volcaniclastic rock; MI = mafic intrusive rock; MI-H = mafic high-level intrusive rock. §Coordinates for samples beginning with the prefix "17MM" are in NAD83; all other samples are reported as NAD27. #Groups presented as the geochemical group (e.g., FN2) following groupings detailed in the text and Figure 10. **Hf and Lu concentrations from UBC-PCIGR measurements except for 17MM samples, which are from ALS (see text and Table S3). ††Initial Hf isotopic compositions calculated using $\lambda = 1.87 \times 10^{-11}$ [163], and present-day CHUR values of $^{176}Hf/^{177}Hf = 0.282785$ and $^{176}Lu/^{177}Hf = 0.0336$ [81]. §§Depleted mantle model ages (T_{DM}) are calculated using $^{176}Hf/^{177}Hf = 0.283238$ and $^{176}Lu/^{177}Hf = 0.03976$ [83]. ##Endmembers used in binary mixing calculations are N-MORB: $\varepsilon Hf = +14.6$ and Hf = 2.05 ppm ([91]; [83]) and average Snowcap assemblage: $\varepsilon Hf = -28.6$ and Hf = 6.1 ppm [5].

Table 4: Whole-rock MC-ICP-MS Sm-Nd isotopic results for rocks in the Finlayson Lake district, Yukon.

Sample	Unit*	Rock type†	UTME§	UTMN§	Age	Group#	Nd ppm**	Sm ppm**	$^{143}Nd/^{144}Nd_m$	2s	εNd_m	$^{147}Sm/^{144}Nd$	$^{143}Nd/^{144}Nd_i$††	εNd_i††	2s	T_{DM}§§	Nd-MORB##	Nd-crust##
17MM-004	LJ	FS	429446	6812106	357.6	FN2	30.00	6.05	0.511888	0.000007	-14.63	0.1244	0.511597	-11.34	0.01	2.14	0.54	0.46
P00-WV-1	LW	FI-HP	439618	6811350	355.2	FN1	149.58	25.17	0.512016	0.000007	-12.14	0.1038	0.511774	-7.93	0.00	1.55	0.69	0.31
P00-WV-11C	LW	FI-HP	434456	6818760	354.9	FN1	93.22	15.65	0.512023	0.000008	-11.99	0.1036	0.511783	-7.77	0.00	1.54	0.70	0.30
98DM-189	LW	FV	435625	6812350	356	FN2	28.24	4.66	0.512056	0.000007	-11.35	0.1019	0.511819	-7.04	0.01	1.47	0.72	0.28
P98-102	LW	FV	439390	6807680	356	FN2	15.38	3.11	0.512063	0.000008	-11.22	0.1248	0.511772	-7.96	0.01	1.84	0.69	0.31
P98-130	LW	FV	434100	6810000	356	FN2	23.07	5.62	0.512094	0.000007	-10.61	0.1502	0.511744	-8.50	0.01	2.52	0.67	0.33
P98-145	LW	FV	434900	6809300	356	FN2	30.81	7.68	0.512109	0.000008	-10.32	0.1537	0.511751	-8.37	0.01	2.64	0.68	0.32
17MM-001	WL	FV	413749	6815933	360.9	FN1	51.00	10.45	0.512282	0.000006	-6.95	0.1264	0.511983	-3.71	0.01	1.49	0.81	0.19
17MM-003	WL	MV	412065	6816318	360.9	MN1	33.20	7.79	0.512480	0.000007	-3.09	0.1448	0.512138	-0.70	0.01	1.45	0.88	0.12
17MM-002	KZK	FV	413907	6815182	362.4	FN2	41.10	7.85	0.511875	0.000006	-14.88	0.1178	0.511595	-11.24	0.01	2.01	0.54	0.46
17MM-031	KZK	FV	415049	6815467	362.8	FN1	73.50	14.10	0.512050	0.000006	-11.46	0.1184	0.511769	-7.84	0.01	1.74	0.69	0.31
17MM-033	KZK	FV	415049	6815467	362.8	FN1	59.20	10.35	0.512175	0.000008	-9.03	0.1079	0.511919	-4.92	0.01	1.38	0.78	0.22
17MM-060	KZK	MI-H	415122	6814798	362.8	MN1	13.10	3.61	0.512551	0.000006	-1.70	0.1700	0.512147	-0.47	0.01	NA	0.88	0.12
17MM-074	KZK	FV	419500	6813355	363.3	FN2	36.10	7.50	0.512069	0.000007	-11.09	0.1282	0.511765	-7.92	0.01	1.90	0.69	0.31
P98-19	KZK	FV	427643	6798057	362.8	FN1	96.94	16.41	0.512042	0.000007	-11.63	0.1045	0.511794	-7.36	0.01	1.52	0.71	0.29
P98-24	KZK	FI-H	426400	6806870	362.8	FN2	29.17	6.33	0.512002	0.000009	-12.41	0.1339	0.511684	-9.51	0.01	2.18	0.63	0.37
P98-26	KZK	FV	426100	6807400	362.8	FN1	65.82	12.75	0.512226	0.000006	-8.04	0.1195	0.511942	-4.47	0.01	1.47	0.79	0.21
P98-52	KZK	FI-H	393911	6811945	362.8	FN1	83.58	13.27	0.511976	0.000007	-12.91	0.0980	0.511744	-8.34	0.01	1.52	0.67	0.33
17MM-005	GLPS	FI	429291	6812095	360.9	FN2	26.90	5.41	0.511896	0.000007	-14.48	0.1241	0.511602	-11.14	0.01	2.12	0.55	0.45
17MM-062	GLPS	FI-HP	415122	6814798	361.9	FN2	38.90	8.23	0.512064	0.000006	-11.19	0.1305	0.511755	-8.14	0.01	1.97	0.68	0.32
P98-39	GLPS	FI	430100	6806650	361	FN2	34.52	6.95	0.511884	0.000006	-14.71	0.1242	0.511590	-11.38	0.01	2.14	0.53	0.47
P98-40	GLPS	FI	429750	6811450	361	FN2	35.71	6.79	0.511869	0.000007	-15.00	0.1174	0.511591	-11.36	0.01	2.01	0.53	0.47
P98-42	GLPS	FI	432000	6807050	361	FN1	45.95	8.94	0.512256	0.000007	-7.44	0.1200	0.511973	-3.91	0.01	1.43	0.81	0.19
17MM-047	Dike in FL	FI	419346	6788812	264	FA1	17.10	3.59	0.512262	0.000010	-7.33	0.1295	0.512038	-5.06	0.21	1.58	NA	NA
17MM-056	FL?	MI	411343	6811450	364	MN1	28.20	6.10	0.512607	0.000007	-0.60	0.1335	0.512289	2.34	0.07	0.99	0.92	0.08
P99-24	SRPS	FI	428487	6793907	352.1	FA2	18.00	3.38	0.511783	0.000008	-16.67	0.1158	0.511516	-13.05	0.01	2.11	0.43	0.57
P99-39	CL	FV	426200	6794195	363.2	FA1	30.28	8.32	0.512586	0.000007	-1.01	0.1696	0.512183	0.25	0.00	NA	0.89	0.11
P99-45	CL	FV	424931	6793923	363.2	FA1	23.05	4.55	0.512214	0.000007	-8.26	0.1217	0.511925	-4.79	0.00	1.52	0.79	0.21

*LJ = Little Jimmy formation; LW = Little Wolverine formation; WL = Wind Lake formation; KZK = Kudz Ze Kayah formation; GLPS = Grass Lakes plutonic suite; FL = Fire Lake formation; SRPS = Simpson Range plutonic suite; CL = Cleaver Lake formation. †Rock type: FS = felsic sedimentary rock; FV = felsic volcanic/volcaniclastic rock; FI-HP = felsic high-level porphyritic intrusive rock; FI-H = felsic high-level intrusive rock; FI = felsic intrusion or pluton; MV = mafic volcaniclastic rock; MI = mafic intrusive rock; MI-H = mafic high-level intrusive rock. §Coordinates for samples beginning with the prefix "17MM" are in NAD83; all other samples are reported as NAD27. #Groups presented as geochemical group (e.g., FN2) following groupings detailed in the text and Figure 10. **Nd and Sm concentrations from UBC-PCIGR measurements except for 17MM samples, which are from ALS (see text and Table S3). ††Initial Nd isotopic compositions calculated using $\lambda = 6.54 \times 10^{-12}$ and present-day CHUR values of $^{143}Nd/^{144}Nd = 0.512638$ [80] and $^{147}Sm/^{144}Nd = 0.1967$ [82]. §§Depleted mantle model ages (T_{DM}) are calculated using $^{143}Nd/^{144}Nd = 0.513113$ and $^{147}Sm/^{144}Nd = 0.2114$ [84]; results are not applicable (NA) if measured $^{147}Sm/^{144}Nd > 0.16$. ##Endmembers used in binary mixing calculations are N-MORB: $\varepsilon Nd = +9$ and Nd = 7.3 ppm ([91]; [84]) and average Snowcap assemblage (crust): $\varepsilon Nd = -17$ and Nd = 31 ppm [5].

Table 5: Modal abundances of accessory minerals in felsic volcanic and plutonic rocks in the Finlayson Lake district.

Sample	Group	Zircon	Apatite	Monazite	Xenotime	Rutile	Titanite	Allanite	Uraninite	Thorite
Wind Lake formation										
17MM-001	FN1	0.02	0.05	0.02	<0.01	0.29	<0.01	<0.01	0	0
Kudz Ze Kayah formation										
17MM-002	FN2	0.02	0.26	0.01	<0.01	<0.01	<0.01	<0.01	<0.01	<0.01
17MM-031	FN1	0.07	0.27	0.04	0.01	0.18	<0.01	<0.01	<0.01	0
18MM-133	FN1	0.08	0.29	0.04	<0.01	0.26	<0.01	0.01	<0.01	<0.01
17MM-074	FN2	0.02	0.13	0.01	<0.01	0.05	0.03	0.03	<0.01	<0.01
Wolverine Lake group										
18MM-102	FN1	0.04	0	0.03	<0.01	0.14	<0.01	0	<0.01	0
P00-WV-1C	FN1	0.07	0.20	0.05	<0.01	0.08	<0.01	<0.01	<0.01	<0.01
P99-WV-4K	FN1	0.04	0.16	0.03	<0.01	0.07	<0.01	<0.01	<0.01	<0.01
P00-WV-12	FN2	0.02	0.27	0.02	<0.01	<0.01	<0.01	<0.01	<0.01	<0.01
18MM-114	FN2	0.02	0.25	0.01	<0.01	0.01	0.04	0.05	<0.01	<0.01
Grass Lakes plutonic suite										
18MM-105	FN2	0.02	0.22	0.02	<0.01	0.11	0.01	0.01	<0.01	<0.01
17MM-005	FN2	0.01	0.27	0.01	<0.01	0.01	<0.01	0.04	<0.01	<0.01
17MM-061	FN1	0.06	0.31	0.03	<0.01	0.13	<0.01	<0.01	<0.01	0
17MM-062	FN2	0.02	0.15	0.01	<0.01	0.05	0.07	0.06	<0.01	<0.01
Simpson Range plutonic suite										
18MM-107	FA2	0.03	0.19	<0.01	0	<0.01	0.38	0.06	<0.01	<0.01
Cleaver Lake formation										
18MM-108	FA2	<0.01	<0.01	<0.01	<0.01	0.02	<0.01	<0.01	0	<0.01

Note: complete modal abundances (in area%) presented in Table S6.

FN2 rocks, distinct Th/Nb, but low Zr/Ti ratios most similar to arc-related felsic rocks in the Cleaver Lake thrust sheet. Group MN1 contains all mafic rocks in the non-arc environment that are characterized by high Ti/V (>20) and Zr/Y (>4; e.g., N-MORB, E-MORB, and OIB; Figures 10(d) and 10(f)).

In the Cleaver Lake thrust sheet, felsic rocks of arc affinity are split into groups FA1 and FA2, which are typically designated as the Cleaver Lake formation (ca. 363 Ma) and Simpson Range plutonic suite (ca. 354–349 Ma), respectively. Group FA1 felsic rocks have higher Zr, REE, Zr/Al_2O_3, and Zr/Ti, lower TiO_2, and less evolved εHf and ε Nd > −5 than group FA2. Arc-related mafic rocks in the Cleaver Lake formation comprise group MA1, which includes MORB to IAT-type mafic rocks that have similar Ti/V and Zr/Y to the non-arc mafic rocks.

In the Fire Lake thrust sheet, mafic rocks of arc affinity are separated into group MA2 (Figures 10(d) and 10(f)). This group contains mafic rocks of the Fire Lake formation that have boninite and IAT geochemical affinities that are characterized by low Ti/V (<20) and Zr/Y (<3; Figures 10(d) and 10(f)).

9. Mineral Liberation Analysis Results (MLA-SEM)

MLA-SEM imaging was completed on thin sections of back-arc and arc rocks in the Finlayson Lake district to test mineral abundances relative to geochemical results. All samples show varying modal abundances of HFSE-REE-bearing minerals that account for <0.7 vol.% of the total rock composition (Table 5; Table S6). Rocks in all groups contain between 0.13 and 0.31% apatite, except for the lowest abundances in 17MM-001 (0.05%), 18MM-102 (0%), and 18MM-108 (<0.01%). Group FN1 rocks contain greater abundances of rutile (0.07-0.29%), zircon (0.04-0.08%), and monazite (0.02-0.05%) relative to the FN2 group. Rocks in group FN2 contain between 0.03 and 0.06% titanite and allanite, whereas these minerals are <0.01% in group FN1 rocks. Xenotime, uraninite, and thorite are typically present as trace constituents below 0.01%. Two arc samples (group FA2) from the Cleaver Lake thrust sheet were analyzed, one monzogranite (18MM-107) and one quartz-porphyritic rhyolite (18MM-108). Sample 18MM-107 has high titanite (0.38%) and allanite (0.06%), with comparable zircon (0.03%) and apatite (0.19%) abundances to group FN2 rocks; all other minerals are traced below 0.01%. Sample 18MM-108, however, contains 0.02% rutile but trace abundances of all other accessory minerals (Table 5).

10. Discussion

10.1. Petrogenesis and Melt Sources of Yukon-Tanana Terrane Arc–Back-Arc Rocks

10.1.1. Petrogenesis of Mafic Rocks. The geochemical and isotopic signatures of mafic rocks in the Yukon-Tanana

terrane provide critical insight into the tectonomagmatic environment of formation, and relative roles that enriched lithospheric mantle, depleted asthenospheric mantle, slab metasomatism, and crustal contamination played in their genesis (Figure 11; [7, 61]). These various components will be evaluated below.

Deciphering the mantle component (i.e., enriched or depleted) in ancient mafic rocks requires utilization of elements (and isotopes) that are immobile, insensitive to fractional crystallization, and reflective of the mantle source regions and crustal contamination and/or slab metasomatism (e.g., [94, 95]). The immobile element ratios of Th/Yb, Nb/Yb, and TiO_2/Yb are useful for delineating mantle sources as these ratios are generally reflective of incompatible enrichment of a mantle source (i.e., MORB-OIB array in Figures 11(d) and 11(e); [94]); however, the Th/Yb ratio is also sensitive to crustal contamination and/or slab fluid components as they typically have higher Th/Yb ratios at a given Nb/Yb ratio and distinctive trajectories in Th/Yb-Nb/Yb space (Figure 11(d); [61, 94–97]). The mafic rocks found in the back-arc region of the Finlayson Lake district that plot predominantly within the MORB-OIB array in Th/Yb–Nb/Yb space (Figure 11(d)) are interpreted to be derived from variably enriched mantle sources. For example, rocks from the lower Kudz Ze Kayah formation have relatively depleted BABB (~N-MORB) signatures (e.g., [48]), the upper Kudz Ze Kayah formation have weakly enriched (~E-MORB) signatures, and the Wind Lake formation has highly enriched (~OIB-like) signatures; metagabbros of the North Lakes intrusion and the lower Kudz Ze Kayah formation (samples 17MM-056 and 17MM-057) plot between E-MORB and OIB (Figure 11(d)). Mafic rocks from the arc regions, however, include IAT affinity rocks of the Cleaver Lake formation and boninite to IAT signature rocks of the Fire Lake formation that plot above the MORB-OIB array proximal to E-MORB and N-MORB, respectively (Figure 11(d)). The variation in incompatible element enrichment between these various rocks potentially reflects mixing and varying contributions from depleted, N-MORB-like asthenospheric melts and enriched lithospheric mantle-derived melts (e.g., [7]). The Hf-Nd isotope results for these rocks support this hypothesis. In particular, the back-arc mafic rocks typically have $\varepsilon Hf_{350\,Ma} = +0.8$ to +2.6 and $\varepsilon Nd_{350\,Ma} = -0.8$ to +2.2 (Figures 12 and 14), which, in the case of Nd data, overlaps with the limited dataset of Piercey et al. [61] (Figure 15); however, several E-MORB basalts in the lowest stratigraphic levels of the Kudz Ze Kayah formation overlap with juvenile $\varepsilon Nd = +8.1$ [48]. Many of the samples with both near-chondritic and juvenile εHf and εNd have flat to positive Nb anomalies and the greatest incompatible element enrichment, indicative of rocks that have not seen slab metasomatism nor crustal contamination, suggesting that these isotopic values are a function of the incompatible element-enriched mantle source they were derived from. It is therefore suggested that (1) the near-chondrite Hf-Nd isotope signatures were generated from a mixture of depleted asthenospheric mantle and a component of preexisting and enriched lithospheric mantle [7, 48, 53] and (2) the juvenile Nd isotope signatures, particularly in the E-MORB samples (c.f., [48]), were generated from a nearly uncontaminated asthenospheric mantle source and erupted following little to no residence time in the lithospheric mantle. These geochemical and isotopic signatures are therefore distinct from other mafic rocks in the Finlayson Lake district that experienced crustal contamination, as evidenced by high Th/Yb and more evolved isotopic signatures (Figures 11(d)–11(f), and 15).

A subset of mafic rocks in the belt displays distinct geochemical ratios with $Nb/La_{PM} < 1$, $Nb/Th_{PM} < 1$, and elevated Th/Yb (Figures 12 and 14) indicative of either a subducting slab input or crustal contamination (Figure 11; [7]). Two boninite and IAT basalt samples from the Fire Lake and Cleaver Lake formations, respectively, have negative Nb anomalies and high Th/Nb, which are interpreted to be generated from the retention of Nb and enrichment of Th due to fluid mobilization from the subducting slab (e.g., Figures 11(d), 11(f), 14(c), and 14(d); [45, 48, 62, 95, 96]). These samples also overlap with rocks that have high εNd (+3 to +7; [48]) and are interpreted to have formed from primitive arc magmas that have not interacted with evolved continental crust. Further, the rocks with BABB signatures in the Kudz Ze Kayah formation also show negative Nb anomalies, slightly elevated Th/Yb, and high $\varepsilon Nd = +8.5$ (Figures 11(d) and 11(f); [48]), which is interpreted to indicate that back-arc affinity magmas were overprinted by a weak subduction signature. In contrast, other mafic rocks with back-arc affinities have high Th/Nb and Th/Yb, lower εHf and εNd (–1 to +3), and 1.0-1.4 Ga model ages (Tables 3 and 4), which suggested that the mafic melts interacted with continental crust (e.g., [61]).

These data illustrate that the mafic rocks in the Finlayson Lake district reflect varying contributions of asthenospheric mantle and continental lithospheric mantle that were overprinted by subducting slab or evolved continental crust components. These results also suggest that different crustal architectures in both the arc and back-arc environment generated the variable isotopic and trace element compositions of these mafic rocks. Back-arc mafic rocks, the exception of the lowest Kudz Ze Kayah formation (i.e., BABB and E-MORB), interacted with old subcontinental lithospheric mantle and/or continental crust during ascent, whereas arc rocks did not. Therefore, some components of evolved lithosphere should be expected during the formation of felsic rocks in the back-arc, which is explored below.

10.1.2. Petrogenesis of Felsic Rocks. Felsic rocks throughout the Finlayson Lake district have distinct geochemical and isotopic signatures that define them as arc or back-arc rocks (e.g., Nb/Y, Zr/Y, Zr/Ti, and SiO_2) and reflect varying contributions from evolved crust and juvenile mantle-derived components (e.g., Nb/Ta ~9-18; $\varepsilon Hf_{350\,Ma} = -17$ to +4; $\varepsilon Nd_{350\,Ma} = -13$ to +0.2; Figures 10, 15, and 16; [6, 7, 17, 45, 48, 61, 70]). Arc rocks from the Cleaver Lake thrust sheet have highly variable isotopic values ($\varepsilon Hf_{350\,Ma} = -17$ to +4; $\varepsilon Nd_{350\,Ma} = -13$ to +0.2) and show distinct crystallization ages, including (1) calc-alkalic to tholeiitic volcanic rocks of the Late Devonian Cleaver Lake

formation ($\varepsilon Hf_{350\ Ma} = -4$ to +5; $\varepsilon Nd_{350\ Ma} = -5$ to +0.2) and (2) calc-alkalic granitoids of the Early Mississippian Simpson Range plutonic suite ($\varepsilon Hf_{350\ Ma} = -17$; $\varepsilon Nd_{350\ Ma} = -13$; Figure 15). These suites of arc-related felsic rocks have a range in HFSE and REE contents from very depleted (tholeiitic rocks) to less depleted but significantly lower concentrations than the back-arc felsic rocks (e.g., Zr and $REE_{sum} < 200$ ppm; Figures 11 and 16), while having isotopic signatures that reflect influence from the variable crustal basement during Late Devonian and Early Mississippian magmatism. Back-arc rocks, however, illustrate a significant decoupling of Hf-Nd isotopes and HFSE-REE contents, where these signatures define two geochemical groups that underwent differing crustal melting processes (Figures 15–17). There is a positive relationship between εHf and εNd and HFSE-REE contents with the VMS-proximal FN1 suite rocks having the higher values when compared to the VMS-distal FN2 rocks. These features are attributed to the variable contributions of mantle and crustal materials, degrees of crustal assimilation, and temperatures of melting and emplacement and are explored further below.

The back-arc geochemical groups, FN1 and FN2, have isotopic and geochemical features that show evidence for contributions from both mantle and crustal sources; however, the degree of crustal melting and contributions from underplated basaltic magmas is variable (Figure 16). The variations in the basaltic/juvenile component are best recorded by (1) distinct Nb/Ta ratios (Figure 16), (2) bulk rock Hf-Nd isotopic compositions (Figure 15), and (3) Th/U in zircon (Figure 9(b)). The Nb/Ta values for group FN1 are ~17 (i.e., mantle-like), whereas FN2 values are ~12 (i.e., crustal-like; [17, 89, 98, 99]), and these also correspond with εHf and εNd values that are most juvenile (i.e., closest to chondrite—group FN1) and most evolved (group FN2; Figure 15), respectively. In zircon crystals, the highest Th/U (>1) are associated with samples that have εHf-εNd greater than ~−8 and Nb/Ta ~17 (e.g., sample 17MM-031, group FN1). However, some samples have very wide ranges in zircon Th/U in a single sample, such as in plutonic samples 96DM-065 and 18MM-105 that gave large ranges of Th/U between 0.4-2.3 and 0.3-2.2, respectively (Figure 9(b)). These variations could reflect mixing between juvenile and evolved magmas in the chamber; however, equally viable is that it reflects potentially varying degrees of disequilibrium crystallization where zircon crystallization is not controlled by specific partition coefficients in the melt (e.g., [100]). Even with the variability in Th/U in some samples, there is a general trend at both the whole rock and mineral scale of more juvenile and higher temperature magmatic rocks proximal to VMS mineralization (i.e., the FN1 population).

Most felsic rocks in the Finlayson Lake district exhibit evidence for melting of Proterozoic to Archean crustal basement [3, 4, 6]. The most common method of crustal melting, regardless of tectonic setting, involves a basaltic heat source as either intrusions or ponding of hot basaltic magmas that melt the overlying crust [101, 102]. In extensional settings, thinning lithosphere can accommodate upwelling asthenosphere into the rift regions leading to partial melting, basalt underplating of the crust, and crustal assimilation [103–106]. Here, we adopt this model to test and explain the variance in crust versus mantle Hf and Nd isotopic components in felsic rocks from the Finlayson Lake district (e.g., [17, 36]). We employed a simple two-component mixing model for both isotopes and trace element ratios using the equation of Faure [107]:

$$R_x^m = \frac{R_x^1 C_1 X + R_x^2 C_2 (1 - X)}{C_1 X + C_2 (1 - X)}, \quad (1)$$

where R_x^m is the ratio of the mixture, R_x^1 and R_x^2 are the compositions of the mantle and crustal endmembers, C_1 and C_2 are the trace element concentrations of the mantle and crustal endmembers, and X is the mixing factor that defines the volume ratio of the mantle to crustal components. The variable X varies between 0 (0% of component C_1) and 1 (100% of component C_1). In these mixing models, the two endmembers were chosen as (1) C_1 = N-MORB basalt (i.e., asthenospheric mantle) and (2) C_2 = evolved Laurentian crust. The basaltic N-MORB component is defined based on the spatial association of most felsic rocks with basalts in the Finlayson Lake district and in the back-arc realm therein the asthenospheric component generally has N-MORB compositions (see previous section; Figures 11(d)–11(f)). The nature of the crustal basement directly beneath Yukon-Tanana terrane rocks in the Finlayson Lake district is enigmatic; however, regionally, the Neoproterozoic to Early Paleozoic Snowcap assemblage has been interpreted as the basement to Yukon-Tanana terrane [5], and we use this as a crustal endmember in our calculations. We utilized the average isotopic compositions of Snowcap assemblage rocks that were more evolved than our most evolved samples, since 100% assimilation of the crust is highly unlikely (e.g., [108]).

Isotopic mixing models indicate that rocks from the Finlayson Lake district formed from variable mixtures of depleted N-MORB mantle melts and crustal melts from the assimilation of preexisting Snowcap assemblage rocks (Figures 15, 17, and 18). In the Cleaver Lake thrust sheet, arc rocks in the Cleaver Lake formation reveal between 9 and 21% Nd and Hf crustal components compared to 48-57% for the Simpson Range plutonic suite. In the Big Campbell thrust sheet, back-arc mafic rocks have isotopic compositions that indicate ~8-13% Nd and Hf contributions from the Snowcap endmember, whereas the felsic rocks vary from 17 to 45% Hf and 19 to 47% Nd from this endmember (Figure 15; Tables 3 and 4). The group FN1 rocks have the lowest contributions from the crustal endmember (17-28% Hf and 19-33% Nd), which also corresponds to the most elevated εHf-εNd, whereas group FN2 rocks have greater crustal contributions (24-45% Hf and 28-47% Nd) that correlate with the most evolved isotopic values (Figure 15). Therefore, it is evident that crust-mantle mixing was a dominant process in the formation of felsic rocks in the Finlayson Lake district and was particularly important in the differences in petrogenetic histories of the group FN1 and FN2 rocks.

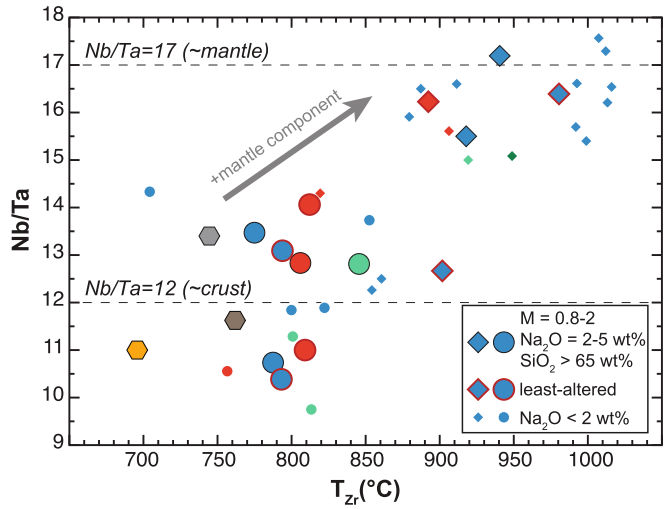

FIGURE 19: Zircon saturation thermometry calculations (T_{Zr} (°C)) relative to Nb/Ta. Temperatures were obtained using the equation of Boehnke et al. [113], which show negligible variation from the original equations of Watson and Harrison [111] and Hanchar and Watson [112]. Samples are parsed based on their alteration intensity, which greatly affects the accuracy of thermometry calculations. Large symbols contain M values of 0.8-2, Na_2O = 2-5 wt.%, and SiO_2 > 65 wt.%, and large symbols with red borders are least-altered rocks. Small symbols contain Na_2O < 2 wt.% and generally follow similar trends to their least-altered equivalents. The grey arrow represents the trajectory of increasing mantle-derived components in the formation of felsic rocks in the Finlayson Lake district (i.e., difference between group FN1 and FN2 compositions).

The εHf-εNd compositions and HFSE-REE abundances for group FN1 rocks are elevated compared to group FN2 rocks; however, the trace element abundances increase, but εHf and εNd are constant in each group, suggesting a decoupling of HFSE-REE from Nd and Hf isotopes. Two-component mixing lines using isotopes and trace element ratios also do not generate unique mixing curves with a single, evolved Snowcap endmember, which may indicate that an additional process beyond crustal contamination generated the high HFSE and REE and low $^{147}Sm/^{144}Nd$ ratios of group FN1 rocks (Figures 17 and 18). The uniquely high HFSE-REE could be explained by two hypotheses: (1) abundances are controlled by fractional crystallization, which would increase the trace element abundances but not further fractionate isotopic compositions (e.g., [43, 109, 110]) or (2) abundances are controlled by variable temperatures of crustal melting, which in turn facilitated variable dissolution of preexisting HFSE-REE-rich minerals into the melt (i.e., high temperature = increased dissolution; [17, 42, 43, 45, 109, 111]). Typical fractionation processes would favor an increase in Zr with increasing SiO_2 in the felsic rocks; however, the FN1 rocks are trachytic to dacitic (i.e., lower SiO_2) and have the highest Zr relative to FN2 rhyolites, which contradicts this trend. Therefore, we prefer the temperature-dependent hypothesis to explain this variation. To test this, zircon saturation thermometry [111, 112] was used to calculate temperatures at which zircon formed in rocks in the Finlayson Lake district. For this, we used the modified equation of Boehnke et al. [113]:

$$\ln D_{Zr}^{zircon/melt} = (10108 \pm 32/T) - (1.16 \pm 0.15)(M - 1) - (1.48 \pm 0.09), \quad (2)$$

where $D_{Zr}^{zircon/melt}$ is the distribution coefficient of Zr between zircon and the silicate melt, for which a stoichiometric concentration of 497,646 ppm Zr and measured whole-rock Zr (in ppm) were used, T is the temperature in Kelvin, and M is the cation ratio expressed as $(Na + K + 2 \cdot Ca)/(Al \cdot Si)$. Alteration was closely monitored by screening for M = 0.8-2, SiO_2 > 65 wt.%, and Na_2O = 2-5% (Figure 19). The calculated zircon saturation temperatures indicate higher-temperature crustal melts (890-980°C) contributed to the generation of group FN1 rocks, whereas distinctly lower-temperature melts (780-850°C) generated rocks in group FN2; the temperature range for groups FN1 and FN2 overlaps with temperatures obtained for FP and QFP porphyritic rocks, respectively, in the Wolverine deposit [17]. Interestingly, the higher zircon saturation temperatures are also associated with lower abundance of crustal components in the group FN1 rocks, which is interpreted to suggest that the dissolution efficiency of HFSE-REE-bearing minerals in the crust was far greater than those associated with lower-temperature FN2 melts (e.g., [42]). The SEM-MLA results also show that FN1 rocks have the highest modal abundances of HFSE-REE minerals (e.g., zircon, monazite, and xenotime; Table 5) and therefore directly relate to the HFSE-REE budget of the whole rock [110, 114, 115]. Moreover, the increased mantle components in the group FN1 rocks likely provided higher temperatures required to increase dissolution efficiency of these minerals in the crust, which in turn led to higher HFSE-REE contents in the ascending melts that are observed in VMS-bearing stratigraphic horizons both in the Kudz Ze Kayah and Little Wolverine formations.

10.1.3. Implications for VMS Mineralization. The whole-rock lithogeochemistry, petrogenesis, and tectonic setting of

VMS-bearing felsic rocks have been extensively studied [34, 36, 43, 116, 117]. Similarly, U-Pb geochronology has provided constraints on the timing of magmatism and mineralization in some VMS districts globally [28, 92, 118–121]. Moreover, there have been studies of shallow subvolcanic intrusions with close spatial and/or temporal ties to VMS-hosting stratigraphy, and these have also been implicated as the primary source of heat for the formation of VMS deposits [31–34, 122]. However, several authors have challenged this hypothesis and argue that these intrusions may not have been the direct heat source for mineralization but rather passive magmatic products in a regional, thermally anomalous geodynamic environment [17, 35, 36].

In the Finlayson Lake district, the Grass Lakes plutonic suite was previously suggested to be the heat driver for mineralization in the Kudz Ze Kayah formation [6]. The new U-Pb dates for the Grass Lakes plutonic suite (ca. 361.8 to 360.9 Ma; Figures 8 and 9) indicate that the intrusive rocks postdate the Kudz Ze Kayah VMS deposit and volcanism and therefore could not be the heat source for VMS mineralization. Additionally, while there is not a large plutonic suite associated with mineralization in the Wolverine Lake group, there are high-level syn-VMS porphyritic intrusions proximal to the Wolverine deposit that have been linked to regional extensional-related magmatism [17]. Despite their variations in timing, these rocks have geochemical and isotopic signatures that suggest potential fertility for VMS mineralization. For example, the FN1 rocks within <100-200 m of the ca. 362.8 Ma Kudz Ze Kayah deposit, the ca. 355.2 Ma Wolverine deposit, and the ca. 354.9 Ma Fisher zone have elevated HFSE-REE concentrations (e.g., Nb/Ta > ~ 15), zircon saturation temperatures (>890°C), and εHf-εNd isotope signatures that are consistent with formation at high-temperatures related to basaltic underplating (Figures 15, 16, and 19). In contrast, VMS-barren FN2 group rocks have distinct U-Pb dates outside of 2s uncertainty from the FN1 rocks, are HFSE-REE poor, and have more evolved εHf-εNd isotope signatures. The spatial association of VMS with magmas indicative of rifting and with evidence of high temperatures of emplacement and more juvenile signatures suggests that basaltic underplating association with back-arc rifting controlled the localization of VMS mineralization in the Finlayson Lake district. Rifting provided the ground conditions (i.e., synvolcanic faults) needed to focus fluid flow (e.g., [123]), whereas the basaltic underplate provided the essential heat needed to drive hydrothermal fluid circulation that formed both large and high-grade VMS deposits in the district (e.g., [17]). The underplating of rifts by basaltic magmas and associated crustal melting are processes likely recorded in many VMS districts globally (e.g., [36]), and further study of both bulk rock and mineral scale chemistry and isotopes is required to test these ideas and their validity.

10.2. Implications for Tectonostratigraphy in the Late Devonian–Early Mississippian Yukon-Tanana Terrane, Finlayson Lake District. Most magmatic rocks that comprise the Finlayson Lake district formed between ca. 363.5 and 354.8 Ma (Figure 9; [30]) and were part of an east-dipping Japan-Japan Sea style arc and back-arc environment along the western Laurentian continental margin (e.g., [2, 6, 7, 15, 124]). This model has been scrutinized by van Staal et al. [50] who argued that the tectonic configuration of the Yukon-Tanana terrane was more like the New Britain-Solomon-New Hebrides arc system at the Australian-Pacific plate boundary (e.g., [125]). Our results allow testing of these models and will utilize the (1) stratigraphic evaluation of mafic rocks in the Fire Lake and Kudz Ze Kayah formations and (2) geological characteristics of the ca. 360-358 Ma deformational event recorded in the Finlayson Lake district. An outcome of our work will be a series of testable models that will help guide future studies reconstructing the potential Late Devonian tectonic configuration of the Yukon-Tanana terrane and related rocks along the western Laurentian margin.

10.2.1. Redefining Geological Relationships of Fire Lake and Kudz Ze Kayah Formations. Mafic magmatism in the Fire Lake formation was previously interpreted to represent arc–back-arc rift initiation on the western Laurentian continental margin that subsequently evolved into a regime dominated by crustal melting and within-plate magmatism in the Kudz Ze Kayah formation [16, 45, 48]. This interpretation relied on three pieces of evidence: (1) ca. 365 Ma dates for mafic intrusions interpreted to be comagmatic with the Fire Lake formation (i.e., North Lakes intrusion; [4, 16]), (2) geochemistry of mafic rocks previously interpreted to represent the initiation and evolution of rifted continental arc (e.g., arc boninite and IAT to non-arc MORB to OIB; [47, 48]), and (3) apparent stratigraphic continuity of mafic rocks of the Fire Lake formation and felsic rocks of the Kudz Ze Kayah formation [16]. We will reevaluate the above in light of recent ideas (i.e., [50]) and new results and geological relationships.

Most mafic rocks in the Kudz Ze Kayah formation have chondritic isotopic compositions (εNd and εHf ~0) that have been interpreted as being mixtures of asthenospheric and enriched lithospheric mantle sources (±crustal/slab influence; see discussion above). The products of this magmatism were predominantly rocks with the most enriched E-MORB to OIB affinities; however, several mafic rocks stratigraphically overlie the North River formation that has primitive BABB to E-MORB affinities with juvenile εNd_i values (+8.1 and +8.5; [48]). These isotopic compositions are significantly more juvenile than the results from the rest of the redefined Kudz Ze Kayah formation and, given their stratigraphic position, are interpreted to be one of the first products related to rift-related magmatism in the nascent continental back-arc basin. At this stage, early rift-related magmas were likely generated by high-temperature mantle melting where the depleted asthenospheric melts (e.g., BABB) interacted with metasomatized mantle from the mantle wedge as the back-arc opened (e.g., [95, 126]). These primitive melts also contained an enriched E-MORB component that ascended through extensional structures in the continental crust with insufficient residence time in enriched lithospheric mantle and continental crust to influence the isotopic compositions. As rifting continued,

relatively deeper, incipient mantle melts would have had increased opportunity to interact with enriched lithospheric mantle and generated weakly alkalic rocks stratigraphically higher in the Kudz Ze Kayah formation (e.g., [94]), which then progressed stratigraphically upwards into a bimodal but felsic-dominated, within-plate volcanic sequence that was subsequently intruded by the North Lakes intrusion (ca. 362.6 to 361.8 Ma) and the Grass Lakes plutonic suite (ca. 361.9 to 360.9 Ma). These observations are interpreted to suggest that the Kudz Ze Kayah formation, as opposed to the Fire Lake formation (c.f., [48]), represents the pre-363.3 Ma marker of bimodal magmatism and back-arc rift initiation in the Yukon-Tanana terrane.

In the redefined Fire Lake formation, the allochthonous ultramafic rocks are overlain by extrusive metavolcanic rocks with affinities common to primitive arcs (e.g., boninite and IAT; [48, 68]). Such associations have been found in modern arcs and in many ophiolites and interpreted to have formed due to rapid rifting and exhumation of ultramafic rocks, as proposed for suprasubduction zone forearc [127–129] and back-arc environments [130–132]. Using examples from modern arcs, we herein propose a revised petrogenetic and geodynamic setting for the redefined Fire Lake formation and associated ultramafic slab. Ultramafic-mafic rocks and high-Ca boninites were generated in the forearc of the nascent arc system following subduction initiation, where rapid extension eventually led to a transfer of extensional stresses from the forearc to the back-arc region (e.g., [128]). Forearc extension and/or incipient back-arc formation thus facilitated deep exhumation of ultramafic mantle rocks in this model. Depleted boninites erupted above the ultramafic-mafic rocks, formed via decompression melting, due to rising asthenospheric melts that passed through a depleted, refractory mantle wedge that had previously extracted melt in the arc proper (e.g., IAT; [48, 133]). These magmas would have depleted the mantle wedge prior to boninite formation and have left an ultradepleted residue that the boninitic rocks could have been derived from (e.g., [134]). The proposed forearc setting provides the most ideal scenario to explain the preservation of oceanic rocks in the Fire Lake formation and the juxtaposition of these rocks near continental affinity rocks, which requires that the Fire Lake formation and associated ultramafic rocks (i.e., the arc initiation suite) are thrust onto the inboard North River formation.

The proposed model for the Fire Lake formation implies that continental crust was absent in the formation of most rocks, in contrast to the suggestions of Piercey et al. [47] who suggested the boninites formed in an environment with stratigraphic continuity with continental crust (e.g., a Havre Trough-type setting in the Kermadec arc; [135, 136]). The new observations and data presented here are not internally consistent with this model, and we suggest the Fire Lake formation formed in a separate oceanic domain proximal but outboard of the continental crust-floored Kudz Ze Kayah formation back-arc and were juxtaposed by thrusting. These observations require stratigraphic redefinition of both geological units and imply that the Kudz Ze Kayah formation, not the Fire Lake formation, records the onset of continental arc–back-arc rifting on the western Laurentian margin in the Late Devonian (pre-363.3 Ma).

10.2.2. Deformation, Uplift, and Erosion (ca. 360–358 Ma): Implications for Tectonics in the Western North American Cordillera. The ca. 360-358 Ma deformation, uplift, and erosion are recorded by the angular unconformity between the Grass Lakes and Wolverine Lake groups [16, 62]; the cause of the deformation and unconformity is poorly understood but broadly correlates with timing of the Late Devonian-Early Mississippian Antler Orogeny in the western United States (e.g., Figure 20; [137–140]). Evidence to support the nature and age of this unconformity includes the following: (1) quartzofeldspathic grits in the Little Jimmy formation have immature textures with angular feldspar laths, interpreted to be representative of deposition that was coincident with or shortly after seafloor volcanism; (2) zircon in this sample that yielded a maximum depositional age of ca. 357.6 Ma indicates deposition coeval with magmatism in the Wolverine Lake group; (3) the unit has geochemical signatures identical to the underlying Kudz Ze Kayah and overlying Little Wolverine formations but has a very evolved isotopic signature in group FN2 (see above); (4) rocks below the unconformity are more highly deformed than those above, having well-developed cleavages, ductile fabrics, and locally exhibit isoclinal folding; (5) relatively undeformed granitoids cut folded granitic dikes, and both were subsequently uplifted and eroded; and (6) the unconformity cuts kilometers of stratigraphy observed as a beveled and tilted erosional feature from the Wind Lake formation down to the North River formation (Figure 2).

New constraints on volcanism in the Wind Lake formation and the new CA-ID-TIMS date of ca. 357.6 Ma for the grit sample (Figures 8(a), 8(f), and 9(a)) indicate that the deformation period occurred between ca. 360.9 Ma and ca. 357.6 Ma. A similar style of unconformity has been recognized in the Money Creek thrust sheet between the Waters Creek and Tuchitua formations, but regional correlations beyond the Finlayson Lake district to other parts of the Yukon-Tanana terrane or North American continental margin are lacking. We interpret this to indicate that deformation at ca. 358 Ma was not more widely recognized in the northern Cordillera due to poor preservation of the back-arc environments in the rock record. Further, this deformation is present during a period of sinistral transpression on the western Laurentian margin [57, 137, 141–146], suggesting that it represents rarely preserved evidence that could be related to the Antler Orogeny in the northern North American Cordillera (Figure 20). If this is the case, the Antler Orogeny would have impacted the entire western North American continental margin during the Late Devonian to Early Mississippian (e.g., [140]), but much of the evidence in the northern Cordillera was then variably erased during younger deformation and metamorphic events.

Despite there being an unconformity between the Grass Lakes and Wolverine Lake groups, its timing suggests it may be unrelated to deformation in the region but due to the evolution of the subsequent rift-drift stage (e.g., [147]). Two types of Grass Lakes granitoids are present immediately

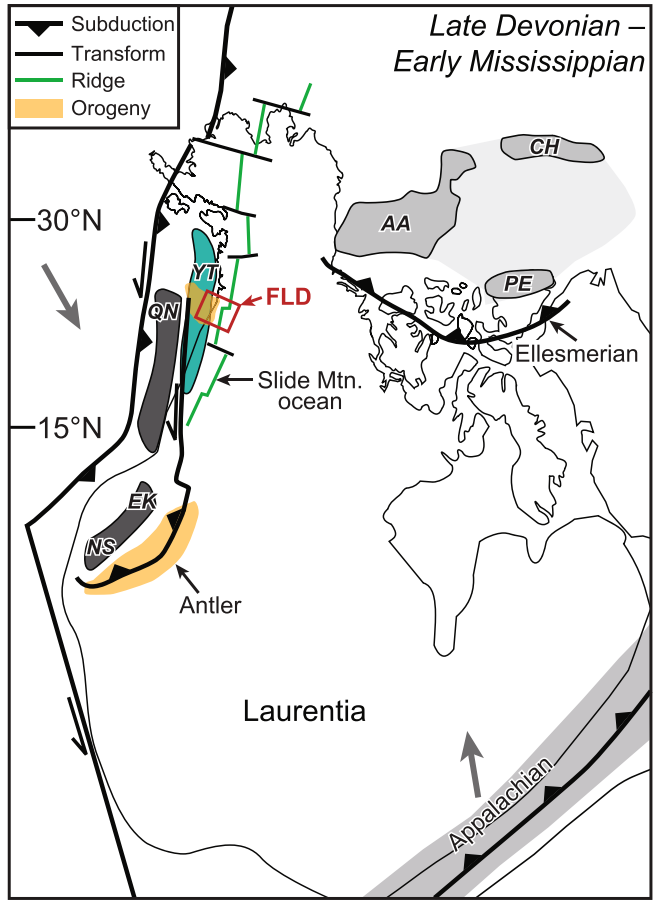

FIGURE 20: Late Devonian to Early Mississippian paleogeography of the Laurentian continental margin, modified after Colpron and Nelson [141] and Beranek et al. [137]. The Antler Orogeny (orange) is related to sinistral transpression along the western Laurentian margin, and the Finlayson Lake district (red box; FLD) is interpreted to contain a previously unrecognized remnant related to this tectonism. AA = Arctic Alaska; CH = Chukotka; EK = Eastern Klamath terrane; FLD = Finlayson Lake district; NS = Northern Sierra terrane; PE = Pearya terrane; QN = Quesnellia; YT = Yukon-Tanana terrane.

beneath the unconformity: (1) strongly deformed granite that preserves isoclinal folds interpreted to correlate with a transpressional deformation event (i.e., Antler Orogeny) and (2) a later, weakly foliated granite that crosscuts the strongly deformed granites above. The latter granitoid intrusion was dated at 357.3 ± 2.8 Ma [16] and, despite the large uncertainty, overlaps with the maximum depositional age and new CA-ID-TIMS date in the grits above the unconformity (Figure 8(a)). The younger cross-cutting granite is located below the unconformity and constrains the upper age limit of deformation, but it also establishes a distinct, post-transpressional magmatic event that preceded uplift and erosion. The ca. 357 Ma granite could also provide a local source for the Little Jimmy formation grits. Therefore, it appears that the erosional unconformity may be slightly younger and thus unrelated to the observed ca. 360-358 Ma transpressional deformation event.

As a result of the "decoupled" nature of deformation and erosion, we propose that the basal Wolverine Lake group unconformity represents a rift-onset unconformity that quickly merged into a breakup unconformity, marking the outboard flank of the Slide Mountain ocean. Early rifting in the Grass Lakes group transitioned upwards into alkalic magmatism but was then aborted [7], then was succeeded by compressional deformation. Post-deformation extension quickly facilitated an abrupt, pre-rift uplift period on the rift flank of the new Wolverine Lake group basin as a regional isostatic response to upwelling mantle [147–149]. The rapid change in topography on the continental back-arc resulted in an erosional surface (i.e., the basal Wolverine Lake group unconformity) that cut kilometers of stratigraphy and deposited sediment into the new low-lying basin between ca. 357.6 and 356.4 Ma (i.e., Little Jimmy formation; Figures 4(b) and 9; e.g., [30]). Continental margin extension in the Wolverine Lake group back-arc then resumed for at least ~1.5 Myr before MORB-type basalts of the Jasper Creek formation were erupted. The Jasper Creek formation includes both E-MORB and N-MORB basalts with εNd_i between −4 and +7 [57], which has been interpreted to suggest that Jasper Creek formation basalts have both lithospheric and asthenospheric mantle components [57]. The presence of lithospheric components suggests a linkage to the continental lithosphere, and the asthenospheric component implies incipient back-arc spreading. Together with

overlying stratigraphic and structural relationships, it suggests that the entire Wolverine Lake group stratigraphic section represents the evolution of crustal breakup, rifting, and the rift-drift transition following lithospheric rupture leading to incipient spreading (Figures 4 and 5; [45, 53, 71]). Further, these relationships fit with regional models for the Yukon-Tanana and Slide Mountain terranes and the development of a back-arc to ocean spreading center on the western Laurentian continental margin. Our results illustrate, however, this Devonian-Mississippian evolution was much more complex than previously recognized (e.g., [7, 16, 48, 124]).

11. Conclusions

Yukon-Tanana terrane rocks in the Finlayson Lake district, Yukon, represent early manifestations of mid-Paleozoic arc–back-arc magmatism immediately adjacent to the Laurentian continental margin which led to a rift-drift transition and the onset of the opening of the Slide Mountain ocean. When interpreted in the context of new structural and stratigraphic interpretations, our integrated geochronological, geochemical, and isotopic results indicate that the back-arc rocks formed during back-arc rifting in the Late Devonian to Early Mississippian (ca. 363.4 to 355.0 Ma), punctuated by a complex period of compressional deformation, post-compressional magmatism, uplift, and erosion between ca. 360 and 358 Ma. The Cleaver Lake arc contains coeval Late Devonian volcanic rocks (ca. 363.2 Ma) and multiple pulses of granitic plutonism between 352 and 348 Ma. The rocks in both the Grass Lakes and Wolverine Lake groups were generated above the continental crust of Laurentian affinity, which we interpret as rocks similar to the Snowcap assemblage that makes up the basement to Yukon-Tanana terrane throughout Yukon, Alaska, and British Columbia. Geochemical and isotopic results from felsic rocks in both rock packages indicate that crustal melting of the Snowcap assemblage occurred at different temperatures and correlates with variable degrees of assimilation. High-temperature (890-980°C) crustal melting facilitated low degrees of assimilation for Nd and Hf (<~35%) that generated rocks with group FN1 geochemical signatures (e.g., εHf and εNd > −8); this group contains rocks proximal to VMS mineralization. Low-temperature signatures (780-850°C), however, correspond to increased assimilation (>40%), evolved isotopic signatures (εHf and εNd < −8), and group FN2 geochemistry. These geochemical distinctions suggest that rocks directly hosting mineralization in the Kudz Ze Kayah and Wolverine VMS deposits were formed from high-temperature crustal melting from an increasingly mantle-derived component, interpreted to result from extensive basaltic underplating during an active period of slab rollback and mantle upwelling.

The conditions favorable for VMS generation were achieved through a series of complex tectonomagmatic configurations beginning in the Late Devonian. We propose that rapid and complex subduction initiation of various oceanic and continental crust blocks, which originated from remnants of an attenuated Laurentian margin, facilitated rapid arc mobility and extension in the back-arc regions. Rapid extension and magmatism in the Kudz Ze Kayah and Wolverine back-arc basins were punctuated by a period of transpressional deformation between ca. 360 and 358 Ma, possibly related to a rarely preserved segment of the Antler Orogeny. We propose that the deformation was separate from later uplift and erosion that define the regional angular unconformity between the two units, an unconformity interpreted as a rift-onset and overlapping breakup unconformity that marks the outboard flank and beginning of the continental margin rifting that led to the rift-drift transition and formation of the Slide Mountain ocean. This study highlights the importance of new, high-precision CA-ID-TIMS U-Pb zircon geochronology and its utility in placing tectonomagmatic processes within tight temporal chronostratigraphic frameworks. Further work in the Finlayson Lake district has the potential to define the earliest Late Devonian history (i.e., pre-Kudz Ze Kayah back-arc) of the Yukon-Tanana terrane and its relationship with the Laurentian continental margin, which can then be translated across the entire North American Cordilleran margin.

Data Availability

All of the data presented in this paper is available from the tables, figures, and supplementary files.

Conflicts of Interest

The authors are not aware of any conflicts of interest related to this research.

Acknowledgments

We acknowledge BMC Minerals and the Yukon Geological Survey for their ongoing support of this project. The new property-scale mapping, stratigraphic relationships, and sampling would not have been possible without tremendous assistance during fieldwork from Robin Black, Neil Martin, and Robert Burke (BMC Minerals) and Dillon Hume, Darcy Baker, Mark Baknes, Roger Hulstein, Ty Maggie, Ron Voordouw, and Victoria Tweedie (Equity Exploration). Jim Crowley, Mark Schmitz, and Craig Hart are thanked for their assistance with U-Pb geochronology, sample collection, organization, and logistics. Wanda Aylward and John M. Hanchar are thanked for their assistance with SEM work and mineral separations and preparation. Maurice Colpron helped with logistics, sample collection, and insightful discussions. Nikola Denisová, Rosie Cobbett, Adam Wiest, and Carly Mueller are thanked for edits on early versions of this manuscript and discussions of Cordilleran tectonics, VMS deposits, and geochemistry. We also thank Equity Exploration, Trans North helicopters, and Tintina Air for their support and transport while conducting field research from 2017 to 2019. Funding for this research was provided by the Yukon Geological Survey, BMC Minerals, NSERC Discovery Grant, an NSERC Collaborative Research and Development Grant, and the Targeted Geoscience Initiative 5 (TGI-5) program of the Geological Survey of Canada to S.J. Piercey and

a GSA Graduate Student Research Grant and SEG Canada Foundation Student Research Grant to M.J. Manor.

Supplementary Materials

A total of 15 supplemental files accompany this paper. The main appendix includes detailed text related to analytical methodology and CA-ID-TIMS and LA-ICP-MS U-Pb zircon geochronology results. Eight figures (Figures S1–S8) and six tables (Tables S1–S6) are also presented that provide imaging and data used in support of the main text. Appendix: analytical methods and CA-ID-TIMS and LA-ICP-MS U-Pb zircon geochronology results. Figure S1: photographs of U-Pb geochronology samples. Figure S2: MLA-SEM thin section scans used for modal abundance calculations. Figure S3: zircon SEM-CL images—17MM samples. Figure S4: zircon SEM-CL images—18MM samples. Figure S5: zircon SEM-CL images—P99/P00/96DM samples. Figure S6: LA-ICP-MS U-Pb zircon geochronology standard results. Figure S7: LA-ICP-MS U-Pb zircon geochronology results. Figure S8: North Lakes metadiorite sample HD-35 concordia diagram. Table S1: LA-ICP-MS U-Pb zircon geochronology standard results. Table S2: LA-ICP-MS U-Pb zircon geochronology results. Table S3: whole-rock lithogeochemical results. Table S4: whole-rock lithogeochemical QA/QC. Table S5: whole-rock Hf-Nd isotope QA/QC. Table S6: SEM-MLA results for accessory mineral abundances. *(Supplementary Materials)*

References

[1] M. Colpron, J. L. Nelson, and D. C. Murphy, "A tectonostratigraphic framework for the pericratonic terranes of the northern Canadian Cordillera," *Paleozoic evolution and metallogeny of pericratonic terranes at the ancient Pacific margin of North America, Canadian and Alaskan Cordillera: Geological Association of Canada Special Paper*, M. Colpron and J. L. Nelson, Eds., vol. 45, pp. 1–23, 2006.

[2] J. L. Nelson, M. Colpron, and S. Israel, "The Cordillera of British Columbia, Yukon, and Alaska: tectonics and metallogeny," *Society of Economic Geologists, Special Publication*, vol. 17, pp. 53–109, 2013.

[3] S. L. Grant, *Geochemical, radiogenic tracer isotopic, and U-Pb geochronological studies of Yukon-Tanana terrane rocks from the Money klippe, southeastern Yukon, [M.Sc. thesis]*, University of Alberta, Edmonton, Canada, 1997.

[4] J. K. Mortensen, "Pre-mid-Mesozoic tectonic evolution of the Yukon-Tanana Terrane, Yukon and Alaska," *Tectonics*, vol. 11, no. 4, pp. 836–853, 1992.

[5] S. J. Piercey and M. Colpron, "Composition and provenance of the Snowcap assemblage, basement to the Yukon-Tanana terrane, northern Cordillera: implications for Cordilleran crustal growth," *Geosphere*, vol. 5, no. 5, pp. 439–464, 2009.

[6] S. J. Piercey, J. K. Mortensen, and R. A. Creaser, "Neodymium isotope geochemistry of felsic volcanic and intrusive rocks from the Yukon–Tanana Terrane in the Finlayson Lake Region, Yukon, Canada," *Canadian Journal of Earth Sciences*, vol. 40, no. 1, pp. 77–97, 2003.

[7] S. J. Piercey, J. L. Nelson, M. Colpron, C. Dusel-bacon, R.-L. Simard, and C. F. Roots, "Paleozoic magmatism and crustal recycling along the ancient Pacific margin of North America, northern Cordillera," in *Paleozoic Evolution and Metallogeny of Pericratonic Terranes at the Ancient Pacific Margin of North America, Canadian and Alaskan Cordillera*, M. Colpron and J. L. Nelson, Eds., vol. 45, pp. 281–322, Geological Association of Canada, Special Paper, 2006.

[8] J. K. Mortensen and G. A. Jilson, "Evolution of the Yukon-Tanana terrane: evidence from southeastern Yukon territory," *Geology*, vol. 13, no. 11, pp. 806–810, 1985.

[9] J. A. Hunt, "Massive sulphide deposits in the Yukon-Tanana and adjacent terranes," in *Yukon Exploration and Geology 1996*, pp. 35–45, Exploration and Geological Services Division, Yukon, Indian and Northern Affairs Canada, 1997.

[10] J. Hunt, "The setting of volcanogenic massive sulphide deposits in the finlayson lake district," in *Yukon Exploration and Geology 1997*, Exploration and Geological Services Division, Yukon, Indian and Northern Affairs Canada, 1998.

[11] D. C. Murphy, "Stratigraphic framework for syngenetic mineral occurrences, Yukon-Tanana Terrane south of Finlayson Lake: a progress report," in *Yukon Exploration and Geology 1997*, Exploration and Geological Services Division, Yukon, Indian and Northern Affairs Canada, 1998.

[12] A. Green, "Fyre Lake Project," NI 43-101 Technical Report R431.2017, prepared for BMC Minerals, Ltd, Yukon Territory, Canada, 2018, June 2019, http://www.sedar.com/.

[13] J. M. Peter, D. Layton-Matthews, S. J. Piercey, G. D. Bradshaw, S. Paradis, and A. Bolton, "Volcanic-hosted massive sulphide deposits of the Finlayson Lake District, Yukon," in *Mineral Deposits of Canada: A Synthesis of Major Deposit-Types, District Metallogeny, the Evolution of Geological Provinces, and Exploration Methods*, W. D. Goodfellow, Ed., pp. 471–508, Geological Association of Canada, Mineral Deposits Division, Special Publication No. 5, 2007.

[14] K. van Olden, A. Green, and G. Davidson, "Kudz Ze Kayah Property," NI 43-101 Feasibility Study Technical Report R173.2019, prepared for BMC Minerals, Ltd, Yukon, Canada, 2019, June 2019, http://www.sedar.com/.

[15] F. Devine, S. D. Carr, D. C. Murphy, W. J. Davis, S. Smith, and M. Villeneuve, "Geochronological and geochemical constraints on the origin of the Klatsa metamorphic complex: Implications for Early Mississippian high-pressure metamorphism within Yukon-Tanana terrane," in *Paleozoic Evolution and Metallogeny of Pericratonic Terranes at the Ancient Pacific Margin of North America, Canadian and Alaskan Cordillera*, M. Colpron and J. L. Nelson, Eds., vol. 45, pp. 107–130, Geological Association of Canada, Special Paper, 2006.

[16] D. C. Murphy, J. K. Mortensen, S. J. Piercey, M. J. Orchard, and G. E. Gehrels, "Mid-Paleozoic to early Mesozoic tectonostratigraphic evolution of Yukon-Tanana and Slide Mountain terranes and affiliated overlap assemblages, Finlayson Lake massive sulphide district, southeastern Yukon," in *Paleozoic Evolution and Metallogeny of Pericratonic Terranes at the Ancient Pacific Margin of North America, Canadian and Alaskan Cordillera*, M. Colpron and J. L. Nelson, Eds., vol. 45, pp. 75–106, Geological Association of Canada, Special Paper, 2006.

[17] S. J. Piercey, J. M. Peter, J. K. Mortensen, S. Paradis, D. C. Murphy, and T. L. Tucker, "Petrology and U-Pb geochronology of footwall porphyritic rhyolites from the Wolverine volcanogenic massive sulfide deposit, Yukon, Canada: implications for the genesis of massive sulfide deposits in continental margin environments," *Economic Geology*, vol. 103, no. 1, pp. 5–33, 2008.

[18] T. E. Krogh, "Improved accuracy of U-Pb zircon ages by the creation of more concordant systems using an air abrasion technique," *Geochimica et Cosmochimica Acta*, vol. 46, pp. 637–649, 1982.

[19] J. M. Mattinson, "Zircon U-Pb chemical abrasion ("CA-TIMS") method: combined annealing and multi-step partial dissolution analysis for improved precision and accuracy of zircon ages," *Chemical Geology*, vol. 220, pp. 47–66, 2005.

[20] M. J. Manor and S. J. Piercey, "Re-evaluating the chronostratigraphic framework for felsic volcanic and intrusive rocks of the Finlayson Lake region, Yukon-Tanana terrane, Yukon," in *Yukon Exploration and Geology 2017*, K. MacFarlane, Ed., pp. 111–128, Yukon Geological Survey, 2018.

[21] Y. Buret, J.-F. Wotzlaw, S. Roozen, M. Guillong, A. von Quadt, and C. A. Heinrich, "Zircon petrochronological evidence for a plutonic-volcanic connection in porphyry copper deposits," *Geology*, vol. 45, no. 7, pp. 623–626, 2017.

[22] C. Chelle-Michou, M. Chiaradia, M. Ovtcharova, A. Ulianov, and J.-F. Wotzlaw, "Zircon petrochronology reveals the temporal link between porphyry systems and the magmatic evolution of their hidden plutonic roots (the Eocene Coroccohuayco deposit, Peru)," *Lithos*, vol. 198, pp. 129–140, 2014.

[23] M. Chiaradia, U. Schaltegger, and R. Spikings, "Time scales of mineral systems—advances in understanding over the past decade," *Society of Economic Geologists, Special Publication*, vol. 18, pp. 37–58, 2014.

[24] S. J. E. Large, J.-F. Wotzlaw, M. Guillong, A. von Quadt, and C. A. Heinrich, "Resolving the timescales of magmatic and hydrothermal processes associated with porphyry deposit formation using zircon U–Pb petrochronology," *Geochronology*, vol. 2, pp. 209–230, 2020.

[25] M. J. Manor, J. S. Scoates, C. J. Wall et al., "Age of the Late Cretaceous ultramafic-hosted Giant Mascot Ni-Cu-PGE deposit, southern Canadian Cordillera: integrating CA-ID-TIMS and LA-ICP-MS U-Pb geochronology and trace element geochemistry of zircon," *Economic Geology*, vol. 112, no. 6, pp. 1395–1418, 2017.

[26] D. J. Condon, B. Schoene, N. M. McLean, S. A. Bowring, and R. R. Parrish, "Metrology and traceability of U-Pb isotope dilution geochronology (EARTHTIME Tracer Calibration Part I)," *Geochimica et Cosmochimica Acta*, vol. 164, pp. 464–480, 2015.

[27] M. D. Schmitz and K. F. Kuiper, "High-precision geochronology," *Elements*, vol. 9, no. 1, pp. 25–30, 2013.

[28] J. K. Mortensen, J. B. Gemmell, A. W. McNeill, and R. M. Friedman, "High-precision U-Pb zircon chronostratigraphy of the Mount Read Volcanic belt in Western Tasmania, Australia: implications for VHMS deposit formation," *Economic Geology*, vol. 110, no. 2, pp. 445–468, 2015.

[29] P.-S. Ross, V. J. McNicoll, J. A. Debreil, and P. Carr, "Precise U-Pb geochronology of the Matagami mining camp, Abitibi greenstone belt, Quebec: stratigraphic constraints and implications for volcanogenic massive sulfide exploration," *Economic Geology*, vol. 109, no. 1, pp. 89–101, 2014.

[30] M. J. Manor, S. J. Piercey, C. J. Wall, and N. Denisová, "High precision CA-ID-TIMS U-Pb zircon geochronology of felsic rocks in the Finlayson Lake VMS district, Yukon: Linking Paleozoic basin-scale accumulation rates to the occurrence of subseafloor replacement-style mineralization," *Economic Geology*, vol. 117, no. 5, pp. 1173–1201, 2022.

[31] I. H. Campbell, J. M. Franklin, M. P. Gorton, T. R. Hart, and S. D. Scott, "The role of subvolcanic sills in the generation of massive sulfide deposits," *Economic Geology*, vol. 76, no. 8, pp. 2248–2253, 1981.

[32] J. M. Franklin, J. W. Lydon, and D. F. Sangster, "Volcanic-associated massive sulfide deposits," *Economic Geology 75th Anniversary Volume*, pp. 485–627, 1981.

[33] A. G. Galley, "Characteristics of semi-conformable alteration zones associated with volcanogenic massive sulphide districts," *Journal of Geochemical Exploration*, vol. 48, no. 2, pp. 175–200, 1993.

[34] T. R. Hart, H. L. Gibson, and C. M. Lesher, "Trace element geochemistry and petrogenesis of felsic volcanic rocks associated with volcanogenic massive Cu-Zn-Pb sulfide deposits," *Economic Geology*, vol. 99, no. 5, pp. 1003–1013, 2004.

[35] A. G. Galley, "Composite synvolcanic intrusions associated with Precambrian VMS-related hydrothermal systems," *Mineralium Deposita*, vol. 38, no. 4, pp. 443–473, 2003.

[36] S. J. Piercey, "The setting, style, and role of magmatism in the formation of volcanogenic massive sulfide deposits," *Mineralium Deposita*, vol. 46, no. 5-6, pp. 449–471, 2011.

[37] D. S. Coleman, W. Gray, and A. F. Glazner, "Rethinking the emplacement and evolution of zoned plutons: geochronologic evidence for incremental assembly of the Tuolumne Intrusive Suite, California," *Geology*, vol. 32, no. 5, pp. 433–436, 2004.

[38] A. F. Glazner, J. M. Bartley, D. S. Coleman, W. Gray, and R. Z. Taylor, "Are plutons assembled over millions of years by amalgamation from small magma chambers?," *GSA Today*, vol. 14, no. 4, pp. 4–11, 2004.

[39] S. R. Paterson, D. Okaya, V. Memeti, R. Economos, and R. B. Miller, "Magma addition and flux calculations of incrementally constructed magma chambers in continental margin arcs: Combined field, geochronologic, and thermal modeling studies," *Geosphere*, vol. 7, no. 6, pp. 1439–1468, 2011.

[40] F. Walker, N. Schofield, J. Millett et al., "Inside the volcano: three-dimensional magmatic architecture of a buried shield volcano," *Geology*, vol. 49, no. 3, pp. 243–247, 2021.

[41] C. T. Barrie, "Zircon thermometry of high-temperature rhyolites near volcanic-associated massive sulfide deposits, Abitibi subprovince, Canada," *Geology*, vol. 23, pp. 169–172, 1995.

[42] M. S. Codeço, A. Mateus, J. Figueiras, P. Rodrigues, and L. Gonçalves, "Development of the Ervidel-Roxo and Figueirinha-Albernoa volcanic sequences in the Iberian pyrite belt, Portugal: metallogenic and geodynamic implications," *Ore Geology Reviews*, vol. 98, pp. 80–108, 2018.

[43] D. R. Lentz, "Petrology, geochemistry, and oxygen isotope interpretation of felsic volcanic and related rocks hosting the Brunswick 6 and 12 massive sulfide deposits (Brunswick Belt), Bathurst mining camp, New Brunswick, Canada," *Economic Geology*, vol. 94, no. 1, pp. 57–86, 1999.

[44] D. R. N. Rosa, C. M. C. Inverno, V. M. J. Oliveira, and C. J. P. Rosa, "Geochemistry and geothermometry of volcanic rocks from Serra Branca, Iberian Pyrite Belt, Portugal," *Gondwana Research*, vol. 10, no. 3-4, pp. 328–339, 2006.

[45] S. J. Piercey, S. Paradis, D. C. Murphy, and J. K. Mortensen, "Geochemistry and paleotectonic setting of felsic volcanic rocks in the Finlayson Lake volcanic-hosted massive sulfide District, Yukon, Canada," *Economic Geology*, vol. 96, no. 8, pp. 1877–1905, 2001.

[46] S. J. Piercey, L. P. Beranek, and J. M. Hanchar, "Mapping magma prospectivity for Cordilleran volcanogenic massive sulphide (VMS) deposits using Nd-Hf isotopes: preliminary results," in *Yukon Exploration and Geology 2016*, K. E. MacFarlane and L. H. Weston, Eds., pp. 197–205, Yukon Geological Survey, 2017.

[47] S. J. Piercey, D. C. Murphy, J. K. Mortensen, and S. Paradis, "Boninitic magmatism in a continental margin setting, Yukon-Tanana Terrane, southeastern Yukon, Canada," *Geology*, vol. 29, no. 8, pp. 731–734, 2001.

[48] S. J. Piercey, D. C. Murphy, J. K. Mortensen, and R. A. Creaser, "Mid-Paleozoic initiation of the northern Cordilleran marginal backarc basin: geologic, geochemical, and neodymium isotope evidence from the oldest mafic magmatic rocks in the Yukon-Tanana Terrane, Finlayson Lake district, southeast Yukon, Canada," *Bulletin of the Geological Society of America*, vol. 116, no. 9, pp. 1087–1106, 2004.

[49] D. J. Tempelman-Kluit, "Transported cataclasite, ophiolite and granodiorite in Yukon: evidence of arc-continent collision," *Geological Survey of Canada*, 1979, Paper 79-14.

[50] C. R. van Staal, A. Zagorevski, W. C. Mcclelland et al., "Age and setting of Permian Slide Mountain terrane ophiolitic ultramafic-mafic complexes in the Yukon: implications for late Paleozoic-early Mesozoic tectonic models in the northern Canadian Cordillera," *Tectonophysics*, vol. 744, pp. 458–483, 2018.

[51] D. C. Murphy, M. Colpron, C. F. Roots, S. P. Gordey, and J. G. Abbott, "Finlayson Lake targeted geoscience initiative (southeastern Yukon), part 1: bedrock geology," in *Yukon Exploration and Geology 2001*, D. S. Emond, L. H. Weston, and L. L. Lewis, Eds., pp. 189–207, Exploration and Geological Services Division, Yukon, Indian and Northern Affairs Canada, 2002.

[52] H. Gabrielse, D. C. Murphy, and J. K. Mortensen, "Cretaceous and Cenozoic dextral orogen-parallel displacements, magmatism, and paleogeography, north-central Canadian Cordillera," in *Paleogeography of the North American Cordillera: Evidence For and Against Large-Scale Displacements*, vol. 46, pp. 255–276, Geological Association of Canada, Special Paper, 2006.

[53] S. J. Piercey, S. J. Paradis, J. M. Peter, and T. L. Tucker, *Geochemistry of basalt from the Wolverine volcanic-hosted massive-sulphide deposit, Finlayson Lake district, Yukon Territory*, Geological Survey of Canada, Current Research, 2002.

[54] Yukon Geological Survey, *Yukon Digital Bedrock Geology*, Yukon Geological Survey, 2018, August 2018, http://www.geology.gov.yk.ca/update_yukon_bedrock_geology_map.html.

[55] S. J. Piercey and D. C. Murphy, "Stratigraphy and regional implications of unstrained Devono-Mississippian volcanic rocks in the Money Creek thrust sheet, Yukon-Tanana Terrane, Southeastern Yukon," in *Yukon Exploration and Geology, 1999*, D. S. Emond and L. H. Weston, Eds., pp. 67–78, Exploration and Geological Services Division, Yukon, Indian and Northern Affairs Canada, 2000.

[56] H. E. Plint and T. M. Gordon, "The Slide Mountain Terrane and the structural evolution of the Finlayson Lake Fault Zone, southeastern Yukon," *Canadian Journal of Earth Sciences*, vol. 34, no. 2, pp. 105–126, 1997.

[57] S. J. Piercey, D. C. Murphy, and R. A. Creaser, "Lithosphere-asthenosphere mixing in a transform-dominated late Paleozoic backarc basin: Implications for northern Cordilleran crustal growth and assembly," in *Geosphere*, vol. 8, no. 3, pp. 716–739, 2012.

[58] M. McDonald, S. Piercey, G. Layne, L. Pigage, and G. Piercey, "Mineral assemblages, textures and in situ sulphur isotope geochemistry of sulphide mineralization from the Cyprus-type ice volcanogenic massive sulphide (VMS) deposit, Yukon, Canada," *Minerals*, vol. 8, no. 11, p. 501, 2018.

[59] C. Sebert, J. A. Hunt, and I. J. Foreman, *Geology and lithogeochemistry of the Fyre Lake copper-cobalt-gold sulphide-magnetite deposit, southeastern Yukon*, Yukon Geological Survey, Open File 2004-17, 2004.

[60] D. Baker, D. Hume, R. Hulstein, M. Baknes, M. J. Manor, and A. O. Nielsen, "Phase I KZK mapping program: property geology," , Unpublished internal report prepared for BMC Minerals, Ltd, 2018.

[61] S. J. Piercey, J. K. Mortensen, D. C. Murphy, S. Paradis, and R. A. Creaser, "Geochemistry and tectonic significance of alkalic mafic magmatism in the Yukon-Tanana Terrane, Finlayson Lake region, Yukon," *Canadian Journal of Earth Sciences*, vol. 39, no. 12, pp. 1729–1744, 2002.

[62] D. C. Murphy and S. J. Piercey, "Finlayson project: geological evolution of Yukon-Tanana Terrane and its relationship to Campbell Range belt, northern Wolverine Lake map area, southeastern Yukon," in *Yukon Exploration and Geology 1998*, C. F. Roots and D. S. Emond, Eds., pp. 47–62, Exploration and Geological Services Division, Yukon, Indian and Northern Affairs Canada, 1999.

[63] M. J. Manor, D. Hume, T. Magee, and V. Tweedie, "2018 Pelly mapping program: Property geology," , Unpublished internal report prepared for BMC Minerals, Ltd, 2018.

[64] S. J. Piercey, H. L. Gibson, N. Tardif, and B. S. Kamber, "Ambient redox and hydrothermal environment of the Wolverine volcanogenic massive sulfide deposit, Yukon: insights from lithofacies and lithogeochemistry of Mississippian host shales," *Economic Geology*, vol. 111, no. 6, pp. 1439–1463, 2016.

[65] G. Bradshaw, J. Peter, S. Paradis, and S. Rowins, "Geological characteristics of the Wolverine volcanic-hosted massive sulphide deposit, Finlayson lake district, Yukon Territory, Canada," in *Yukon Exploration and Geology, 2000*, Exploration and Geological Services Division, Yukon, Indian and Northern Affairs Canada, 2001.

[66] F. Devine, D. C. Murphy, and S. D. Carr, "Yukon-Tanana terrane in the southern Campbell Range, Finlayson Lake belt, southeastern Yukon: the geological setting of retrogressed eclogite of the Klatsa metamorphic complex," *Canadian Journal of Earth Sciences*, vol. 44, no. 3, pp. 317–336, 2007.

[67] D. C. Murphy, "Preliminary geological map of Grass Lakes area, Pelly Mountains, southeastern Yukon," in *Exploration and Geological Services Division, Yukon, Indian and Northern Affairs Canada*, Open File 1997-3, 1997.

[68] D. C. Murphy, M. Colpron, S. P. Gordey, C. F. Roots, G. Abbott, and P. S. Lipovsky, "Preliminary bedrock geological map of northern Finlayson Lake area (NTS 105 G) Yukon Territory (1:100 000 scale)," in *Exploration and Geological Services Division*, Yukon, Indian and Northern Affairs Canada, 2001.

[69] D. C. Murphy, R. Kennedy, and A. Tizzard, "Geological map of part of Waters Creek and Fire Lake map areas (NTS 105G/

1, part of 105G/2), southeastern Yukon (1:50 000 scale)," in Yukon Geological Survey Open File 2004-11, 2004.

[70] S. J. Piercey and B. S. Kamber, "Lead isotope geochemistry of shales from the Wolverine volcanogenic massive sulfide deposit, Yukon: implications for Pb isotope vectoring in exhalative ore systems," *Economic Geology*, vol. 114, no. 1, pp. 47–66, 2019.

[71] G. D. Bradshaw, S. M. Rowins, J. M. Peter, and B. E. Taylor, "Genesis of the Wolverine volcanic sediment-hosted massive sulfide deposit, Finlayson Lake District, Yukon, Canada: mineralogical, mineral chemical, fluid inclusion, and sulfur isotope evidence," *Economic Geology*, vol. 103, no. 1, pp. 35–60, 2008.

[72] V. I. Davydov, J. L. Crowley, M. D. Schmitz, and V. I. Poletaev, "High-precision U-Pb zircon age calibration of the global carboniferous time scale and Milankovitch band cyclicity in the Donets Basin, eastern Ukraine," *Geochemistry, Geophysics, Geosystems*, vol. 11, no. 2, p. 22, 2010.

[73] M. D. Schmitz and V. I. Davydov, "Quantitative radiometric and biostratigraphic calibration of the Pennsylvanian-early Permian (Cisuralian) time scale and pan-Euramerican chronostratigraphic correlation," *Bulletin of the Geological Society of America*, vol. 124, no. 3-4, pp. 549–577, 2012.

[74] O. M. Burnham, "Trace element analysis of geological samples by inductively coupled plasma mass spectrometry (ICP–MS) at the Geoscience Laboratories: Revised capabilities due to method improvements," in *Summary of field work and other activities*, vol. 6226, pp. 38-1–38-10, Ontario Geological Survey, Open File Report, 2008.

[75] W. Pretorius, D. Weis, G. Williams, D. Hanano, B. Kieffer, and J. Scoates, "Complete trace elemental characterisation of granitoid (USGS G-2, GSP-2) reference materials by high resolution inductively coupled plasma-mass spectrometry," *Geostandards and Geoanalytical Research*, vol. 30, no. 1, pp. 39–54, 2006.

[76] D. Weis, B. Kieffer, C. Maerschalk et al., "High-precision isotopic characterization of USGS reference materials by TIMS and MC-ICP-MS," *Geochemistry, Geophysics, Geosystems*, vol. 7, no. 8, p. 30, 2006.

[77] D. Weis, B. Kieffer, D. Hanano et al., "Hf isotope compositions of U.S. geological survey reference materials," *Geochemistry, Geophysics, Geosystems*, vol. 8, no. 6, p. 15, 2007.

[78] T. Tanaka, S. Togashi, H. Kamioka et al., "JNdi-1: a neodymium isotopic reference in consistency with LaJolla neodymium," *Chemical Geology*, vol. 168, no. 3-4, pp. 279–281, 2000.

[79] J. Blichert-Toft, C. Chauvel, and F. Albarède, "Separation of Hf and Lu for high-precision isotope analysis of rock samples by magnetic sector-multiple collector ICP-MS," *Contributions to Mineralogy and Petrology*, vol. 127, no. 3, pp. 248–260, 1997.

[80] J. Blichert-Toft and F. Albarède, "The Lu-Hf isotope geochemistry of chondrites and the evolution of the mantle-crust system," *Earth and Planetary Science Letters*, vol. 148, no. 1-2, pp. 243–258, 1997.

[81] A. Bouvier, J. D. Vervoort, and P. J. Patchett, "The Lu-Hf and Sm-Nd isotopic composition of CHUR: constraints from unequilibrated chondrites and implications for the bulk composition of terrestrial planets," *Earth and Planetary Science Letters*, vol. 273, no. 1-2, pp. 48–57, 2008.

[82] S. B. Jacobsen and G. J. Wasserburg, "Sm-Nd isotopic evolution of chondrites," *Earth and Planetary Science Letters*, vol. 50, no. 1, pp. 139–155, 1980.

[83] J. D. Vervoort and J. Blichert-Toft, "Evolution of the depleted mantle: Hf isotope evidence from juvenile rocks through time," *Geochimica et Cosmochimica Acta*, vol. 63, no. 3-4, pp. 533–556, 1999.

[84] S. L. Goldstein, R. K. O'Nions, and P. J. Hamilton, "A Sm-Nd isotopic study of atmospheric dusts and particulates from major river systems," *Earth and Planetary Science Letters*, vol. 70, no. 2, pp. 221–236, 1984.

[85] B. Schoene, J. L. Crowley, D. J. Condon, M. D. Schmitz, and S. A. Bowring, "Reassessing the uranium decay constants for geochronology using ID-TIMS U-Pb data," *Geochimica et Cosmochimica Acta*, vol. 70, no. 2, pp. 426–445, 2006.

[86] Y. Ishikawa, T. Sawaguchi, S. Iwaya, and M. Horiuchi, "Delineation of prospecting targets for Kuroko deposits based on modes of volcanism of underlying dacite and alteration halos (in Japanese with English abs.)," *Mining Geology*, vol. 26, pp. 117–206, 1976.

[87] R. R. Large, J. B. Gemmell, H. Paulick, and D. L. Huston, "The alteration box plot: a simple approach tounderstanding the relationship between alteration mineralogy andlithogeochemistry associated with volcanic-hosted massive sulfide deposits," *Economic Geology*, vol. 96, no. 5, pp. 957–971, 2001.

[88] W. MacLean and T. Barrett, "Lithogeochemical techniques using immobile elements," *Journal of Geochemical Exploration*, vol. 48, no. 2, pp. 109–133, 1993.

[89] S. M. McLennan, "Relationships between the trace element composition of sedimentary rocks and upper continental crust," *Geochemistry Geophysics Geosystems*, vol. 2, no. 4, 2001.

[90] W. McDonough and S. Sun, "The composition of the earth," *Chemical Geology*, vol. 120, no. 3-4, pp. 223–253, 1995.

[91] S. S. Sun and W. F. McDonough, "Chemical and isotopic systematics of oceanic basalts: implications for mantle composition and processes," in *Magmatism in the Ocean Basins*, vol. 42, no. 1, pp. 313–345, Geological Society of London, Special Publication, 1989.

[92] P.-S. Ross and J. H. Bédard, "Magmatic affinity of modern and ancient subalkaline volcanic rocks determined from trace-element discriminant diagrams," *Canadian Journal of Earth Sciences*, vol. 46, no. 11, pp. 823–839, 2009.

[93] J. W. Shervais, "Ti-V plots and the petrogenesis of modern and ophiolitic lavas," *Earth and Planetary Science Letters*, vol. 59, no. 1, pp. 101–118, 1982.

[94] J. A. Pearce, "Geochemical fingerprinting of oceanic basalts with applications to ophiolite classification and the search for Archean oceanic crust," *Lithos*, vol. 100, no. 1-4, pp. 14–48, 2008.

[95] J. A. Pearce and D. W. Peate, "Tectonic implications of the composition of volcanic arc magmas," *Annual Review of Earth and Planetary Sciences*, vol. 23, no. 1, pp. 251–285, 1995.

[96] J. A. Pearce, P. E. Baker, P. K. Harvey, and I. W. Luff, "Geochemical evidence for subduction fluxes, mantle melting and fractional crystallization beneath the South Sandwich island arc," *Journal of Petrology*, vol. 36, no. 4, pp. 1073–1109, 1995.

[97] K. H. Wedepohl, "The composition of the continental crust," *Geochimica et Cosmochimica Acta*, vol. 59, no. 7, pp. 1217–1232, 1995.

[98] M. G. Barth, W. F. Mcdonough, and R. L. Rudnick, "Tracking the budget of Nb and Ta in the continental crust," *Chemical geology*, vol. 165, no. 3-4, pp. 197–213, 2000.

[99] T. H. Green, "Significance of Nb/Ta as an indicator of geochemical processes in the crust-mantle system," *Chemical Geology*, vol. 120, no. 3-4, pp. 347–359, 1995.

[100] X. Wang, W. L. Griffin, J. Chen, P. Huang, and X. Li, "U and Th contents and Th/U ratios of zircon in felsic and mafic magmatic rocks: improved zircon-melt distribution coefficients," *Acta Geologica Sinica*, vol. 85, no. 1, pp. 164–174, 2011.

[101] H. E. Huppert and R. S. J. Sparks, "The generation of granitic magmas by intrusion of basalt into continental crust," *Journal of Petrology*, vol. 29, no. 3, pp. 599–624, 1988.

[102] A. B. Thompson, "Some time-space relationships for crustal melting and granitic intrusion at various depths," *Geological Society Special Publication*, vol. 168, no. 1, pp. 7–25, 1999.

[103] D. McKenzie and M. J. Bickle, "The volume and composition of melt generated by extension of the lithosphere," *Journal of Petrology*, vol. 29, no. 3, pp. 625–679, 1988.

[104] D. McKenzie and R. K. O'Nions, "Partial melt distributions from inversion of rare earth element concentrations," *Journal of Petrology*, vol. 33, p. 1453, 1992.

[105] C. H. Langmuir, E. M. Klein, and T. Plank, "Petrological systematics of mid-ocean ridge basalts: constraints on melt generation beneath ocean ridges," in *Mantle Flow and Melt Generation at Mid-Ocean Ridges*, vol. 71, pp. 183–280, American Geophysical Union, Geophysical Monograph, 1992.

[106] M. Wilson, "Magmatism and the geodynamics of basin formation," *Sedimentary Geology*, vol. 86, no. 1-2, pp. 5–29, 1993.

[107] G. Faure, *Principles of Isotope Geology*, John Wiley & Sons, Second edition, 1986.

[108] A. B. Thompson, L. Matile, and P. Ulmer, "Some thermal constraints on crustal assimilation during fractionation of hydrous, mantle-derived magmas with examples from Central Alpine Batholiths," *Journal of Petrology*, vol. 43, no. 3, pp. 403–422, 2002.

[109] F. Bea, "Controls on the trace element composition of crustal melts," *Transactions of the Royal Society of Edinburgh: Earth Sciences*, vol. 315, pp. 33–41, 1996.

[110] F. Bea, "Residence of REE, Y, Th and U in granites and crustal protoliths; implications for the chemistry of crustal melts," *Journal of Petrology*, vol. 37, no. 3, pp. 521–552, 1996.

[111] E. B. Watson and T. M. Harrison, "Zircon saturation revisited: temperature and composition effects in a variety of crustal magma types," *Earth and Planetary Science Letters*, vol. 64, no. 2, pp. 295–304, 1983.

[112] J. M. Hanchar and E. B. Watson, "Zircon saturation thermometry," *Reviews in Mineralogy and Geochemistry*, vol. 53, no. 1, pp. 89–112, 2003.

[113] P. Boehnke, E. B. Watson, D. Trail, T. M. Harrison, and A. K. Schmitt, "Zircon saturation re-revisited," *Chemical Geology*, vol. 351, pp. 324–334, 2013.

[114] E. B. Watson and T. M. Harrison, "Accessory minerals and the geochemical evolution of crustal magmatic systems: a summary and prospectus of experimental approaches," *Physics of the Earth and Planetary Interiors*, vol. 35, no. 1-3, pp. 19–30, 1984.

[115] G. R. Watt and S. L. Harley, "Accessory phase controls on the geochemistry of crustal melts and restites produced during water-undersaturated partial melting," *Contributions to Mineralogy and Petrology*, vol. 114, no. 4, pp. 550–566, 1993.

[116] C. M. Lesher, A. M. Goodwin, I. H. Campbell, and M. P. Gorton, "Trace-element geochemistry of ore-associated and barren, felsic metavolcanic rocks in the Superior Province, Canada," *Canadian Journal of Earth Sciences*, vol. 23, no. 2, pp. 222–237, 1986.

[117] J.-L. Pilote and S. J. Piercey, "Petrogenesis of the Rambler Rhyolite formation: controls on the Ming VMS deposit and geodynamic implications for the Taconic Seaway, Newfoundland Appalachians, Canada," *American Journal of Science*, vol. 318, no. 6, pp. 640–683, 2018.

[118] W. Bleeker and R. R. Parrish, "Stratigraphy and U-Pb zircon geochronology of Kidd Creek: implications for the formation of giant volcanogenic massive sulphide deposits and the tectonic history of the Abitibi greenstone belt," *Canadian Journal of Earth Sciences*, vol. 33, no. 8, pp. 1213–1231, 1996.

[119] W. Bleeker, R. R. Parrish, and S. Sager-Kinsman, "High-precision U-Pb geochronology of the Late Archean Kidd Creek deposit and Kidd volcanic complex," *Economic Geology Monograph*, vol. 10, pp. 43–69, 1999.

[120] C. T. Barrie, Y. Amelin, and E. Pascual, "U-Pb geochronology of VMS mineralization in the Iberian Pyrite belt," *Mineralium Deposita*, vol. 37, pp. 684–703, 2002.

[121] V. J. McNicoll, J. B. Whalen, and R. A. Stern, "U-Pb geochronology of Ordovician plutonism, Bathurst mining camp, New Brunswick," *Economic Geology Monograph*, vol. 11, pp. 203–218, 2003.

[122] J. M. Franklin, H. L. Gibson, I. R. Jonasson, and A. G. Galley, "Volcanogenic massive sulfide deposits," in *Economic Geology 100th Anniversary Volume*, pp. 523–560, 2005.

[123] N. Denisová and S. J. Piercey, "Lithostratigraphy, lithogeochemistry and tectono-magmatic framework of the ABM replacement-style volcanogenic massive sulfide (VMS) deposit, Finlayson Lake District, Yukon, Canada," *Economic Geology*, in press.

[124] J. L. Nelson, M. Colpron, S. J. Piercey, C. Dusel-bacon, D. C. Murphy, and C. F. Roots, "Paleozoic tectonic and metallogenetic evolution of pericratonic terranes in Yukon, northern British Columbia and eastern Alaska," in *Paleozoic Evolution and Metallogeny of Pericratonic Terranes at the Ancient Pacific Margin of North America, Canadian and Alaskan Cordillera*, M. Colpron and J. L. Nelson, Eds., vol. 45, pp. 323–360, Geological Association of Canada, Special Paper, 2006.

[125] S. Meffre and A. J. Crawford, "Collision tectonics in the New Hebrides arc (Vanuatu)," *The Island Arc*, vol. 10, no. 1, pp. 33–50, 2001.

[126] B. Taylor and F. Martinez, "Back-arc basin basalt systematics," *Earth and Planetary Science Letters*, vol. 210, no. 3-4, pp. 481–497, 2003.

[127] J. W. Shervais, "Birth, death, and resurrection: the life cycle of suprasubduction zone ophiolites," *Geochemistry, Geophysics, Geosystems*, vol. 2, no. 1, p. 45, 2001.

[128] R. J. Stern and S. H. Bloomer, "Subduction zone infancy: examples from the Eocene Izu-Bonin-Mariana and Jurassic California arcs," *Geological Society of America Bulletin*, vol. 104, no. 12, pp. 1621–1636, 1992.

[129] E. Todd, J. B. Gill, and J. A. Pearce, "A variably enriched mantle wedge and contrasting melt types during arc stages following subduction initiation in Fiji and Tonga, southwest Pacific," *Earth and Planetary Science Letters*, vol. 335-336, pp. 180–194, 2012.

[130] J.-L. Bodinier and M. Godard, "Orogenic, Ophiolitic, and Abyssal Peridotites," in *The Mantle and Core, Treatise on Geochemistry*, O. Orogenic, A. Peridotites, H. D. Holland, and K. K. Turekian, Eds., vol. 3, Elsevier-Pergamon, Oxford, 2nd edition, 2014.

[131] G. D. Harper, "The Josephine ophiolite, northwestern California," *Geological Society of America Bulletin*, vol. 95, no. 9, pp. 1009–1026, 1984.

[132] J. A. Pearce, T. Alabaster, A. W. Shelton, and M. P. Searle, "The Oman ophiolite as a Cretaceous arc-basin complex: evidence and implications," *Philosophical Transactions of the Royal Society of London. Series A, Mathematical and Physical Sciences*, vol. 300, no. 1454, pp. 299–317, 1981.

[133] T. J. Falloon and A. J. Crawford, "The petrogenesis of high-calcium boninite lavas dredged from the northern Tonga ridge," *Earth and Planetary Science Letters*, vol. 102, no. 3-4, pp. 375–394, 1991.

[134] J. A. Pearce, M. F. Thirlwall, G. Ingram, B. J. Murton, R. J. Arculus, and S. R. Vander Laan, "Isotopic evidence for the origin of boninites and related rocks drilled in the Izu-Bonin (Osagawara) forearc, Leg 125," *Proceedings of the Ocean Drilling Program: Scientific Results*, vol. 125, pp. 237–261, 1992.

[135] J. A. Gamble and I. C. Wright, "The Southern Havre Trough Geological Structure and Magma Petrogenesis of an Active Backarc Rift Complex," *Backarc Basins*, 1995.

[136] L. M. Parson and I. C. Wright, "The Lau-Havre-Taupo back-arc basin: a southward-propagating, multi-stage evolution from rifting to spreading," *Tectonophysics*, vol. 263, no. 1-4, pp. 1–22, 1996.

[137] L. P. Beranek, P. K. Link, and C. M. Fanning, "Detrital zircon record of mid-Paleozoic convergent margin activity in the northern U.S. Rocky Mountains: implications for the Antler orogeny and early evolution of the North American Cordillera," *Lithosphere*, vol. 8, no. 5, pp. 533–550, 2016.

[138] J. G. Johnson and A. Pendergast, "Timing and mode of emplacement of the Roberts Mountains allochthon, Antler orogeny," *Geological Society of America Bulletin*, vol. 92, no. 9, pp. 648–658, 1981.

[139] T. H. Nilsen and J. H. Stewart, "The Antler orogeny – mid-Paleozoic tectonism in western North America," *Geology*, vol. 8, no. 6, pp. 298–302, 1980.

[140] M. T. Smith, W. R. Dickinson, and G. E. Gehrels, "Contractional nature of Devonian-Mississippian Antler tectonism along the North American continental margin," *Geology*, vol. 21, no. 1, pp. 21–24, 1993.

[141] M. Colpron and J. L. Nelson, "A Palaeozoic Northwest Passage: incursion of Caledonian, Baltican and Siberian terranes into eastern Panthalassa, and the early evolution of the North American Cordillera," *Geological Society, London, Special Publications*, vol. 318, pp. 273–307, 2009.

[142] P. H. Cashman and D. M. Sturmer, "Paleogeographic reconstruction of Mississippian to Middle Pennsylvanian basins in Nevada, southwestern Laurentia," *Palaeogeography, Palaeoclimatology, Palaeoecology*, vol. 584, 2021.

[143] T. F. Lawton, P. H. Cashman, J. H. Trexler, and W. J. Taylor, "The Late Paleozoic southwestern Laurentian borderland," *Geology*, vol. 45, pp. 675–678, 2017.

[144] G. M. Linde, J. H. Trexler, P. H. Cashman, G. Gehrels, and W. R. Dickinson, "Detrital zircon U-Pb geochronology and Hf isotope geochemistry of the Roberts Mountains allochthon: new insights into the early Paleozoic tectonics of western North America," *Geosphere*, vol. 12, no. 3, pp. 1016–1031, 2016.

[145] G. M. Linde, J. H. Trexler, P. H. Cashman, G. Gehrels, and W. R. Dickinson, "Three-dimensional evolution of the Early Paleozoic western Laurentian margin: new insights from detrital zircon U-Pb geochronology and Hf isotope geochemistry of the harmony formation of Nevada," *Tectonics*, vol. 36, no. 11, pp. 2347–2369, 2017.

[146] D. M. Sturmer, J. H. Trexler, and P. H. Cashman, "Tectonic analysis of the Pennsylvanian Ely-Bird Spring Basin: Late Paleozoic tectonism on the southwestern Laurentia margin and the distal limit of the ancestral Rocky Mountains," *Tectonics*, vol. 37, no. 2, pp. 604–620, 2018.

[147] D. Franke, "Rifting, lithosphere breakup and volcanism: comparison of magma-poor and volcanic rifted margins," *Marine and Petroleum Geology*, vol. 43, pp. 63–87, 2013.

[148] J. Braun and C. Beaumont, "A physical explanation of the relation between flank uplifts and the breakup unconformity at rifted continental margins," *Geology*, vol. 17, no. 8, pp. 760–764, 1989.

[149] D. Falvey, "The development of continental margins in plate tectonic theory," *The APEA Journal*, vol. 14, no. 1, pp. 95–107, 1974.

[150] M. Colpron and J. L. Nelson, "A digital atlas of terranes for the Northern Cordillera: British Columbia Ministry of Energy and Mines," *British Columbia Geological Survey GeoFile*, vol. 11, 2011.

[151] S. J. Piercey, *Petrology and tectonic setting of felsic and mafic volcanic and intrusive rocks in the Finlayson Lake volcanic-hosted massive sulphide (VHMS) district, Yukon, Canada: A record of mid-Paleozoic arc and back-arc magmatism and metallogeny, [Ph.D. thesis]*University of British Columbia, Vancouver.

[152] J. A. Pearce, "Sources and settings of granitic rocks," *Episodes*, vol. 19, no. 4, pp. 120–125, 1996.

[153] J. A. Winchester and P. A. Floyd, "Geochemical discrimination of different magma series and their differentiation products using immobile elements," *Chemical Geology*, vol. 20, pp. 325–343, 1977.

[154] J. A. Pearce, N. B. W. Harris, and A. G. Tindle, "Trace element discrimination diagrams for the tectonic interpretation of granitic rocks," *Journal of Petrology*, vol. 25, no. 4, pp. 956–983, 1984.

[155] D. R. Lentz, "Petrogenetic evolution of felsic volcanic sequences associated with Phanerozoic volcanic-hosted massive sulphide systems: the role of extensional geodynamics," *Ore Geology Reviews*, vol. 12, no. 5, pp. 289–327, 1998.

[156] J. D. Vervoort, P. J. Patchett, J. Blichert-Toft, and F. Albarède, "Relationships between Lu-Hf and Sm-Nd isotopic systems in the global sedimentary system," *Earth and Planetary Science Letters*, vol. 168, no. 1-2, pp. 79–99, 1999.

[157] R. A. Creaser, P. Erdmer, R. A. Stevens, and S. L. Grant, "Tectonic affinity of Nisutlin and Anvil assemblage strata from the Teslin tectonic zone, northern Canadian Cordillera: constraints from neodymium isotope and geochemical evidence," *Tectonics*, vol. 16, no. 1, pp. 107–121, 1997.

[158] J. J. Ryan, A. Zagorevski, and S. J. Piercey, "Geochemical data of Yukon-Tanana and Slide Mountain terranes and their successor rocks in Yukon and northern British Columbia," in *Geological Survey of Canada Open File 8500*, 2018.

[159] C. N. Garzione, P. J. Patchett, G. M. Ross, and J. A. Nelson, "Provenance of Paleozoic sedimentary rocks in the Canadian Cordilleran miogeocline: a Nd isotopic study," *Canadian Journal of Earth Sciences*, vol. 34, no. 12, pp. 1603–1618, 1997.

[160] N. D. Boghossian, P. J. Patchett, G. M. Ross, and G. E. Gehrels, "Nd isotopes and the source of sediments in the Miogeocline of the Canadian Cordillera," *Journal of Geology*, vol. 104, no. 3, pp. 259–277, 1996.

[161] M. D. Schmitz and B. Schoene, "Derivation of isotope ratios, errors, and error correlations for U-Pb geochronology using ^{205}Pb-^{235}U-(^{233}U)-spiked isotope dilution thermal ionization mass spectrometric data," *Geochemistry, Geophysics, Geosystems*, vol. 8, pp. 1–20, 2007.

[162] A. H. Jaffey, K. F. Flynn, L. E. Glendenin, W. C. Bentley, and A. M. Essling, "Precision measurement of half-lives and specific activities of U^{235} and U^{238}," *Physical Review C*, vol. 4, pp. 1889–1906, 1971.

[163] E. Scherer, C. Münker, and K. Mezger, "Calibration of the Lutetium-Hafnium Clock," *Science*, vol. 293, pp. 683–688, 2001.